Sirte University
Faculty of Science
Department of Chemistry

Enhanced Photocatalytic Activity of (NiO and ZnO) by Doping Ag Nanoparticles Using Green Synthesis *Thymeala Hirsuta* Extract

Student Name
HAMEEDAH MISBAH ZAYD

Under Supervision
Professor Dr. Hamid. M. Younis
Dr. Salima. M. Hussein Mohamed

Thesis Submitted in Partial Fulfilment of the Requirements for the Degree Master of Science in Chemistry

Academic Year 2024-2025

DECLARATION

I am Hameedah M. Zayd, and I confirm that the work in this thesis, unless otherwise referenced, is the researcher's work and has not been previously submitted to meet the requirements of an award at this University or any other higher education or research institution. I furthermore cede the copyright of this thesis to Sirte University.

Student name: Hameedah M. Zayd

Signature: 

Date: 15\4\ 2025

ACKNOWLEDGEMENTS

First and foremost, I am grateful to Allah Almighty, who helped me succeed. I also want to thank my parents for their irreplaceable and invaluable support.

I want to express my heartfelt gratitude to my sister for her unwavering support, encouragement, and understanding throughout my research journey. Her constant motivation and belief in me have been invaluable.

I also thank Associate Professor Dr Hamid M. Younis for his supervision and guidance in this research work. His continuous support and valuable contributions finally brought this research forward.

I would also like to thank Dr. Siti Khadijah Mohd for teaching me about the FESEM instrument and the FESEM images of catalysts. I am also immensely indebted to Dr. Norazzizi and the School of Chemical Sciences, USM University, for the specialised insights, advice, and support that have been crucial in bringing this research to fruition.

Researcher

DEDICATION

To the nine-year-old girl who stepped onto the university grounds for the first time, her eyes filled with dreams waiting to be fulfilled, and to the determination and resolve in her gaze, you chose to belong here. Today, you have turned that dream into reality.

Finally, to all those who still dream of knowing and changing the world, may this thesis stand as a testament to hard work, perseverance, and the relentless pursuit of excellence.

Hameedah Misbah Zayd

TABLE OF CONTENTS

LIST OF FIGURES

LIST OF TABLES

LIST OF ABBREVIATIONS

Symbol	Definition
A	Absorbance
CB	Conductive Band
CR	Congo Red
DPPH	2,2-diphenyl-1-picrylhydrazyl
e^-	Electron
h^+	Hole
TEM	Transmission Electron Microscopy
Vis	Visible
Ppm	Parts per million
M	Molarity, mol/Liter
FESEM	Field-Emission Scanning Electron Microscopy
EDX	Dispersive X-ray Spectrometry
UV-vis	Ultraviolet-visible spectroscopy
NPs	Nanoparticles
Ag	Silver
Pd	Palladium
Au	Gold
ZnO	Zinc Oxide
VB	Valance Band
NiO	Nickel Oxide
Ev	electron Volt
·OH	Hydroxyl radical

H+	Proton
H_2O_2	Hydrogen peroxide
Hv	Photon
TiO_2	Titanium dioxide
MOFs	Metal-Organic Frameworks
CO_2	Carbon dioxide
Al	Aluminium
N	Nitrogen
F	Fluorine
V_{Zn}	Zn Vacancies
g-C_3N_4	Graphene Carbon Nitrate
0-D	Zero-Dimensional
1-D	One-Dimensional
2-D	Two-Dimensional
3-D	Three-Dimensional
XRD	X-Ray Diffraction
UV	Ultraviolet light
PVD	Physical Vapour Deposition
Rh B	rhodamine B
MO	Methyl Orange
MB	Methylene Blue
FEG	Field Emission Gun

ABSTRACT

The green approach to synthesising photocatalysts Nanoparticles is considered a feasible alternative to traditional methods. This study adopted green synthesis using *Thymeala Hirsuta* extract as a capping, stabilising, and reduction agent to produce pure ZnO and NiO NPs, which were then surface-modified by silver nanoparticles. The structure analysis of photocatalysts nanoparticles confirmed the formation of a spherical shape with a diameter equal to 3.05 nm,3.044 nm, 3.346 nm and 3.434 nm for ZnO, NiO, Ag-ZnO and Ag-NiO NPs, respectively. Due to a decrease in NPs size and formation 0-D and doping by silver NPs causing a reduction in band gap energy value Eg of pure ZnO and NiO NPs, was 3.3 eV for ZnO NPs and 3.15 eV for Ag-ZnO NPs and the band gap energy of NiO NPs equal 3.16 eV and Ag-NiO was 3.14 eV, which improved photocatalytic activity of pure photocatalysts at Ph 7 were with a degradation rate of 74.62% and 98.32% for Ag doping ZnO NPs. The Ag doping NiO NPs also showed a high level of photodegradation activity, with degradation rates of 76.59% and 51.37% for NiO NPS, respectively. Increasing photocatalytic activity in an alkaline medium confirms the stability of photocatalysts during the study and the reusability of prepared photocatalysts.

CHAPTER 1
INTRODUCTION

1.1 BACKGROUND OF THE STUDY

Nanomaterials are characterised by structural features at the nanoscale, typically consisting of tiny particles ranging from 1 to 100 nanometres. Single crystals of nanoparticles are usually called nanocrystals, and aggregates are named nano-powders [1]. These nanoparticles can contain metals, dielectrics, or semiconductors. They can be engineered into core-shell geometries, which exhibit novel electrical and optical properties due to quantum size effects that increase their natural energy gap compared to bulk materials. Examples include quantum wells, nano-powders, nano-shells, nanowires, nanorods, carbon nanotubes, nanomembranes, and nano-coatings, which are frequently combined into nanocomposites [2].

Nanomaterials in energy applications have enhanced chemical, electronic, mechanical, and optical properties due to an increased surface-to-volume ratio and quantum size effects. This makes them unique compared to bulk materials. Numerous methods for synthesising photocatalysts have been established: physical, hydrothermal, solvothermal, sol-gel, and co-precipitation. However, they could become costly and involve dangerous chemicals, significantly threatening environmental integrity and biological systems [3]. Various synthesis methods, including eco-friendly approaches such as using plant extracts, are being developed to create nanomaterials like ZnO, TiO_2, NiO, and nanocomposites with better environmental and safety profiles [1,2].

The above features make the plant extracts a more favourable choice compared to other synthesis methods. This opens the prospects for nano-sized semiconductors. Among the semiconductors that can be used for photocatalytic purposes, zinc oxide (ZnO) and nickel oxide (NiO) are the most promising candidates for a variety of applications, including composite anodes for fuel cells, gas sensing technologies, bright windows, supercapacitors, and water treatment. ZnO and NiO have a wide band gap energy, so they exhibit high photocatalytic activity under UV irradiation but low activity in the visible range; hence, to improve the photoactivity of ZnO and NiO in the visible region, the researchers use metals and non-metals doped photocatalysts or photocatalysts composites. Some studies have

focused on green synthesis using plant extract, biomass, and algae [4]. This study was the first to combine green synthesis and controlling morphology and size nanoparticles; the selection of *Thymelaea hirsuta* was based on its high content of flavonoids, saponins, and alkaloids that act as reduction, capping, and stabilise agents due to their ability to inhibit growing atoms of nanomaterial to the small diameter of semiconductors, which are expected to facilitate nanoparticle formation and enhance their physical properties. This new methodology contributes to the growing field of green nanotechnology and opens ways to use underutilised plant species to fabricate nanomaterials. It bridges nanotechnology and plant biotechnology in reducing metal ions using plant extracts without applying high pressure, energy, temperature, or toxic chemicals. The surface area and morphology of photocatalysts in the semiconductors can be improved by doping with different metals and nonmetals. This phenomenon inhibits the recombination of electron-hole pairs and increases visible light absorption by introducing defect states in the band gap [5].

Moreover, when semiconductor materials doping with metal and non-metal dopants enhance their photocatalytic activity, extending promising applications in water treatment, environmental purification, and solar energy conversion. Doping also changes the electronic structure and facilitates the creation of localised band gap energy, enhancing the charge carriers' confinement efficiency and hindering recombination. This effect is especially favourable in applications requiring constant photocatalytic activity under illumination with sunlight since using a more significant percentage of the light spectrum is possible. In the present work, ZnO and NiO nanoparticle-based photocatalysts, modified and synthesised with various plant extracts by a simple, nontoxic, inexpensive, and eco-friendly process to create a highly efficient photocatalyst characterised by low toxicity, are reported [6,7].

1.2 Definition OF ZnO and NiO as Photocatalysts

ZnO is a semiconductor material with a wide bandgap, featuring a direct bandgap of 3.37 eV at room temperature. It has impressive optical properties, including transparency to visible light and strong absorption of UV radiation. Due to their small size, ZnO nanoparticles have a high surface area, making them useful for many applications. These nanoparticles can adopt various shapes, such as spheres, cylinders, and cubes, which impact their surface area and crystal facets. Spherical nanoparticles have more even surface energy and are more effective in photocatalysis. However, anisotropic materials like cubes or rods can show crystal planes that would be suitable for photocatalysis; particles can be reduced

in size and spherical in nature with control over the used extract concentration [8]. Higher concentrations typically yield smaller, spherical nanoparticles, while more dilute solutions tend to produce larger nanoparticles with varied shapes [9]. Standard methods for synthesising ZnO nanoparticles include sol-gel controlled precipitation and vapour transport, which are some ways to make these tiny particles. ZnO nanoparticles work well to break down organic dyes that pollute water when exposed to UV or visible light. They are also used in sunscreens because they can block UV rays. The nanoparticles are also applied in electronics, such as transparent conductive films, sensors, and varistors. The nanoparticles are also found in biomedical use as antimicrobial, drug, antibacterial, and antifungal. Some issues, such as clumping together and stability, may influence how effectively they work. Also, toxicity issues require cautious handling and analysis [10].

NiO is a green crystalline solid material with ferromagnetic properties. It is a wide-bandgap (3.6–4.0 eV) p-type semiconductor with extreme chemical stability. When NiO is synthesised in nanostructures, its properties change depending on the particle size. Due to their small size, NiO nanoparticles have a high surface area, which makes them useful in photocatalytic applications [11].

1.3 Zinc Oxide and Nickel Oxide Modified with Noble Metals

The methodology to improve the photocatalytic activity of semiconductors like ZnO NPs is doping with noble metallic or non-metallic nanoparticles. The Noble metals that are used to decrease the wide band gap energy of these metallic oxides, such as silver (Ag) and palladium (Pd), have been separately doped onto ZnO nano photocatalysts using methods like borohydride reduction [3]. Incorporating noble metal nanoparticles onto the surfaces of ZnO and NiO significantly enhances the photocatalytic efficiency. These noble metals act as co-catalysts, promoting charge separation and reducing the recombination of photogenerated electron-hole pairs. The modified ZnO and NiO photocatalysts exhibit improved degradation of organic pollutants under light irradiation [12].

1.4 Problem Statement

Traditional synthetic methods for synthesising metal oxides, including pure ZnO and NiO NPs and their doping with metals, are conventionally performed using hazardous chemicals and expensive procedures that harm environmental integrity and biological

systems [12]. This challenge requires the development of eco-friendly and cost-effective green synthesis methods using plant extracts that can act as natural stabilising and reducing agents. The goal of this study is to control the size and morphology of nanoparticles to improve high photocatalytic efficiency and reduce toxicity and environmental impact. Green synthesis approaches utilise non-toxic and renewable materials, water as a solvent, and biological reducing and stabilising agents such as biomolecules and phytochemicals from microbes and plants, promoting efficient energy consumption and minimising contamination [14].

It becomes helpful in applications due to the unusual properties of the nanoparticles for surface or quantum effects. However, classical synthesis involves hazardous solvents and toxic chemical ingredients that increase energy consumption with cost and environmental risks. Researchers continuously develop environmentally benign synthesis processes that rely on non-toxic and renewable starting materials. The use of microorganisms and plant extracts in synthesising metal and metal-based hybrid nanoparticles is gaining popularity as a new research focus [12]. This study employs a rapid and straightforward bio-approach, using *Thymelaea hirsuta* extract to synthesise pure ZnO and NiO NPs and to dope them with silver NPs. The research aims to address the following key questions:

1. How does *Thymelaea hirsuta* extract and the variation in its concentration short-time reaction to a salt solution affect the morphology and size of synthesised pure ZnO and NiO nanoparticles (NPs)?
2. How does adding silver NPs influence the morphology and size of pure ZnO and NiO nanoparticles?
3. How do the morphology and size of pure nanoparticles impact the photocatalytic activity of the photocatalysts?
4. How do doping ZnO and NiO nanoparticles with surface silver NPs affect their photocatalytic activity?

1.5 Objectives of the Study

The research aims to develop an eco-friendly method for synthesising ZnO and NiO nanoparticles from plant extracts, focusing on minimising environmental impact and maximising cost-effectiveness. The research further seeks to optimise the process to provide consistent control over the shape and size of the nanoparticles, with a preference for smaller

growth of nanoparticles. Furthermore, it aims to study the influence of doping Ag on ZnO and NiO nanoparticles in terms of morphological and structural properties, as well as the implications of the resulting changes on the photocatalytic activity. Finally, it aims to search for potential applications of the nanoparticles synthesised to fields such as environmental remediation and renewable energy harvesting.

The main objectives of this study are summarised in the points below:

1. Investigating the Effect of *Thymelaea Hirsuta* Extract: Study shows how increasing the concentration of *Thymelaea hirsuta* extract in a short-time reaction to a salt solution influences the morphology and size of synthesised pure ZnO and NiO nanoparticles (NPs).
2. Determine the Impact of Silver Nanoparticles (NPs): study shows how the coating of silver NPs affects the morphology and size of pure ZnO and NiO NPs.
3. Measurement Photocatalytic Efficiency: Study shows the effect of pure ZnO and NiO nanoparticles' morphology and size under UV, dark and solar light.
4. Effects of silver NPs coating: Study shows how doping ZnO and NiO nanoparticles with silver NPs affects their photocatalytic activity.

1.6 Significance of the Study

Improving photocatalytic activity through green synthesis is vital to promoting environmental sustainability. The key contributions of this study are summarised in the following points:

1. **Plant-mediated green synthesis reduces toxic chemical and energy-intensive equipment, ensuring safety and sustainability**. The nanoparticles produced through this method can be effectively applied in photodegradation processes without causing negative environmental impacts.
2. **Exploring the role of bioactive compounds in *thymelaea hirsuta* extract** in controlling the final size and shape of nanoparticles.

3. **Enhanced photocatalytic efficiency under the visible spectrum**, enabling more effective solar energy utilisation for environmental applications.

1.7 Scope of Study

The scope of this study is limited to the preparation of zinc oxide and nickel oxide nanoparticles coated with silver nanoparticles to generate highly stable zinc oxide doped with silver nanoparticles (Ag-ZnO) and nickel oxide doped with silver nanoparticles (Ag-NiO) using the green synthesis method within a short time frame. The optimisation process was based only on the properties of the bioactive compounds in the plant extract and their ability to oxidise silver ions, aiming to enhance the photocatalytic activity of the synthesised photocatalysts under the visible range.

1.8 Organisation of the Thesis

This dissertation is organised into five chapters, Chapter 1 provides an introduction to the study, including the problem statement, aims, and objectives. Chapter 2 presents a comprehensive review of the literature, covering the synthesis of ZnO and NiO, silver doping, and surface modification using various organic and inorganic methods. Chapter 3 details the experimental section, including materials, procedures, characterisation techniques, and the optimisation of as-synthesised ZnO and NiO nanoparticles for their application in water treatment through the measurement of photocatalytic activity. Chapter 4 discusses and highlights the key findings derived from this research. Finally, Chapter 5 presents the conclusions of the study and offers suggestions for future research directions.

CHAPTER 2

LITERATURE REVIEWER

2.1 A Brief Overview of Green Photocatalysis

Green photocatalysis, using light to power chemical reactions in concert with sustainable and non-toxic materials, is one alternative to conventional catalysis that will reduce the ecological footprint by diminishing harmfully employed chemicals and energy. The search for appropriate metal oxide semiconductors to serve as photocatalysts for the degradation or remediation of contaminants and pollutants present in water bodies using solar energy is among the most essential tasks in material science. The photocatalytic material should have appropriate properties of the desired bandgap for absorption of a wide range of the solar spectrum to dissociate water molecules and remain stable in the water environment throughout the reaction processes. In addition, it must be economically viable, easy to process, readily available, and non-toxic to the environment [15].

Green photocatalysts, such as ZnO, an n-type semiconductor with a wide bandgap of about 3.37 eV, exhibit excellent performance in the generation of reactive species due to their efficient UV light absorption and high efficiency in the degradation of organic dyes in wastewater and water splitting for hydrogen and oxygen production [4]. NiO, having a bandgap between 3.1 and 3.6 eV, is frequently used in heterojunction systems to separate charge and visible-light utilisation. The modified band gap energy of NiO and ZnO synergised their properties, leading to an extension in the light absorption range and an enhancement in the photocatalytic efficiency to become these photocatalysts have several applications: solar energy in the treatment of wastewater, purification of air, CO_2 reduction, and hydrogen production, with huge potential to give sustainable solutions for environmental and energy challenges [5,7,12].

2.2 Photocatalysis

Photocatalysis is an advanced oxidation process in which chemical reactions occur under light and a suitable catalyst. The photocatalytic reaction depends primarily on wavelength or light (photon) energy and the catalyst. Generally, semiconducting materials serve as catalysts and sensitisers for light-induced redox reactions owing to their electronic structure, consisting of a full valence and an empty conduction band [16].

This is unique in that the reaction occurs only when the photocatalyst and light energy are simultaneously present; the absence of either one would prevent the reaction.

The process of photocatalysis generally involves three key steps:

- **Excitation of electron-hole pairs**: Light irradiation with an energy larger than or equal to the band gap energy of the photocatalyst shining on the catalyst generates electron-hole pairs.

- **Migration of the photogenerated electrons and holes**: The electrons migrate to the surface of the photocatalyst in the conduction band, while the holes do the same in the valence band. They reductively or oxidatively react at the surface with adsorbed oxygen and water molecules to form $\bullet O^{2-}$ and •OH active radical species.

- **Secondary reactions**: The radical species formed to attack the pollutant molecules, decomposing them into innocuous products.

The mechanisms of photocatalysis at each step (e.g., for ZnO) are represented by Equations 1–7 [3,4,5,16]:

$$ZnO + h\nu(light) \rightarrow e^-_{(CB)} + h^+_{(VB)} \ldots\ldots 1$$

$$H_2O + h^+_{VB} \rightarrow \cdot OH + H^+ \ldots\ldots 2$$

$$O_2 + e^-_{CB} \rightarrow O_2^- \ldots\ldots 3$$

$$O_2^- + H^+ \rightarrow \cdot HO_2 \ldots. 4$$

$$2 \cdot HO_2 \rightarrow H_2O_2 + O_2 \ldots. 5$$

$$H_2O_2 + O_2^- \rightarrow \cdot OH + OH^- + O_2 \ldots. 6$$

$$\cdot OH + \text{Organic Dye} \rightarrow \text{Degradation} + \text{Oxidize Product} \ldots. 7$$

These processes are schematically illustrated in Scheme 1, which depicts the mechanism of photocatalytic reactions using a homogeneous semiconductor photocatalyst such as ZnO (with a bandgap of 3.2 eV) excited by UV light irradiation.

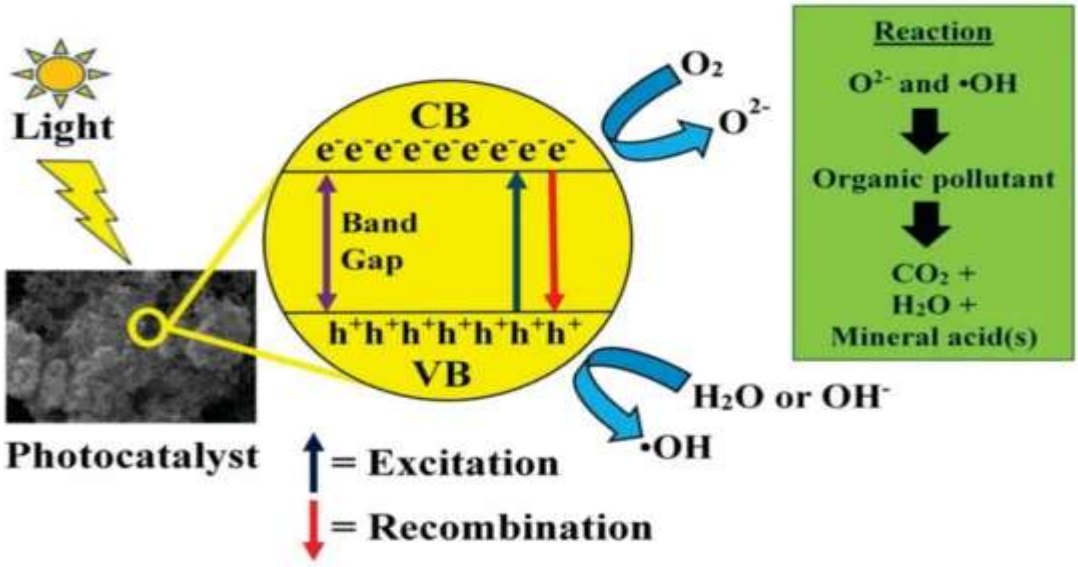

Figure 1: Schematic representation of semiconductor photocatalytic mechanism [4].

2.3 Photocatalysts

A photocatalyst is a substance that can be excited by light absorption, thus enabling various chemical reactions. It acts as a catalyst, using light energy, mainly from ultraviolet or visible light, to form reactive species, such as electron-hole pairs that eventually react with other reactants to drive several chemical changes. Photocatalysis has become indispensable in various applications, including environmental remediation, energy conversion, and synthesis of valuable chemical substances [16,18].

The fundamental process of photocatalysis involves the absorption of photons by semiconductor materials, which leads to the jump of electrons in the valence band to the conduction band, hence producing electron-hole pairs. The efficiency of photocatalysis relies on how the material absorbs light, separates and transports the charge carriers' electrons and holes and enhances their interaction with the reactants efficiently. The holes can oxidise the reactants, but the electrons participate in the reduction reactions.

Some properties determine whether a photocatalyst is effective:

- Broad light absorption spectrum.
- Efficient Charge Separation.
- High catalytic activity.

Widely used photocatalytic materials are semiconductors like titanium dioxide (TiO_2), zinc oxide (ZnO), and graphene oxide, which are mainly preferred for being stable, non-toxic, and capable of absorbing ultraviolet light [4,6]. More advanced photocatalysts include MOFs with tenable structures designed for particular applications and noble metal nanoparticles, like platinum and silver, improving photocatalytic efficiency by promoting charge separation [6].

Photocatalysts have significant environmental applications, including the degradation of organic pollutants in water and air and energy production, including hydrogen generation via water splitting and CO_2 reduction for solar energy conversion. Developing more efficient photocatalysts is crucial for advancing sustainable energy technologies and environmental protection [20].

2.4 Issues with Photocatalysts

The key challenges in evaluating the efficiency of these photocatalysts include the rapid recombination of photogenerated electron-hole pairs, reduced adsorption of dye molecules on the catalyst's surface, and a lower charge transfer rate relevant to the degradation of dye molecules. These metal oxide photocatalysts exhibit better activity in degrading organic dyes when illuminated with ultraviolet light due to their high band gap values. It is worth noting that only about 5% of the solar spectrum consists of UV light, and these materials work within this narrow energy range, making most of the solar energy go to waste [6,11].

Since visible light accounts for approximately 43% of the solar spectrum, there is a pressing need to develop photocatalysts sensitive to visible light [3]. To address these challenges, researchers have explored photocatalysts with diverse morphologies, as variations in morphology can significantly influence their surface and optical properties. Tailoring these properties can enhance photocatalytic performance, leading to improved photocatalytic activity [21].

2.4.1 Semiconductors as Photocatalysts at the Nanoscale

Semiconductors are materials capable of absorbing light and creating charge carriers, electrons, and holes with the help of light; such materials are used for photocatalytic purposes. According to the literature, photocatalysis is caused by light in which a

semiconductor material catalyses a chemical reaction without undergoing depletion. It tends to produce electron-hole pairs to enhance redox reactions on the surface [22].

Semiconductor materials at the nanoscale show distinct properties that contribute significantly to their photocatalytic activity, which is most suitable for applications in environmental remediation and the production of renewable energy. At the nanoscale, semiconductors have a more excellent surface area-to-volume ratio, allowing more interaction with reactants and increasing photocatalytic efficiency. The higher surface area allows for more significant production of electron-hole pairs upon photon absorption since the smaller particle size and quantum confinement effects at the nanoscale increase the dynamics of charge carriers and reduce recombination rates [23].

Photocatalysts, including titanium dioxide (TiO_2), zinc oxide (ZnO), and nickel oxide (NiO), demonstrate enhanced photocatalytic performance when in nanoscale configurations. This enhancement is attributed to their capacity to effectively absorb ultraviolet or visible light, producing highly reactive entities such as hydroxyl radical (•OH) and superoxide anion radical ($\cdot O_2^-$) [2,8,12].

These reactive entities play a crucial role in the degradation of contaminants, the generation of hydrogen via water splitting, and the reduction of carbon dioxide. The ability to tune the properties of semiconductors at the nanoscale, such as bandgap and doping processes and surface modifications, significantly enhances their photocatalytic activity. Thus, semiconductors at the nanoscale become versatile tools for different applications, including self-cleaning surfaces, water purification, and solar energy conversion. Combining semiconductor photocatalysis with nanotechnology offers promising prospects for solving global environmental problems and promoting sustainable energy solutions [14].

2.4.2 The Types of Semiconductors Used in Photocatalysis

The types of Semiconductors are classified by their intrinsic properties and the presence of impurities, which affect their electrical and optical properties, especially in applications like photocatalysis:

- Intrinsic semiconductors are pure, undoped materials whose electrical behaviour is wholly determined by the inherent atomic structure. Examples include pure ZnO and TiO_2; most photocatalytic processes depend on their ability to absorb UV light and form

electron-hole pairs. However, wide bandgaps have restricted their ability to perform photocatalytic activity in the UV spectrum range.

- Extrinsic or doping semiconductors are purposely doped with various impurities to alter their electrical behaviour by introducing extrinsic charge carriers. For instance, n-type semiconductors, of which Al-doped ZnO is an example, exhibit an electron-rich profile with surplus electrons as the majority of charge carriers. The hole carriers dominate p-type semiconductors, represented by NiO [25,26].

Doping also extends the capability of spectral light absorption, by which extrinsic semiconductors will work more effectively in the visible light region. This, again, is very useful in pollutant degradation, water splitting, and CO_2 reduction. In a nutshell, the classification of semiconductors in photocatalysis is based on their purity-intrinsic versus extrinsic-where doping plays an essential role in enhancing their photocatalytic efficiency and light absorption spectrum. Photocatalysts can facilitate photoreactions such as pollutant degradation, water splitting, and CO_2 reduction under light irradiation. Indeed, many types of photocatalysts have been developed with different properties and mechanisms [8].

2.5 Band Gap Energy

2.5.1 Band Gap Energy of ZnO Nanoparticles

Zinc Oxide (ZnO) is widely known as an essential n-type semiconductor with a bandgap energy of approximately 3.37 eV. Its extensive exploration has been encouraged by its prospective applications in photocatalysis due to its relatively wide bandgap, enabling it to absorb ultraviolet (UV) light efficiently. Unlike most other wide-bandgap semiconductors, ZnO has a direct bandgap, meaning electrons in the valence band can transition to the conduction band without changing momentum (k values). This makes ZnO better at absorbing light and participating in photocatalytic reactions when illuminated with UV light. The direct bandgap nature of ZnO allows for fast electron transitions, thus minimising carrier recombination and improving photocatalytic activity. The direct bandgap nature of ZnO is quite different from many other semiconductor materials, such as silicon (Si), which have indirect bandgaps that require modifications in k values for the transition of electrons [27,28]. This anisotropy, as in the case of the bandgap, directly affects the absorption and emission characteristics of the material and thereby renders ZnO especially applicable in optoelectronic and photocatalytic applications requiring high efficiency.

Several studies have demonstrated that the direct bandgap of ZnO allows it to achieve high photoluminescence and strong UV absorption, which is favourable in environmental applications, including the degradation of organic pollutants, water splitting, and CO_2 reduction. The photocatalytic activity of ZnO can be further enhanced by doping or coupling with other materials, which would shift its light absorption to a broader range of wavelengths, including visible light [19,27,29].

The diagram illustrating the direct bandgap properties of ZnO gives an apparent visual image of the energy band structure, including conduction and valence bands and a direct transition in the energy diagram **Figure** 2 from [30]. In this case, it has been depicted that electron transitions between the VB and the CB take place without any change in momentum, which is contrary to the case for indirect semiconductors. This property is essential in increasing the efficiency of photocatalytic processes because direct electron transitions enable faster charge separation, lower recombination, and more photo-generated carriers available for the reaction.

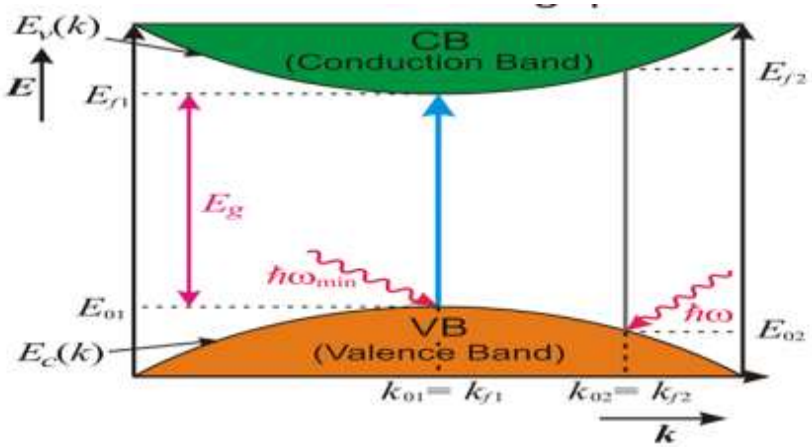

Figure 2: Direct transition from VB to CB of semiconductors [30].

2.5.2 Band Gap Energy of NiO Nanoparticles

Nickel oxide (NiO) nanoparticles have been widely studied for their photocatalytic properties, in which the bandgap energy of the material dictates the efficiency of NiO in both solar energy conversion and environmental remediation processes. The p-type semiconductor material has a relatively narrow bandgap, reported to range between 3.1 and 3.6 eV [30,31]. This makes NiO capture the visible light, thus qualifying for photocatalytic activity in the natural sunlight region. However, the bandgap of NiO is an indirect bandgap system, meaning transitions of electrons from the valence band to the conduction band

require a change in momentum assisted by phonons. As shown in **Figure** 3 from [30], this indirect gap typically arises via a phonon-assisted process, where the electron interacts with lattice vibrations to conserve momentum, a salient feature in transition metal oxides such as NiO.

The indirect bandgap properties of NiO bring both benefits and challenges for photocatalytic applications. On the one hand, they allow the localisation of charge carriers and, therefore, may improve the material's chemical stability [30].

On the other hand, the momentum change required for exciting electrons results in less effective electron transitions than direct bandgap materials, limiting light absorption efficiency. Moreover, its photocatalytic activity can be improved remarkably by structural changes and the design of composite materials. The bandgap tuning strategies for NiO continue to be an active area of research to expand its applicability for solar-driven reactions and environmental remediation [31,34].

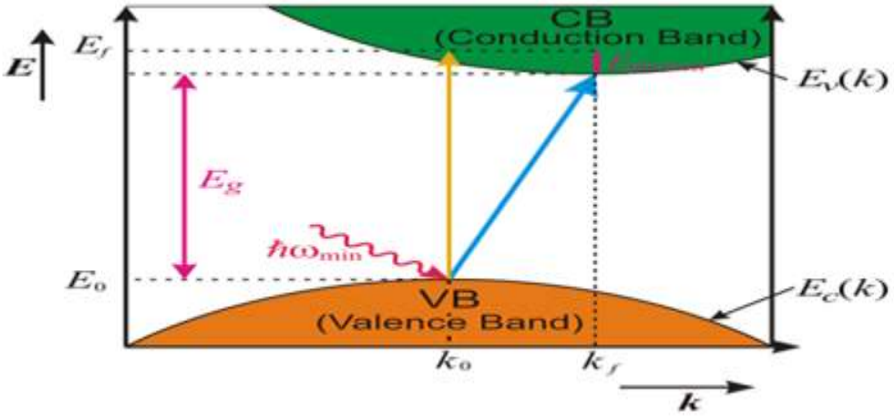

Figure 3: Indirect transition from VB to CB of semiconductors [30].

2.5.3 Modifying Band Gap Energy of Photocatalysts in Visible Light Spectrum

Continuous research on photocatalysis, through changing semiconductor band gap energy, has aimed to seek active photocatalysts within the visible light region to utilise solar energy. When semiconductor band gap values decrease, the material absorbs longer wavelengths of light, shifting its absorption spectrum from UV to visible light.

This is called a redshift or bathochromic effect, in which the improved ability of a photocatalyst to absorb visible light is developed since it constitutes most of the solar spectrum. In return, the increase in photocatalytic reaction efficiencies arises because the photocatalyst can harness more solar energy, thus becoming more applicable for applications like solar water splitting and environmental remediation [4,19,34].

2.5.3.1 Surface Doping of Semiconductor Photocatalysts

The surface doping of semiconductor photocatalysts has garnered significant attention in recent years due to its possibility of enhancing photocatalytic efficiency in the visible light range. Coupling photocatalysts with support materials like metals with narrower band gaps or forming nanocomposite materials with polymer has been reported to enhance photodegradation efficiency in visible light irradiation [35].

Sohrabnezhad and Seifi [36] studied the green synthesis of Ag/Zno nanocomposites prepared using *Urtica dioica* leaf extract. Silver metal nanoparticles were deposited over the ZnO nanocomposite to enhance the photocatalytic activity, using $AgNO_3$ as a source of silver ions and Urtica dioica leaf extract as a reducing agent, respectively. The Ag/ZnO nanocomposite was characterised by X-ray diffraction (XRD); the powder X-ray diffraction showed that Ag/ZnO nanoparticles were located on the surface MMT layers. The diffuse reflectance spectra of the nanocomposite indicated a strong surface plasmon resonance (SPR) absorption band in the visible region, resulting from metallic Ag nanoparticles. The photocatalytic activity of the nanocomposite was studied for the destructive reaction of methylene blue dye under visible light. The results showed that modifying the ZnO nanocomposite with silver nanoparticles increased the percentage of methylene blue (MB) degradation from 38.95% to 91.95%. The composite matrix was essential in reducing electron-hole recombination in the nanocomposite.

Nagasundari *et al*. [37] reported simple Phyto-assisted synthesis of zinc oxide nanowires (ZnO NWs), and their silver (Ag) doping by co-precipitation method has been reported. The synthesised Ag-doped ZnO NWs photocatalytic action on the UTI antibiotic nitrofurantoin (NFT) and the dye methylene blue (MB) has been reported. UV-vis spectroscopy, FTIR, XRD, SEM, TEM, EDAX, and particle size analyser determined the synthesised NPs' optical, biocomponents, structural and chemical properties. The photocatalytic activity of Phyto-assisted synthesised Ag-doped ZnO nanowires (NWs) was

investigated for antibiotic NFT and dye methylene blue (MB) degradation. The degradation efficiency and dye removal were evaluated quantitatively. The analysis of the UV-vis absorption spectrum revealed the occurrence of a surface plasmon resonance (SPR) band in the range of 370 nm to 400 nm with blue and redshifts. The vast bandgap energy (3.37 eV - 2.75 eV) reduction indicated the inclination of noble metal Ag on the surface of ZnO NWs. The synthesised Ag-doped ZnO nanowires achieved photocatalytic degradation of about 78.51% of the antibiotic NFT and 92.43% of MB dye in 150 min under UV irradiation. The present study establishes the likelihood of photocatalytic degenerative potency of the antibiotic nitrofurantoin and methylene blue employing photosynthesised zinc oxide nanowires.

Liu *et al.* [38] synthesised spherical Ag-ZnO NPs by a two-step chemical method. The ZnO-MSs with 70 nm diameter were first synthesised using ultrasonic technology. The Ag-NPs with a 20–50 nm diameter were subsequently anchored onto the surface of the synthesized ZnO-MSs via a microwave polyol process. The structural, morphology, and optical properties of the synthesised materials were analysed by various analytical techniques, including X-ray diffraction (XRD), field emission scanning electron microscopy (FESEM), transmission electron microscopy (TEM), high-resolution transmission electron microscopy (HRTEM), X-ray photoelectron spectroscopy (XPS), UV-visible absorption spectroscopy, and photoluminescence spectroscopy. The findings indicate that the surface plasmon resonance absorption band of Ag/ZnO composites is considerably broadened, and the PL intensity of heterostructure composites exhibits fluctuation upon increased Ag loading.

The photocatalyst activity of Ag/ZnO composites was ascertained by degrading rhodamine B (RhB) solution under ultraviolet (UV) and visible light illumination. The synthesised Ag/ZnO composites' degradation rate was more than three times faster than that of pure ZnO-MSs when they were illuminated with UV light. This effect resulted from the Schottky barriers formed at the interfacial areas between ZnO mesoporous structures and Ag nanoparticles. Besides, Ag/ZnO composites exhibit enhanced photocatalytic activity compared to ZnO-MSs under visible light irradiation, which is predominantly due to efficient electron transfer from plasmon-excited $Ag_{(0)}$ nanoparticles to ZnO-MSs because of the intense confinement of surface plasmon resonance (SPR). The recombination rate of

electron-hole pairs is minimal, and there is a prolonged lifetime of electron-hole pairs, because of which degradation efficiency is enhanced.

Furthermore, Dhiman *et al.* [39] underline the excellent antibacterial activity realised by Ag/ZnO nanocomposites with an initial band gap of 3.44 eV tuned to 3.1 eV. Increased surface area, besides the surface plasmon resonance (SPR) effects arising from silver, contributed much toward enhancing bactericidal properties, thus rendering these nanocomposites very strong against a broad spectrum of pathogens.

Hira Naseer and Tahir Iqbal [40] reported that doping ZnO with Ag when ZnO is doped with silver NPs decreases the ZnO NPs band gap value and changes it from UV-based to the visible region of the solar spectrum. The calculated band gaps of different Ag dopant concentrations, ranging from 0.5% to 2%, decreased from 3.37 eV to 2.80 eV.

2.5.3.2 Doping Engineering in Photocatalysts

2.5.3.2.1 Cation-Doped Semiconductor Photocatalyst

Cation-doped semiconductors are one of the most significant strategies in semiconductor engineering, as they can decrease the band gap energy related to photocatalysts, such as ZnO, by incorporating cation ions in lattices. Pure ZnO usually exhibits a band gap of approximately 3.37 eV, thus limiting its utility in visible-light-driven processes. However, it has been well established that doping of cations such as aluminium (Al) in ZnO can cause a narrowing in the bandgap by replacing Al^{+3} with Zn^{+2} in the ZnO lattice to approximately 3.1 eV and further doping with cobalt (Co) could also reduce it to approximately 2.83 eV [41].

The narrowing of bandgap energy is due to the formation of localised energy states within the band gap, which promotes electronic transitions. Such localised states allow electrons to be lifted into the conduction band at lower energies, improving the optical absorption characteristics of the material. Cation-doped ZnO thus exhibits increased sensitivity to visible light and has great potential in several applications, including photocatalysis and optoelectronics. The careful choice of dopants and their concentrations are essential in optimising the doped semiconductor's desired electronic and optical properties [42].

2.5.3.2.2 Anion-Doped Semiconductor Photocatalyst

Anion doping of semiconductor NPs is one important method of modifying their electronic and optical properties. In general, incorporating anions such as nitrogen (N), sulphur (S), or carbon (C) into the crystal lattice changes the band gap energy, enhancing performance in various applications [43].

For instance, N-doped TiO_2 nanoparticles extend light absorption into the visible spectrum, enhancing photocatalytic efficiency under sunlight [43]. Similarly, S-doped ZnO nanoparticles show enhanced photocatalytic activity through mid-gap states that promote charge carrier separation. Further, the carbon-doped NiO nanoparticles show better electrochemical performance and stability, which makes them suitable for energy storage. Such developments highlight the importance of anion doping in developing high-performance semiconductor NPs that are useful for environmental and energy applications [44,45].

Improve the photocatalytic activity of NiO with doping elements such as nitrogen (N), which has been shown to significantly enhance its structural and optical properties, particularly for photocatalytic applications. Doping introduces additional energy levels within the band gap, reducing band gap energy, which improves the material's effectiveness under visible light. For instance, band gap energies of about 3.2 eV for undoped NiO and 3.0 eV for nitrogen-doped NiO have been reported, indicating a trend of decreasing band gap with increasing doping levels. The decrease favours visible light absorption and consequently enhances the photocatalytic degradation of pollutants like methylene blue [46].

2.5.3.3 Vacancy Engineering in Photocatalysts

2.5.3.3.1 Cation-Vacancy Engineering in Photocatalysts

In enhancing the photocatalytic efficiency of photocatalysts, there has been a conventional need to lower band gap energy values in semiconductors by strategically engineering vacancies that create vacancies by removing atoms or ions in the semiconductor lattice. Zinc vacancy is a cation vacancy that changes band gap energy to improve the optical properties of zinc oxide lattice [47]. Pan *et al.* [48] reported that 7.5 mol% abundant Zn vacancies had been successfully introduced into undoped ZnO using a simple solvothermal

method followed by calcination in air. They were doubtlessly proved both by characterisations and computations. Consequently, with Zn vacancies, some new properties were induced in ZnO, such as p-type conductivity, room-temperature ferromagnetism, and high photocatalytic activity. Abundant Zn vacancies can be formed during the synthesis of ZnO. This may imply that metal defects would be readily engineered in undoped metal oxides, probably giving rise to many unexpected properties; hence, a broadening of synthetic strategy and application scope can be expected in energy areas.

2.5.3.3.2 Anion-Vacancy Engineering in Photocatalysts

Wang *et al.* [49] found the formation of the oxygen vacancy in a crystal introduces considerable effects on the electronic property of ZnO. High oxygen vacancy concentration incorporation can be achieved with precursors such as ZnO. Synthesised ZnO assumes the yellow tint, with the red shifting of the absorbance edge toward longer wavelengths. These phenomena were further proved by Raman and XPS spectra: the concentration of oxygen vacancies of ZnO annealed in the air decreased at higher annealing temperatures, which agrees with the result from the theoretical calculation. With increasing oxygen vacancies, the bandgap was narrowed down, increasing the absorption of visible light in ZnO. It is further confirmed by the enhanced photocurrent response upon irradiation of ZnO with visible light, inferring the narrowing bandgap. ZnO with oxygen vacancies is active and efficient for the photodecomposition of 2,4-dichlorophenol under visible light irradiation.

2.5.4 Morphology of Photocatalyst Nanoparticles

Two aspects are considered for photocatalysts (as nanomaterials). One is the extended surface area of the nanomaterials compared with their bulk counterpart. Increased surface area can raise the catalytic activity of the Photocatalysts. The second aspect is to modify their structure at a small scale, namely, changing the shape of the nanomaterial photocatalysts. This can make them have a larger surface area, be flatter, and have more active sites for chemical reactions. According to their confinement situation, nanomaterials can be classified into zero-dimensional, one-dimensional, two-dimensional, and three-dimensional nanomaterials.

The 0-D materials are those in which electron movement is restricted in all three directions. In the 1- and 2-D nanomaterials, the same is confined in two and one dimensions, respectively 3-D; there is no confinement in any dimension; hence, electrons can freely move in all three dimensions. These materials maintain their energy bands, similar to bulk materials, but can still exhibit unique properties arising from their nanostructured features: 3-D structures, hierarchical frameworks, porous architectures, and interconnected networks [51]. **Figure** 4 from [51] shows that the 0-D materials are the nanoparticles/quantum dots, whereas the 1- and 2-D materials correspond to the wires/rods and nanosheets.

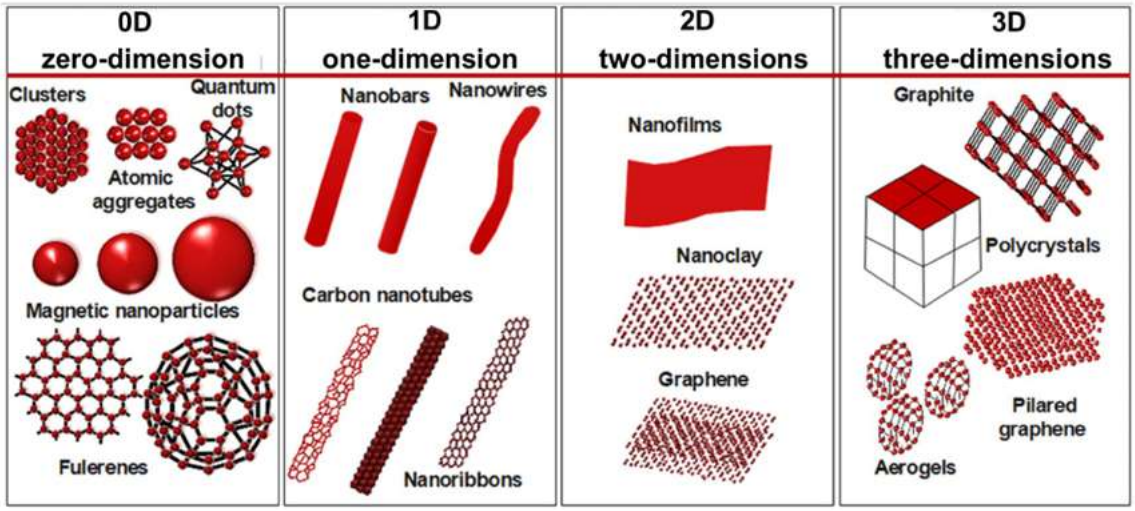

Figure 4: Schematic illustration of dimensional nanostructures of photocatalysts [51].

2.5.4.1 Zero-Dimensional Photocatalysts Nanoparticles

Zero-dimensional nanoparticles are materials whose dimensions fall in the nanoscale range, generally below 100 nm in size. Their properties are unique primarily because of their small scale and excellent surface-to-volume ratio. Examples of 0D NPs include quantum dots, fullerenes, and some kinds of metal or metal oxide nanoparticles. These would be spherical or near-spherical, isolated particles rather than extended objects [50]

Ba-Abbad *et al.* [52] used the sol-gel method to synthesise ZnO nanoparticles and produced spherical morphologies by optimising the process parameters using the D-optimal design method. They studied several variables, such as precursor concentration, pH, and reaction temperature, to control the size and morphological features of the nanoparticles. In another study, Kajbafvala *et al.* [53] prepared ZnO nanostructures with spherical and flower-like geometries using a microwave-assisted method by varying the heating rate of the solution, as shown in **Figure** 5. Then, the photocatalytic activity of the ZnO nanostructures

was determined using methylene blue (MB) as an organic dye under UV light irradiation. After four hours of UV irradiation, the spherical and flower-like ZnO nanostructures degraded MB by 78% and 17%, respectively.

The enhanced activity obtained in the spherical ZnO particles is due to their higher specific surface area of 98 m^2/g compared with flower-like ZnO morphology, which possesses a specific surface area of 22.9 m^2/g. Additionally, Peter et al. reported that the large surface area favours high adsorption rates. In contrast, the quantum confinement of photoinduced carriers leads to low recombination that enhances the photocatalytic activity of ZnO dots compared with its three different morphologies: ZnO flakes, rods, and dots.

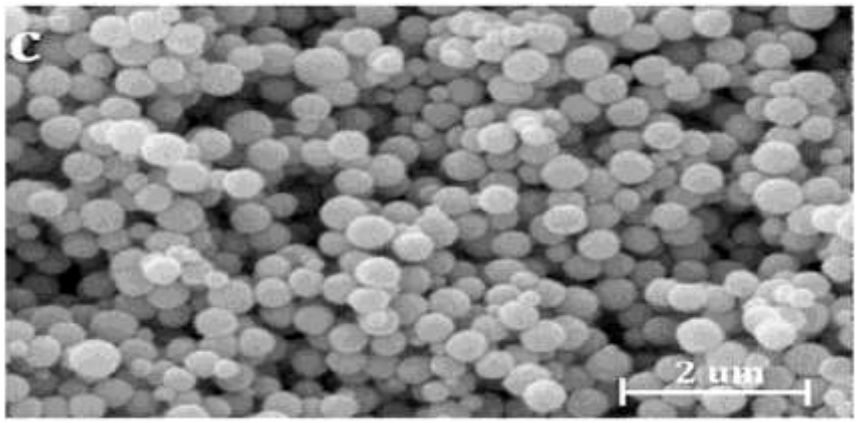

Figure 5: SEM image of ZnO NPs at Zero-Dimensional [53].

2.5.4.2 One-Dimensional Photocatalysts Nanoparticles

One-dimensional (1D) nanoparticles, such as ZnO nanowires and NiO nanorods, are nanostructures with much larger length than the width and height, exhibiting rod-like or wire-like shapes. They have large aspect ratios; due to quantum confinement effects, they exhibit unique properties and are promising for various applications in sensing, photodetection, and field emission [50].

Ezhilarasi and co-workers [54] investigated the biosynthesis of nickel oxide nanorods (NiO NRs) using Phoenix dactylifera extract as a green reducing agent and a capping agent. The biosynthesised NiO NRs showed a crystalline face-centred cubic (FCC) structure; TEM analysis revealed rod-shaped nanostructures with an average diameter of 32 ± 5 nm, showing high dispersion and less agglomeration, as shown in Figure 6. The optical band gap of 3.62 eV promised enhanced light absorption and photocatalytic activity, which demonstrated the degradation of 4-chlorophenol. It is cytotoxic, causing oxidative stress for

bacterial damage and death. The ability of NiO NRs to induce reactive oxygen species (ROS) and good antibacterial action. These findings indicate an eco-friendly synthesis approach for multifunctional NiO NR applications in photocatalysis, biomedicine, and Environmental remediation.

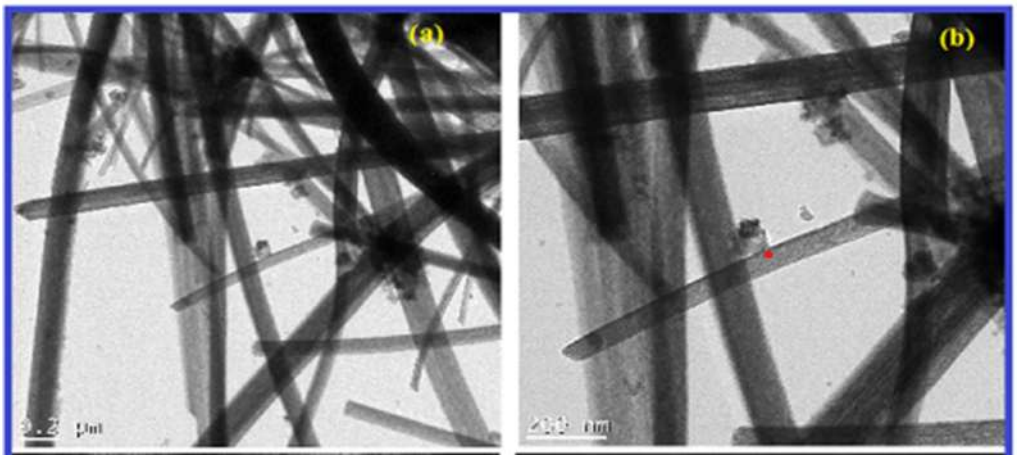

Figure 6: TEM images of ZnO NPs at One-Dimensional [54].

2.5.4.3 Two-Dimensional Photocatalysts Nanoparticles

All 2D nanomaterials have atomic-scale thickness and large surface areas in various morphologies, including sheets, ribbons, flakes, plates, and wrinkled or rippled surfaces. Various morphologies in different forms provide such nanomaterials with unique electrical, thermal, and mechanical properties, increasing their value for applications such as flexible electronics, sensors, and photocatalysts. Since their morphology is tenable, optimisation against a particular technological development is important in nanotechnology [50].

Moghaddas SM and co-workers [55] synthesised ZnO nanosheets through a hydrothermal method; the resulting structures had a reasonably uniform distribution with an average thickness of about 75 nm. Morphological examination, further supported by FESEM observation (**Figure** 7), showed that the nanosheets, although on the nanometer scale, were slightly agglomerated. X-ray diffraction patterns confirmed the tetragonal structure of ZnO without any extra peaks, which suggests high purity. EDX analysis also confirmed this further, as the weight percentages of oxygen and zinc were 27.12% and 72.88%, respectively. UV-vis spectrophotometry analysis showed the photocatalytic characteristics of the produced ZnO nanosheets. A distinct absorption peak at around 384

nm was associated with a bandgap energy of 3.29 eV, indicating that the nanosheets can promote electrons jumping from the VB to the CB, an important factor for their photocatalytic efficacy.

Further, the photocatalytic activity of the ZnO nanosheets was evaluated by examining their ability to degrade dye in the presence of ultraviolet light (UV). The results showed that the degradation of the dye was highly enhanced under UV irradiation compared to the case in the dark, which indicates the predominance of the photocatalytic degradation process over mere adsorption. It involves the excitation of electrons that generate highly oxidising cavities and hydroxyl radicals, which can decompose the pollutants into harmless substances such as water and carbon dioxide. These findings underpin the potential applications of ZnO nanosheets in environmental remediation, specifically in degrading organic pollutants and dyes. Their high surface area and effective photocatalytic properties make them promising candidates for water treatment and purification.

Wang J *et al.* [56] have taken up a comprehensive study on the diverse properties, including dimensions, morphology, band gap energy, and applications, of Ag/ZnO nanosheet (NS) arrays. Scanning electron microscopy (SEM) images in **Figure** 7 showed that ZnO NSs, without silver nanoparticle (NP) decoration, are densely covered with vertically oriented structures. When decorated with Ag NPs, these NSs showed good adhesion of Ag, especially at the edges, with an average Ag NP diameter of about 120 nm. The XPS and XRD analyses confirmed the existence of metallic Ag NPs and a hexagonal wurtzite structure of ZnO. The optical properties of the Ag/ZnO NSs were characterised by PL and UV-vis spectroscopy.

PL spectra revealed two emission peaks at 373 and 550 nm, respectively, assigned to near-band edge and deep-level emissions. As confirmed by the interaction, the effective charge transfer between ZnO and Ag NPs resulted in a decreased recombination rate and PL intensity. UV-vis absorption spectroscopy showed an extra absorption peak at 430 nm, which points out the localised surface plasmon resonance (LSPR) effect of Ag NPs and dramatically improves the optical properties of the NSs. These Ag/ZnO NSs showed excellent surface-enhanced Raman scattering (SERS) ability, which is promising for chemical sensing and environmental monitoring applications. The improved SERS performance mechanism is ascribed to the LSPR effect of Ag NPs and the resonant cavity

effect generated by ZnO arrays. In addition, the charge transfer between Ag NPs, ZnO, and probe molecules such as crystal violet (CV) further amplifies the SERS signals.

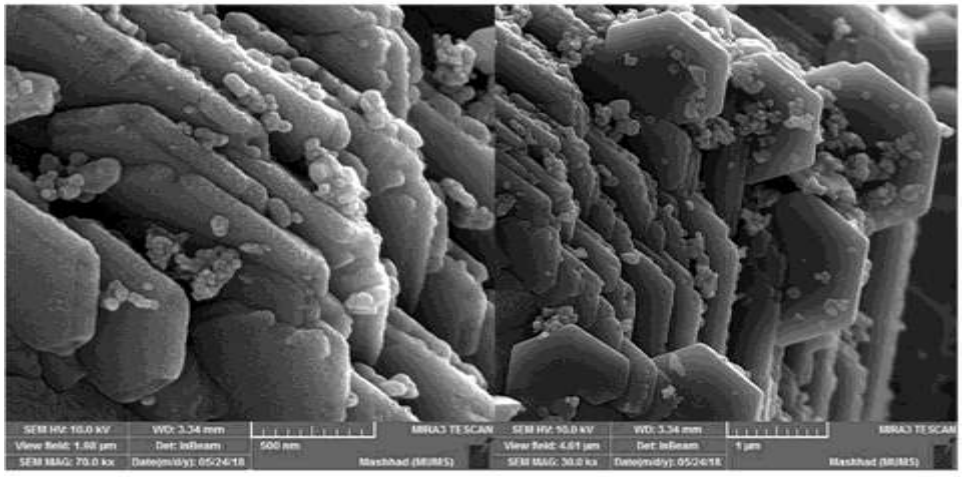

Figure 7: FESEM images of ZnO nanosheet at different magnifications [56].

The unique combination of features, including size, morphology, band gap energy, and excellent optical properties, makes Ag/ZnO nanostructures potentially useful for a variety of applications, including photocatalysis, chemical sensing, and environmental remediation.

2.5.4.4 Three-Dimensional Photocatalysts Nanoparticles

The 3D nanomaterials, by definition, have extended structures in all three dimensions. Usually, many 0D nanoparticles or any other nanostructures are aggregated to form the bulk material. One fantastic example of a 3D nanomaterial is nanoflowers. They represent hierarchical structures that appear flower-like on the nanoscale and are generally made of metals, oxides, or carbon compounds [50].

Khedkar *et al.* [57] prepared three-dimensional (3D) Ag-NiO nanocomposites (NC) and uncoated NiO nanoparticles. The latter belonged to a face-centred cubic lattice structure whose peaks represented specific crystal planes. At the same time, Ag-NiO NCs provided additional peaks ascribed to Ag, proving both materials' crystalline nature. The NiO nanostructures depicted a hexagonal morphology with an average size of ~86 nm, and Ag NPs were well dispersed in the NiO matrix with an average size of ~54 nm. The optical properties showed band gap values of 3.60 eV for NiO and 3.47 eV for Ag-NiO NC. These

Ag-NiO nanocomposites showed higher photocatalytic activity, degrading 94% of methylene blue (MB) in 288 seconds, compared to the 93% degradation displayed by pristine NiO in 648 seconds. The interfacial electronic interactions between Ag and NiO enhanced the photocatalytic activity of the Ag-NiO nanocomposites.

Ferreira RM *et al.* [58] report that a high-surface-to-volume ratio, nickel-based hierarchical material was synthesised through a simple, scalable, and low-cost hydrothermal method. The procedure allowed obtaining gram-scale NiO nanoflowers with very well-defined geometries, uniform sizes, ca. 15 ± 8 nm thick, and diameters more significant than one μm. SEM images (**Figure** 8) showed the detailed morphology, and TEM and HRTEM images confirmed the nanoflowers' self-assembly growth mechanism and polycrystalline nature. The Rietveld refinement method proved the pure NiO phase with high crystallinity. Electrochemical tests demonstrated that these nanoflowers provided improved electron transfer and sensitivity, showing high efficiency in applications such as hydrazine detection in electrochemical sensors. The high activity is attributed to the enhanced active sites, large specific surface area, and efficient electron transfer properties of the nanoflowers.

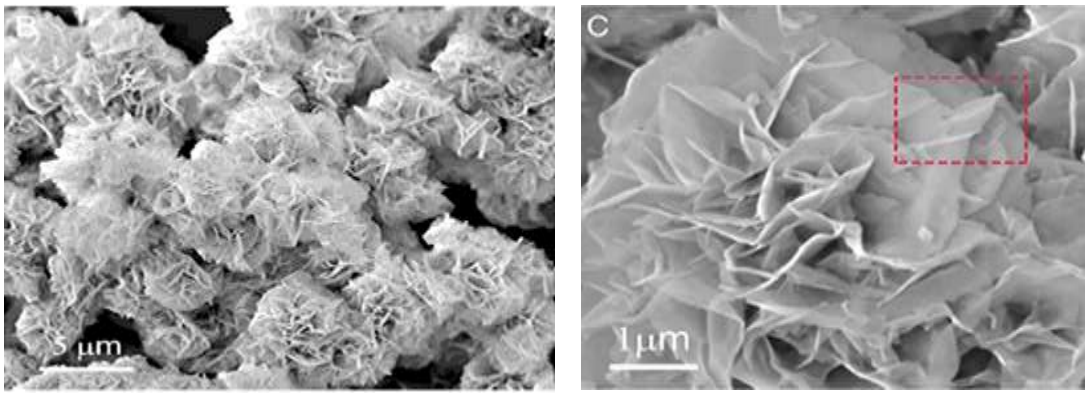

Figure 8: SEM images of NiO NPs at different magnifications [58].

2.5.5 Synthesis Strategies of Photocatalysts Nanoparticles

The two unique methodologies for combining NPs are top-down and bottom-up, as shown in **Figure** 9 from [59]. Top-down using various techniques such as grinding, milling and sputtering or thermal/laser ablation. The suitable bulk material is broken down into smaller, fine particles by size reduction. Meanwhile, bottom-to-top NPs are formatted by chemical and biological methods through the self-assembly of atoms into new nuclei that grow into particles of nano size. Among these methods are electrochemical and chemical

reduction approaches. Each of these mechanisms converts one of the physical factors, such as thermolysis changes in temperature, ball friction pressure, ion implantation pH, and laser ablation radiation changes.

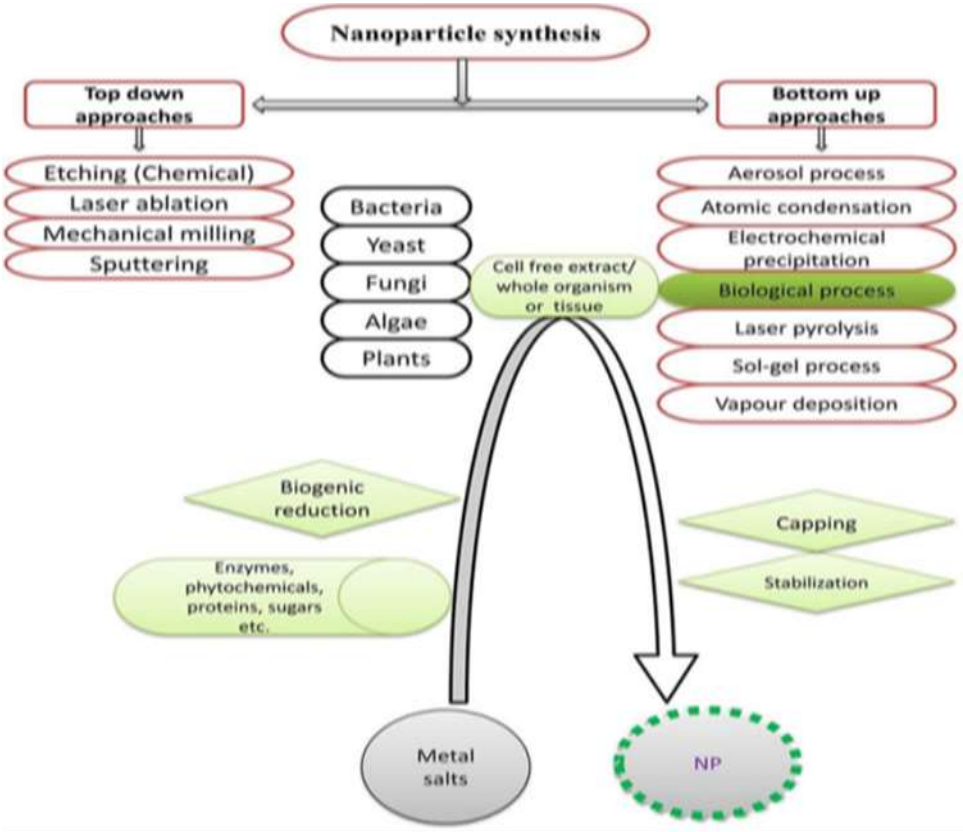

Figure 9: Photocatalysts NPs synthesis methodologies [59].

Optimisation and maintenance of optimised parameters are essential to investigate nanoparticles' desired shape and size (NPs). However, most physical techniques have drawbacks, such as time-consuming processes, high operational parameters, expensive equipment, and pollution from milling media and/or the atmosphere. These methods can also consolidate the powder product without maintaining the nanocrystalline microstructure, and recycling and disposal of nanomaterials lack established safe policies. Moreover, physical approaches are also considered harmful to the environment because of the toxicity involved.

Chemical synthesis, on the other hand, can synthesise bulk amounts of nanoparticles very quickly. Some of the methods under this approach include co-precipitation, sol-gel processing, radiofrequency plasma method, solvothermal synthesis, and chemical vapour

deposition. The techniques employed use potent reducing agents to reduce nanoparticles and capping agents to control the size and stabilise the formed nanoparticles, like oleic acid, thioglycerol, and triethanolamine. Nonetheless, this technique employs hazardous chemicals that can be dangerous to biological entities [59,60].

The fabrication of nanoparticles may be carried out by three major approaches: physical, chemical, and green approaches. Physical approaches include physical vapour deposition (PVD), thermolysis, microwave-assisted synthesis, pulsed laser methods, high-energy ball milling, laser ablation, melt mixing, ion implantation, electric arc deposition, and sputter deposition. These methods change physical parameters such as temperature, pressure, pH, and radiation. However, most physical methods involve more extended periods, higher costs, and even environmental hazards due to pollution and the release of dangerous waste material. The synthesised nanoparticles usually exhibit a significant distribution in size and shape resulting from the special procedure and parameter conditions [61,62].

The green synthesis of nanoparticles has certain advantages over conventional methods. It is an eco-friendly approach in which natural resources like plant extracts can be used. The plant-mediated synthesis of nanoparticles is a cost-effective technique that employs the natural chemical reactions of plants to synthesise nanoparticles at room temperature and neutral pH [56,59].

Figure 10 shows that the green chemistry route uses plant extracts as reducing and stabilising agents and can be scaled up for green industrial manufacturing. It is biocompatible, scalable, and suitable for biomedical applications since most plant phytochemicals can manipulate nanoparticle properties. Some leading plants utilised include *Neem* and *Moringa oleifera*, indicating the method's potential in reducing the environmental footprint and producing highly useful nanomaterials. Shown are methods of plant-mediated synthesis of nanoparticles. The prepared plant extracts' phytochemicals (proteins, enzymes, polysaccharides, vitamins, carbohydrates, amino acids, and organic acids) reduce the metal ions to their elemental form, leading to nucleation and growth of nanoparticles. The phytochemicals stabilise these nanoparticles to prevent aggregation. The nano-size and morphology of the nanoparticles can be controlled by adjusting factors such as concentration, pH, temperature, and reaction time, avoiding the use of hazardous chemicals altogether [63].

Green synthesis is cost-effective, energy-efficient, and can be achieved through a single-step, one-pot, biocompatible method. It is also highly suitable for large-scale production. It also ensures human health safety and reduces environmental impact by avoiding toxic waste and pollution. Besides, nanoparticles synthesised by the green synthesis method exhibit better biocompatibility and stability, making them applicable in medicine, agriculture, and environmental remediation. **Table** 1 summarises the comparative study of different synthesis methods, including the starting materials used and the properties of the nanoparticles formed [60,63].

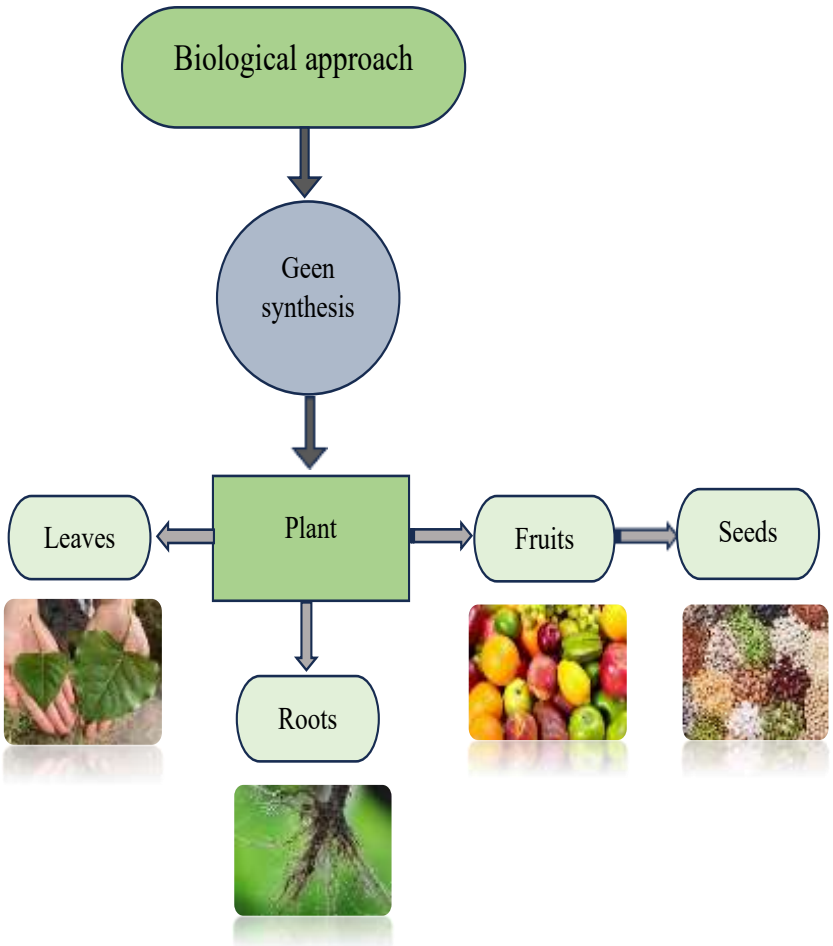

Figure 10: Various methods of plant-mediated synthesis of nanoparticles.

Table 1: Comparison between various synthesis methods of prepared nanoparticles.

photocatalyst	Method	Starting materials	Size (nm)	Morphology	Ref
ZnO	Sol-gel	zinc acetate dihydrate, oxalic acid dihydrate, ammonia, hydrochloric acid, absolute ethanol	20	Spherical	[52]
ZnO	Electrochemical	Zn electrode, oxalic acid dihydrate, potassium chloride, sodium hydroxide and nitric acid	50-100 150-200	Spherical & Cylindrical	[64]
ZnO	Microwave & hydrothermal	Zinc nitrate hexahydrate, zinc acetate dehydrate, hydrazine hydrate and ammonia	50-150	Needle & flower	[65]
Ag-ZnO	Microwave & hydrothermal	zinc acetate dihydrate, carbinol, silver nitrate, sodium borohydride,	30-40	Spike	[66]
Ag-ZnO	Green	*Ginger* oil, zinc acetate dihydrate, silver nitrate	/	Nanorod	[67]
NiO	Green	Nickel (II) nitrate, *Senna auriculata flower*	20	Quasi-spherical	[68]
Ag-NiO	sol-gel	Nickel nitrate hexahydrate, anhydrous citric acid, sodium hydroxide, sodium borohydride	15-20	Spherical	[69]

2.5.6 Applications of Pure and Doping Photocatalyst Nanoparticles

Photocatalyst nanomaterials, such as pure nickel oxide (NiO) and zinc oxide (ZnO) nanoparticles, are highly useful in energy and the environment. Pure NiO has been appreciated for its stability, low toxicity, and eco-friendliness, thus making it suitable for application in gas sensors and electrochemical devices.

On the other hand, Pure ZnO shows vigorous oxidative activity and stability under ultraviolet light, which is beneficial for UV protection, antibacterial coating, and water purification. In the case of NiO or ZnO, foreign atom doping can significantly enhance photocatalytic activity [66,70].

For example, the visible-light absorption and photocatalytic performance are improved by doping NiO, thus showing better environmental remediation and hydrogen production. Similarly, doping of ZnO with metals or non-metals enhances charge separation. It inhibits electron-hole recombination, thereby increasing its efficiency toward the degradation of organic contaminants and treatment of wastewater [70,71,72].

- **Environmental Remediation:** Decomposition of Toxic Pollutants.
- **Photocatalytic CO_2 Reduction.**
- **H_2 Production via Water Splitting.**
- **Photocatalytic Disinfection of Bacterial Species.**

Using plant extracts, Noorullah and Zainab [71] prepared eco-friendly silver-zinc oxide (Ag-ZnO) nanocomposites. It shows the benefits of using plant extracts, like their easy availability and low toxicity, instead of traditional chemical methods. The present study also discusses the efficiency of the prepared nanocomposites as photocatalysts and their potential use in environmental cleaning. Photocatalytic activity percentages are reported to be 86% and 21% for *Aloe vera* and *Hibiscus sabdariffa*, respectively, for the degradation of Methylene Blue (MB) dye. All these findings demonstrate that the prepared Ag/ZnO nanocomposite is an efficient photocatalyst, especially when combined with Aloe vera extract.

Rani *et al.* [73] synthesised flake-shaped ZnO nanoparticles (NPs) using a green and sustainable method using Azadirachta indica fruit peel extract. The fruit peel extract served as a natural reducing and stabilising agent, enabling the formation of ZnO NPs with a hexagonal wurtzite crystalline structure. Additionally, the ZnO NPs demonstrated excellent photocatalytic activity, with degradation efficiency of 88.53% for methylene blue and 83.08% for rhodamine B dye for 240 min under sunlight irradiation. Moreover, the ZnO NPs also demonstrated effective antibacterial activity against *Escherichia coli,*

Pseudomonas aeruginosa, Staphylococcus aureus, and *Streptococcus pneumoniae*, with MIC values of 140 µg/mL, 135 µg/mL, 130 µg/mL, and 130 µg/mL, respectively. Furthermore, the ZnO NPs also exhibited excellent supercapacitor performance with a specific capacitance value of 794.96 F/g and energy density of 22.34 Wh/kg at 5 mV/s. This research will elucidate the encouraging capabilities of *Azadirachta indica fruit peel* extract in the green synthesis of ZnO nanoparticles for various applications in antibacterial activity, energy storage, and photocatalytic processes.

Al-Zaqri *et al.* [68] green synthesised NiO nanoparticles using flower extract from *S. auriculata*, which resulted in the removal of MB dye to over 97% under UV light irradiation for as long as 90 min. Due to an electron relay effect, biosynthesized NiO NPs would represent efficient redox photocatalysts. This increases the reduction rate by increasing the rate of electron relay transfer within donor-acceptor molecules. The critical feature is the size of the metal oxide nanoparticles, as a decrease in the particle size-to-surface area increases the catalyst's effectiveness many-fold. NiO NP's antibacterial activity was studied against microorganisms like *S. aureus*, *B. subtilis*, *P. aeruginosa*, and *E. coli*, giving inhibition zones in the 20-23 mm range. These findings underpin the potential of natural resources in the sustainable synthesis of nanoparticles, with applications both in environmental remediation and as antibacterial treatments.

Yadav *et al*. [74] prepared Ag-doped ZnO NPs by using turmeric root extract as a reducing agent of Ag^{+}. The photocatalytic water splitting to hydrogen production in the presence of Ag/ZnO NPs was carried out in a 20 mL quartz glass reactor equipped with a closed gas-circulating system. The catalyst 8 mg was sonicated in the solution of water and ethanol 6 mL and 2 mL, respectively, for 30 min with deaerating by argon/nitrogen bubbling for 10-15 min and measured by gas chromatography under room temperature 25°C. A water-ethanol system has been used in the study for the photocatalytic H2 evolution activity of the Ag/ZnO NPs calcined at 400°C for three h. The amount of hydrogen gas generated was plotted as a function of UV exposure time, and it was found that 214 mmol/g·h of H_2 was produced after 2.5 hours of UV exposure. Hydrogen gas generation ceased when the UV light was turned off, which confirmed that UV irradiation drove the gas evolution. Thus, Ag/ZnO NPs were highly effective photocatalysts for hydrogen generation from water-splitting reactions.

Singh *et al.* [75] synthesised NiO NPs using a cell-free extract of filamentous green macroalgae Spirogyra sp., which is well documented to contain polyols, amines, and carbonyl compounds. Then, the synthesised material was assessed for some biological applications. Thus, 50% of the target activity is inhibited at an inhibitory concentration of 10 milligrams per litre (IC50:10 mg L^{-1}). NiO NPs have antibacterial activity against *Bacillus subtilis*, and *Escherichia coli* bacterial strains were found to be 10 mg/L. Showing dose-dependent activities, NiO NPs have MICs at 10 mg/L. At low doses, for instance, 5 mg/L, NPs stimulate the growth of the root and shoot by about 15%. The same Nanoparticles, at high concentrations, such as 45 mg/L, delay the seed germination of Mung Bean inhabitation and their seeding development. Moreover, the NiO NPs showed evident antioxidant activities by DPPH and TAC assays. They concluded that green biosynthesised NiO NPs possess reliable in vitro biochemical properties for applications in both biomedical and agricultural industries.

Rajalakshmi *et al.* [76] synthesised pure and different concentrations, viz. 2%, 5%, 10%, and 15% of the silver-doped Nio nanoparticles, using a green synthesis method in an aqueous flower extract of *Moringa oleifera Lam*. The flower extract of MO contains several bioactive constituents that can be used with strong reducing, stabilising, and capping agents to prepare pure and Ag: NiO NPs. The antibacterial and antifungal activity of biosynthesised pure and silver-doped NiO nanoparticles was evaluated using Agar-well diffusion methods. The antibacterial and antifungal activity of pure NiO and Ag-doped NiO nanoparticles was synthesised using *Moringa oleifera* flower extract as a reducing agent against Ag variation (2%, 5%, 10%, 15%).

The synthesised nanoparticles were screened against Gram-positive bacteria, such as *Staphylococcus aureus* and *Bacillus cereus*, Gram-negative bacteria, such as *Salmonella typhimurium*, *Escherichia coli*, *Klebsiella pneumonia*, and *Pseudomonas aeruginosa*, and the fungal strain *Candida albicans*. The zone of inhibition studies indicated that Ag-doped NiO nanoparticles exhibited enhanced antimicrobial activities compared to pure NiO and showed maximum activity at 15% doping of Ag. The smaller particle size of the nanoparticles contributed to their increased antimicrobial activity. It was concluded that Ag-doped NiO nanoparticles exhibit superior antibacterial and antifungal activities, with higher efficacy against bacterial strains than fungal strains.

Besides the above-mentioned studies, Table 2 comparatively presents related research on applying pure and photocatalysts doping with silver NPs synthesised by green approaches and their photocatalytic efficiency in Photocatalytic degradation of Organic Pollutants.

Table 1: Summarise some studies on applying pure and doping photocatalysts with silver NPs synthesised by green approaches.

photocatalyst	Plant Scientific name	Size/shape	Light source	Pollutant	E %	R
ZnO NPs	*Moringa Oleifera*	52 nm/spherical	Sunlight/180 min	Titan yellow Congo red	96% 97%	[77]
ZnO NPs	*Hagenia abyssinica*	27.8 nm/hexagonal	Sunlight/120 min	MO	83%	[78]
ZnO NPs	*Calliandra haematocephala*	19.45 nm/nanoflower	Sunlight/270 min	MB	88%	[79]
ZnO NPs	*Monsonia burkeana*	20 nm/hexagonal	UV/48 min	MB	48%	[80]
ZnO NPs	*Commelina benghanlensis* 10g *Commelina benghanlensis* 20g *Commelina benghanlensis* 30g	60-80 nm /Flaky 8-12 nm/Spherical 8-10 nm/Spherical	UV/120 min UV/120 min UV/120 min	MB MB MB	55% M 55% 81%	[81]
Ag-ZnO NPs	*Prunus cerasifera* + 1.6%Ag^{+} *Prunus cerasifera* + 1.8%Ag^{+} *Prunus cerasifera* + 2.0%Ag^{+}	82.46 – 101.98 nm/ spherical 72.11 – 128.06 nm/linear 72.11-100 nm/irregular	Sunlight/35 min Sunlight/20 min - -	RB OS - -	85.52 74.11 - -	[82]
ZnO NPs **Ag-ZnO NPs**	*Crataegus monogyna*	30-35 nm/spherical 55-70 nm/spherical	UV/90 min UV/90 min Sunlight/90 min Sunlight/90 min UV/90 min UV/90 min Sunlight/90 min Sunlight/90 min	MO BV10 MO BV10 MO BV10 MO BV10	80.1% 82.2% 67.4% 76.5% 89.8% 94.2% 75.3% 84.7%	[83]
NiO NPs	*Azadirachta indica (neem)*	10.5 nm/cubic	Sunlight/30 min	MB	72.6%	[84]
NiO NPs	*Calotropis gigantea latex*	28 nm/hexahedral	Sunlight/30 min	nitro phenol CR	95% 94%	[85]
NiO NPs	starch powder	28.6 nm/spherical	UV/270 min	MB	80%	[86]
NiO NPs **Ag-NiO NPs**	*Aloe Vera* gel *Aloe Vera* gel + Ag^{+}6%	Irregular flaky 20 nm/Irregular flaky	UV/120 min UV/120 min	FB FB	62.9% 98%	[87]

2.5.7 Sunlight-Driven Photocatalysts

Optimised for sunlight activation, metal oxide semiconductors quickly become efficient photocatalysts for environmental remediation. Modifying the bandgap or introducing dopants can enhance their ability to absorb a more significant fraction of the solar spectrum, thus improving sunlight utilisation for catalytic processes. Under sunlight, these photocatalysts generate highly reactive species; Hydroxyl radicals (·OH) and superoxide anions ($\cdot O_2^-$) play a key role in degrading organic chemicals in aquatic matrices. The long-term stability offered by these compounds in water mediums ensures sustainable existence, and their ability to work even without any external energy source exhibits their eco-friendly character [18,54,88]. These substances are also often inexpensive, simple to fabricate, and non-polluting, making them apt for extensive water treatment and pollution control. They can efficiently harvest solar energy and are considered critical solutions to environmental challenges on a sustainable and renewable basis [89].

The following factors affect the photocatalytic activity of photocatalysts:

- **Dye concentrations**: The dye concentration is critical for how the photocatalytic reaction proceeds. The amount of catalyst must, on average, degrade an appropriate level of dye, and some of the dye must adhere to the catalyst's surface to be exposed for absorption. The second effect under stimulated light, from the former's original concentration, is proportional; hence, the original dye concentration must be determined. Typically, the quantitative requirement of the photocatalyst increases with a higher dye concentration; however, the percentage degradation decreases.

- **Amount of catalysts**: The quantity of catalysts in a photocatalytic process primarily affects dye degradation. Increasing the number of photocatalysts can increase the percentage of photodegradation in a heterogeneous photocatalytic process. This increase makes more active sites within the reaction available, producing more reactive radicals required for photodegradation.

- **pH**: pH of the solution also plays a critical role in the entire process of degradation and may facilitate or retard the photocatalytic reaction based on the nature of the material and the pollutant. By changing the surface charge, solution pH may control the adsorption on the catalysts' surfaces, more so metal oxide nanoparticles. The tuning

behaviour of adsorption may affect the degradation rate significantly. Under acidic conditions, it can increase the positive charge on the catalyst's surface, favouring the adsorption of negatively charged pollutants and, therefore, the photodegradation rate. Oppositely, a fundamental solution could enhance a negative charge on its surface, which is further used to enhance or reduce the adsorption of various types of pollutants, affecting the overall efficiency of the photodegradation treatment process. Thus, pH should be carefully controlled and maintained to optimise the photocatalytic degradation efficiency.

- **Surface morphology**: Some parameters of surface morphology, such as particle size and shape, are very important for photodegradation. Each structural morphology provides a more direct pathway between the photocatalyst surface and the organic contaminant. The speed of photocatalytic reactions can be modified by the number of photons that strike the photocatalyst surface; different morphologies may vastly increase the speed of the reactions.

  There are some advantages of different morphological types:

  - Nanoparticles provide a large surface area for pollutant adsorption, which improves degradation efficiency.

  - Nanorods and nanowires improve the charge transport property, helping to reduce the recombination rate of the electron-hole pair.

  The unique two-dimensional structure of nanosheets allows appropriate light absorption and pollutant contact. Besides, a nanoparticle's size has remarkable effects on its photocatalytic activity. Smaller particles have increased surface area to volume and will have relatively more active sites for the reaction. Such an increase in active sites increases the interaction of catalysts with a pollutant and boosts the rate of the photodegradation process.
- **Irradiation time and intensity of the light**: the photodegradation of the contaminant is highly intensified by the intensity of the incident light and exposure time. At low light intensity levels, the photodegradation rate is high due to increased exciton (electron-hole pairs) formation yield, which reduces the same pairs' recollection. This, in turn, increases the number of reactive species that could effectively degrade pollutants. On the other hand, under higher light intensities and above, a negative proportion of the

percentage of photodegradation to light intensity is obtained. This is because the increase in light intensity shows more recombination rates for the electron-hole pairs, decreasing both the catalytic activity and the efficiency of the photodegradation process. More importantly, irradiation time is another variable that affects photodegradation efficiency [90,91,92].

More extended irradiation periods give more time for forming reactive species, therefore intensifying the utilisation of pollutants. However, the amount of irradiation is not beyond a limit that optimises photodegradation, with no considerable additional irradiation inducing enhanced photodegradation because of the saturation of reactive sites onto the photocatalyst. In another study, Malato *et al.* [93] proved that the ideal light intensity and irradiation time should be attained to enhance photodegradation efficiency. Chatterjee and Dasgupta [94] also reported that the balance between light intensity and exposure time is essential in reducing the adverse effects of increased electron-hole recombination.

- **Surface Dopants on the Dye Degradation**: Many methods of synthesising ZnO and NiO nanomaterials can absorb those photons even at relatively minimal energy levels. This can be done by band gap engineering by incorporating both metals and non-metals into photocatalytic materials to change and keep alternating the valence and conduction bands. Transition metal doping, for example, with Fe, Cr, and V, was reported to successfully decrease the band gap and enhance the ability of the material to absorb visible light effectively. Non-metal impurity doping with nitrogen, carbon, and sulphur is also an important factor in diversifying the light response of the ZnO and NiO photocatalysts using the mid-band states to enable visible light absorption [90].

  Surface modification may also be reached when ZnO and NiO are combined with organic molecules and other semiconductors. For instance, the attachment of organic dyes on either ZnO or NiO surfaces should enhance their absorption range. Embedding ZnO and NiO with other semiconductors, such as CdS, TiO_2, and WO_3, is also expected to improve the overall photocatalytic activity due to charge separation and reduction of electron/hole recombination [44,95].

  These changes would enable increased light absorption, but they would also produce reactive oxygen species, which are also used in the chemical degradation of the dye and other contaminants.

2.5.8 Characterisation Methods of Photocatalysts Nanoparticles

2.5.8.1 Transmission Electron Microscopy (TEM)

Transmission electron microscopy (TEM) is a method that uses an electron beam to study and analyse specimens to obtain detailed information about the size of nanoparticles and their interior makeup. On the other hand, scanning electron microscopy (SEM) looks at the surface of samples to assess characteristics. TEM allows for the penetration of samples to obtain details on internal characteristics. In TEM, thermal emission heats an electron source, typically from a filament, most commonly fabricated from tungsten. It is sensitive to an accelerating voltage of 60 to 100 kilovolts (kV). The user can manage this accelerated electron energy according to the analysis requirements. The electron beam passes along the vacuum column in the microscope, which is then focused by a series of electromagnetic gradients or lenses inside the column. In conjunction with control apertures located across the column, these lenses control the electron beam width and degree of focus by preventing unwanted electrons, thus ensuring that an accurate and coherent beam reaches the sample [96]. When the electron beam eventually hits the sample, several different events take place. The effective beam, thus, passes through the sample without deflection, while the rest is scattered or absorbed by the constituent atoms within the sample being probed. The image is then formed on a fluorescent screen, showing areas of the sample as shades of grey as the electron distribution varies at different points, as shown in **Figure** 11 from [97].

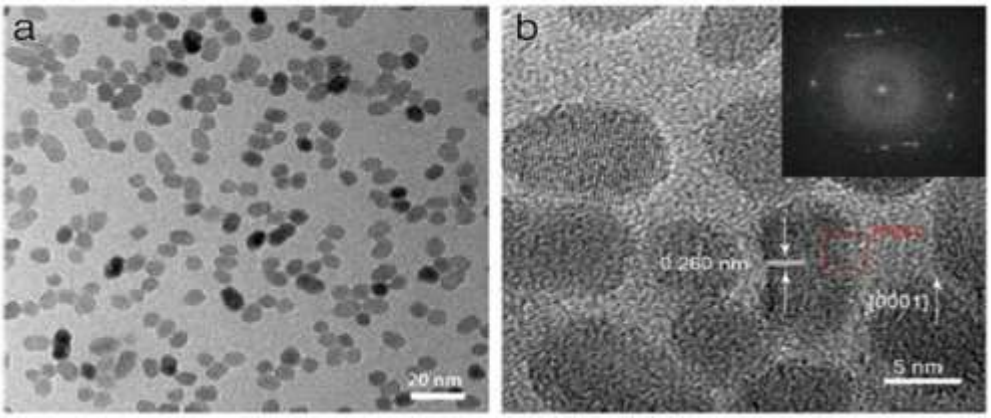

Figure 11: Transmission electron microscopy images of ZnO NPs [97].

Dark regions indicate the area of the microscope into which electrons have been absorbed or highly scattered—the denser or heavier the atomic regions—while bright

regions indicate minimal electron absorption or scattering, showing lighter atomic elements [97].

2.5.8.2 Field Emission Scanning Electron Microscopy (FESEM)

Field Emission Scanning Electron Microscopy is a very sophisticated imaging method that employs a field emission gun (FEG) for generating an electron beam of very high coherence and focus, enabling imaging of materials at very high resolutions, typically at the nanometre or sub-nanometre level. This technique is particularly effective for observing various materials' surface morphology and topography at higher resolution than conventional Scanning Electron Microscopes (SEM) [97]. FESEM finds typical applications in nanotechnology, material science, biology, and the semiconductor industry, where surface details of finer features must be analysed.

One of FESEM's advantages is that it can image the delicate structures of conductive and non-conductive materials with little sample preparation. Compared to traditional SEM, FESEM employs a lower accelerating voltage, with less sample damage and electron beam penetration, and is best suited to image weak or soft materials. The FESEM's high resolution enables researchers to study the morphology of nano-scale structures such as thin films, nanoparticles, and individual nanostructures and obtain valuable information regarding their properties and behaviour [98].

2.5.8.3 Fourier Transform Infrared (FTIR) Spectrometry

Fourier Transform Infrared (FTIR) spectrometry is among the most prevalent analysis techniques used in the characterisation of photocatalysts, especially those metal oxide nanoparticles like nickel oxide (NiO) and zinc oxide (ZnO). The method gives information regarding the functional groups via metal-oxygen bond vibration and the surface chemistry of materials. FTIR spectra typically exhibit characteristic absorption peaks for metal-oxygen vibrations that identify the type of metal oxide. Zn-O stretching vibration, for example, is typically observed between 400–600 cm^{-1}, as shown in **Figure** 12. At the same time, Ni-O vibrations are also observed within the same range, allowing their differentiation and identification [97,98].

FTIR can also detect surface modifications, adsorbed species, or organic impurities, which are very important in establishing the photocatalyst properties of such materials [84,66,124]. FTIR is an important method in photocatalysis studies and nanoparticle research.

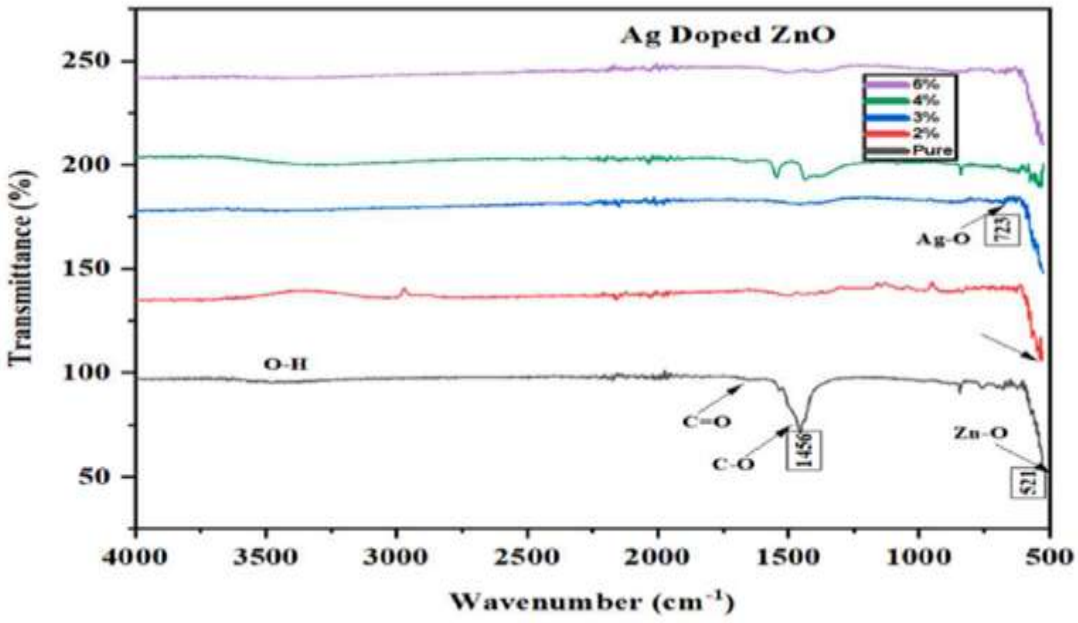

Figure 12: FTIR Spectra of Pure and ZnO NPs doping with silver [98].

2.5.8.4 Ultraviolet-visible (UV/Vis) Spectroscopy

Ultraviolet-visible (UV-vis) spectroscopy is a critical analytical method to monitor the photocatalytic degradation of organic contaminants by photocatalysts like ZnO and NiO NPs. Researchers can determine the efficacy of photocatalytic performance based on this method by monitoring the change in the absorption of contaminants at one wavelength with time following exposure to the light source. The absorbance of a contaminant, such as methylene blue (MB), rhodamine B (RhB), or methyl orange (MO), is typically determined before and after exposure to visible or UV light in the presence of the photocatalyst. ZnO nanoparticles, for example, also exhibit better photocatalytic activity due to their wide bandgap and high absorbance of UV light, enabling them to generate reactive oxygen species (ROS) that break down organic contaminants into more straightforward, less toxic molecules. Experiments have established that progressive diminishment of absorbance at a pollutant's characteristic wavelength ,e.g., 664 nm for methylene blue or 554 nm for rhodamine B, indicates its degradation in photocatalyst conditions. UV-vis spectroscopy also determines the reaction kinetics, e.g., the degradation rate constant, which provides

quantitative data on ZnO-based photocatalyst activity. This makes UV-vis spectroscopy essential in ascertaining the breakdown of pollutants and the rational development of photocatalyst materials for environmental cleanup [99,100].

2.5.8.5 UV-vis Diffuse Reflectance Spectroscopy (UV-vis DRS)

UV-vis Diffuse Reflectance Spectroscopy (UV-vis DRS) is among the most common techniques for identifying photocatalysts' band gap energy, mainly metal oxides such as ZnO and NiO NPs. An approximation of the optical band gap can be achieved using the Kubelka-Munk function to treat the reflectance spectrum of the solid sample. Native ZnO, with its expansive band gap energy (circa 3.2 eV), absorbs mainly in the UV region, limiting its activity under visible light. Some alterations, like doping or loading ZnO with transition metals (e.g., Ag, Cu, or Ni), significantly lower its band gap energy, enhancing its visibility in the visible light range.

UV-Vis DRS can compare the absorption edge of pure ZnO and modified ZnO in a manner that can quantify this increase. It has, for example, been shown that metal-doped ZnO results in a redshift of the absorption edge, which reveals a reduction of the band gap so that visible light can be utilised for photocatalysis. Such a reduction of the band gap is required to improve the photocatalytic activity of ZnO, which can be used in environmental purification applications and solar energy conversion, for example. It renders UV-Vis DRS an advantageous method in photocatalyst optimisation [99,101].

2.5.8.6 Energy Dispersive X-ray (EDX) Spectrometry

Energy Dispersive X-ray (EDX) spectrometry is a sophisticated technique for analysing the elemental composition of materials such as metal oxide nanoparticles and doping. EDX has the accuracy to measure the occurrence and distribution of zinc and nickel in defining ZnO and NiO nanoparticles and in determining their respective elemental transitions, i.e., the K-alpha and L-beta transitions, which are associated with their respective absorption energies, as shown in **Figure** 13. For Ag-doped ZnO nanoparticles, EDX assists in identifying the existence and amount of silver dopants. This is crucial in relating the alterations of the structural and electronic character of ZnO caused by silver doping.

Identification of such elements through EDX is done by mapping the peaks of each element at specific energy levels. For instance, Zn is marked by a well-defined K-alpha peak around 8.6 keV; the K-alpha peak around 7.5 keV marks Ni; and silver in Ag-doped ZnO nanoparticles is marked by characteristic peaks around three keV. Comprehensive studies, for instance, those by Kumar et al., and Sharma et al., illustrate the utility of EDX in confirming the stoichiometry and homogeneity of ZnO and NiO and Ag-doped Zno nanoparticles. This is important for the optimisation of the electronic and photocatalytic properties of these materials [102].

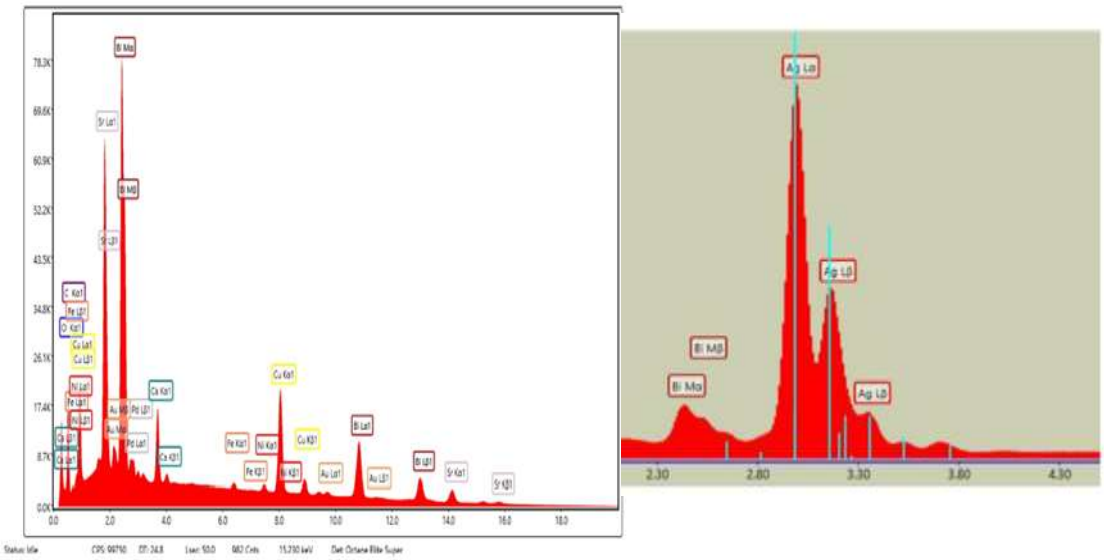

Figure 13: Typical spectrum of EDX with element peaks [102].

Characteristic X-rays, or X-ray lines, seen in energy-dispersive X-ray spectroscopy (EDX) result when vacancies are produced in the inner electron orbits of an atom, which create "holes." The electrons from outer, higher energy orbits fill the vacancies by emitting X-rays equal to the difference in energy between the shells. These X-ray lines are named according to the shell on which the vacancy occurs (i.e., K, L, M) and the shell from which the electron jumps (i.e., α for one shell higher, β for two shells higher, etc.), as shown in **Figure** 14 [103].

For instance, a Kα transition is when an electron from the L shell (n = 2) fills a vacancy in the K shell (n = 1), and a Kβ transition is when an electron from the M shell (n = 3) fills the vacancy. The subdivision of larger shells with principal quantum numbers (n) into subshells leads to individual X-ray lines being formed. For L to M shell transitions, even more X-ray lines are allowed, but only a few are typically resolved and of value for EDX

analysis. For instance, the closely spaced lines Kα1 and Kα2 will represent one peak in an EDX spectrum because they have a minimal energy difference [104].

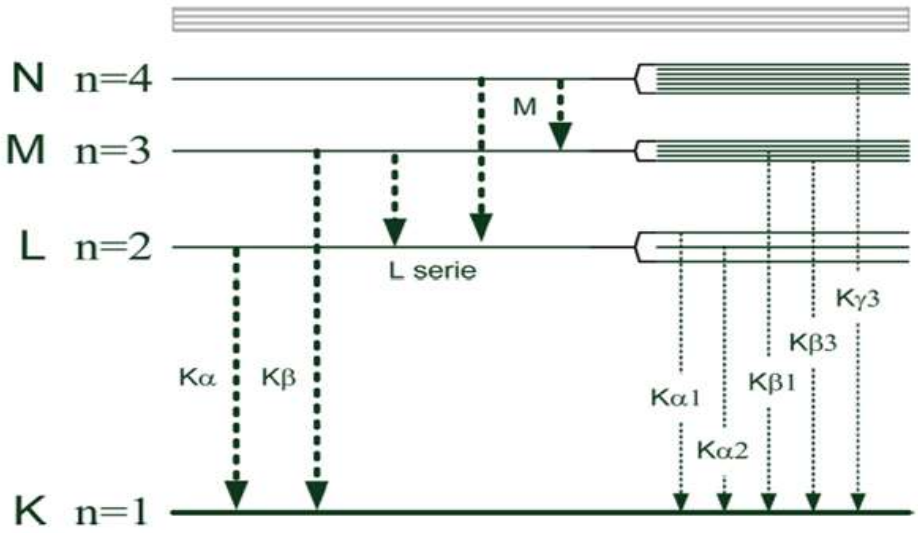

Figure 14: nomenclature of X-ray lines [103].

2.6 Advances and Trends in Utilizing Metal Oxide Nanoparticles as Photocatalysts for Dye Degradation and Water Purification.

The relentless industrial activities worldwide have created an urgent need for effective and sustainable methods to tackle environmental contamination, particularly in water resources. Among the various pollutants, synthetic dyes from the textile and manufacturing industries pose a significant threat due to their toxic and non-biodegradable nature. In this context, metal oxide nanoparticles have emerged as a promising solution, offering enhanced photocatalytic properties for the degradation of these persistent dyes. This review explores recent advancements and emerging trends in using metal oxide nanoparticles, such as NiO and ZnO, as photocatalysts for dye degradation and water purification. By examining the latest research and technological developments, this study highlights the potential of these nanomaterials to significantly contribute to sustainable water treatment practices (Table 3).

Table 2 :Summary of research and technological developments in photocatalytic nanomaterials.

Year	Research focus	Contributions	References
1970	Discovery of TiO_2 as a photocatalyst.	Fujishima and Honda demonstrated the photocatalytic splitting of water using TiO_2 under UV light.	[1,18,23,56]
1980s	Discovery of more metal Oxides.	Research was initially focused on ZnO and SnO_2 as other metal oxide photocatalysts for environmental remediation.	[5,18,20]
1990s	Significant development.	Researchers have studied the fading of organic dyes such as methylene blue (MB) and rhodamine B (RB) with assistance from TiO_2 and ZnO.	[2,6]
2000s	Entry of Metal oxide nanoparticles as photocatalysts.	Synthesis of metal oxides like ZnO and TiO_2 NPs by traditional methods to improve photocatalytic activity under UV light	[16,22,60]
2005s	Modified metal oxide NPs.	Doping metal and nonmetal to decrease band gap energy improves the photocatalytic activity of metal oxides like ZnO and TiO_2 under UV light.	[7,36,38,45]
2010s	Visible light activation.	Focus on engineering photocatalysts NPs active in the visible light spectrum to degrade organic dyes.	[47,48,52]

2015s	Hybrid photocatalysts.	Research focuses on synthesising photocatalyst composites like ZnO/NiO and ZnO/graphene.	[14,20]
2020s	Green synthesis of metal oxide NPs.	Synthesis of metal oxides like ZnO, NiO and TiO_2 NPs using different plant extracts.	[9,31,48]
2022s	Modified metal oxides.	Plant extract and biogenic routes are used to modify the band gap energy of metal oxides by metal and non-metal.	[39,56,69]
2024s	Formation of heterojunction.	Plant extract and biogenic routes can be modified by forming a composite with organic frameworks.	[69,71]
2025s *This study*	Modify morphology and size of NPs using a new plant under solar energy.	Improve photocatalytic activity of ZnO and NiO NPs from UV light to visible light to degrade organic dye, decreasing band gap energy by: - Using a new plant extract to synthesise pure photocatalyst NPs by different parameters and controlling size NPs. - Using a new plant extract to dope photocatalysts with silver atoms NPs at different parameters and controlling the size of silver NPs. - Controlling the morphology of pure and doping photocatalysts using a high concentration of plants with adjusted temperature degree and reaction time.	

CHAPTER 3

EXPERIMENTAL SECTION AND MATERIALS

3.1 Experimental Site:

The photocatalysts were synthesised in the Biochemistry Laboratory at the Faculty of Medicine, University of Sirte. The USAINS Biomics Laboratory determined the optical bandgap energy and explored functional groups. The analysis of chemical structure, surface properties, and data interpretation was carried out in the Nano-Optoelectronics Research Laboratory at USM Penang, Malaysia.

3.2 Materials and Apparatus:

All chemicals used in this dissertation were obtained from chemical companies and utilised in their pure form without further purification. Wild *Thymelaea hirsuta leaves* and *roots* were collected from the Dhehir area in Sirte City. To ensure the accuracy and reliability of the experiments, all glassware was thoroughly cleaned before use. This involved washing twice with distilled water (DW) and ethanol, followed by drying in an oven. Detailed information on the materials and preparation methods is provided in **Table 4**.

Table 3: The using chemicals.

Substance	Company	Purity%
Ethanol	Carlo Erba	99%
Zinc Acetate	Clariant	-
Nickel (ii) Chloride hexahydrate	Carlo Erba	-
Silver Nitrate	Carlo Erba	98.8%
Sodium hydroxide	Merck	-
Methylene blue dye technical (MB)	BDH	-

Various apparatuses and glassware were utilised to synthesise and characterise pure and doped photocatalyst nanoparticles. These included:

- **Heating and drying equipment:** Electric oven, electric furnace, hot plate with magnetic stirrer, and heater.
- **Measuring instruments:** Electronic balance, pH meter, and measuring cylinders.
- **Laboratory glassware:** Beakers, ceramic crucibles, pipettes, test tubes, and glass rods.
- **Separation equipment:** Centrifuge.

3.3 Experimental Parts

3.3.1 *Thymeala Hirsuta* – Extract Preparation

The concentrated *Thymelaea hirsuta* extract was initially prepared by washing and cutting the leaves and roots, followed by drying and blending them into small pieces using a mixer. Subsequently, 5 g and 20 g of *Thymeala hirsuta* powder were mixed with DI water, about 500, and boiled at 100 °C for two hours using a hot Plate with a Magnetic Stirrer. After that, the mixtures were cooled to room temperature, and the extracts, connected to the vacuum pump device, were filtered with Whatman No. 1 filter paper. These extracts were used as a reduction agent to synthesise ZnO, NiO, Ag-ZnO, and Ag-NiO NPs [105].

3.3.2 Green Synthesis of Pure ZnO Nanoparticles

The synthesis of zinc oxide nanoparticles (ZnO NPs) was carried out using a modified green method. First, 50 mL of Zn $(CH_3CO_2)_2 \cdot 2H_2O$ solution (0.5 M) was measured and poured into a 500 mL beaker. 100 mL of *Thymeala hirsuta* extract (5 g/100L) was incorporated into the Zinc acetate solution at room temperature, a drop at a time. The solution's pH was adjusted to 8 by adding drops of 1 M NaOH solution, and the solution was stirred for two hours at 50°C to obtain a deep yellow paste solution, followed by filtration. Meanwhile, the colour changes of the aqueous solution from light yellow to pale white indicated the reduction of zinc salt.

The filtrate was then washed using absolute ethanol and distilled water to remove and clean it from organic compounds or any oils found on the surface of nanoparticles during synthesis, and dried at 120°C in an oven for two hours. The obtained paste was further transformed in a ceramic crucible and annealed at 500°C for three hours, yielding a light white powder. The final step in obtaining the samples involved crushing them into fine white powder using a mortar, after which they were reserved for characterisation. To synthesise

larger quantities of ZnO NPs, the reactant quantities were scaled up by a factor of ten [80,81].

3.3.3 Green Synthesis of Pure NiO Nanoparticles

The synthesis of NiO nanoparticles (NPs) was carried out using a modified green method. First, 50 ml of $NiCl_2 \cdot 6H_2O$ solution (0.5 M) was poured into a beaker with a capacity of 500 ml. 100 mL of *Thymeala hirsuta* extract (5 g/100L) was added to the Nickel (II) chloride solution at room temperature, drop by drop. The solution's pH was adjusted to 8 by adding drops of 1 M NaOH solution. The solution was stirred for four hours at 50°C to obtain a green solution, followed by centrifugation of the precipitate, and then washed with distilled water and ethanol. The resulting filtrate was allowed to dry in the oven for 2 hours at 100 °C. The obtained paste was washed with absolute ethanol and distilled water, transformed in the ceramic crucible, and annealed at 500°C for three hours, resulting in a black powder. Lastly, the resulting samples were ground down into fine black powders with a mortar and stored for characterisation to synthesise large amounts of NiO NPs. The reactant quantities were multiplied by ten [74,76,84].

3.3.4 Methodology to Improve Photocatalytic Activity of Photocatalysts by Green Synthesis

To synthesise photocatalysts that have band energy more minor and have improved conductivity, three approaches were combined:

1- Formation of cation or anion vacancies:

Formation of (V_{Zn}) in a zinc oxide lattice and (V_o) in a nickel oxide lattice is done by annealing at high temperatures to enhance crystalline and using a reducing agent [47,49].

2- Reducing the size of silver nanoparticles to the atomic scale:

This is done by adding silver nitrate to a zinc oxide or nickel oxide solution in the presence of a weak reducing agent and controlling the temperature and reaction time to avoid agglomeration [81].

3- Surface doping with silver NPs:

Stabilising and fixing agents, such as polymers, were used to dope silver nanoparticles onto the surface of zinc oxide or nickel oxide, ensuring uniform distribution and preventing agglomeration [82,99].

These three methodologies were applied using the *Thymeala hirsute* extract, which contains compounds that act as stabilising and reducing agents. This enables the same triple approach (formation of vacancies, particle size reduction, and surface doping) [106]. Additionally, the *Thymelaea hirsute* extract offers the advantages of green synthesis, making the process more environmentally friendly and cost-effective.

Key Contributions of *Thymelaea hirsuta* Extract:

- **Formation of vacancies for oxygen, zinc and nickel:**

  Extract *Thymeala hirsuta* contains polyphenolic compounds and flavonoids that act as mild reducing agents, which helps reduce Metal ions inside the metal oxide lattice and leads to oxygen vacancy formation.
- **Reduction of silver particles to the atomic scale:**

  Extract *Thymeala hirsuta* from leaves containing tannins, saponins and flavonoids and use a significant amount of plant powder to form a higher concentration of extract, which works to form small silver nanoparticles without agglomeration.
- **Surface doping:**

  Extracting *Thymeala hirsuta* from the root contains some polymers, such as carbohydrates like plant gum, which act as coating and fixing agents on the surface of zinc and nickel oxide without agglomeration.

3.3.5 Green Synthesis of Doped ZnO and NiO NPs with Ag NPs

3 g of silver nitrate was added to the solution containing 15 g of pure NiO or ZnO NPs prepared in the second step, which was poured into a 500 ml beaker under stirring. With continuous stirring, a 100 ml concentrated *Thymeala hirsuta* extract (20 g/100 L) was incorporated into the same beaker for two hours at 50°C. The precipitate was deposited at the bottom of the flask. Finally, the mixture was centrifuged for 10 minutes at 8,000 rpm, and the powder was collected and washed with distilled water and ethanol. The obtained powder was dried at 120°C in the oven for two hours and then calcinated at 500°C for two hours, as shown in **Figure** 15 [74,76].

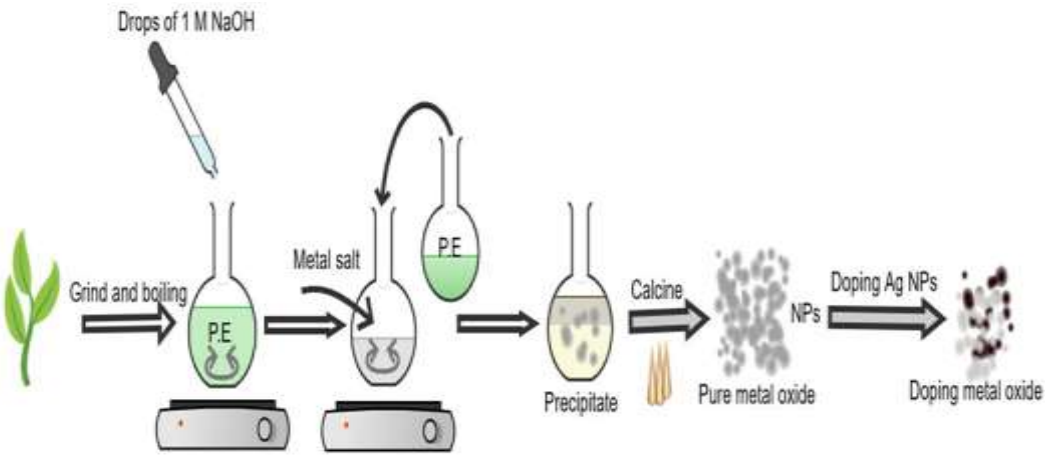

Figure 15 :Proposed schematic for forming Ag-Metal oxide spherical (metal Oxide-S).

3.3.6 Instrumentation and Characterisation Techniques

The prepared pure and doped photocatalysts were characterised using DRS, FT-IR, TEM, FESEM, and EDX. Instruments used to study photocatalytic activity applications were a CAMAG UV lamp cabinet with a wavelength of 254/366 nm as the UV light source and a UV-vis spectrophotometer (SPECODR -210) to study the absorption of organic dye concentration at degradation reaction of dye.

- **UV-Vis Diffuse Reflectance Spectroscopy (DRS):** The optical reflectance of the prepared photocatalysts was analysed using a Perkin Elmer Lambda 35 UV-Vis spectrophotometer (Perkin Elmer, Inc., USA) in the wavelength range of 200–800 nm.

- **Fourier-transform infrared Spectroscopy (FTIR):** FTIR spectra were recorded using a Shimadzu IR Spirit FTIR spectrometer in the range 400–4000 cm^{-1} through the KBr method with $8cm^{-1}$ resolution, which was utilised for structural analysis of the chemical compounds.

- **Transmission electron microscope (JEM _1011, JEOL, Tokyo, Japan):** TEM images were recorded to measure the size distribution of the prepared pure and doped metal oxide nanoparticles at magnifications 5000x, 20000x, 10000x, and 100000x. Samples for investigation using transmission electron microscopy were prepared by dispersing the nanoparticles ultrasonically at 185 W in 100% ethanol for 10 min. A drop of the dispersed solution was deposited on a carbon lace film supported by a

copper grid. The sample was air-dried, and the nanoparticles were imaged with TEM. ImageJ software was utilised to measure the diameters of individual nanoparticles from the TEM images.

- **Field Emission Scanning Electron Microscopy (FESEM) with EDX:** FESEM images and EDX analysis were performed using a SUPRA55 microscope (CARL ZEISS, Germany) at magnifications of 50,000× and 100,000× with a working distance of 5.3 mm. This was used to study the morphology and chemical composition of the pure and doped metal oxide nanoparticles [97,98,99].

3.4 Absorption Spectra Test of The Methylene Blue Dye

An absorption spectra test for methylene blue dye was used to determine the maximum absorbance (λ_{max}) of MB dye from the position absorption peak in an aqueous solution by UV-vis spectrophotometer. A series of standard solutions with concentrations of 18, 16, 14, 12, 10, and 8 ppm were prepared from a 20 ppm MB stock solution. The absorbance of these solutions was measured within the wavelength range of 500–800 nm [107].

3.5 Photocatalytic Activity of Prepared Photocatalysts NPs

To evaluate the photocatalytic performance of the prepared photocatalysts, their activity was assessed through the photodegradation of methylene blue (MB) dye. The degradation process was monitored at a wavelength of 665 nm, corresponding to the maximum absorbance of MB, using a UV-Vis spectrophotometer. Following a modified method, the experiments were conducted under UV light irradiation (366 nm) and direct sunlight on clear days.

First, 10 mg of methylene blue dye was dissolved in 1 Liter of distilled water. Then, 100 mL of the dye solution was transferred to a 250 mL beaker, and 60 mg of the photocatalyst was added. The mixture was adjusted to a pH of 7 and stirred for 30 minutes using ultrasonication in dark conditions at room temperature to achieve adsorption-desorption equilibrium. The photocatalytic activity of ZnO, NiO, Ag-ZnO, and Ag-NiO nanoparticles (NPs) was initially tested in dark conditions using UV-Vis spectrophotometry, with the absorbance recorded at zero minutes. Subsequently, the solution was exposed to sunlight

for 140 minutes, and the dye degradation efficiency was calculated using the following equation (1):

$$Degradation\ Efficiency\ (\%) = (Ao - At)\ /Ao * 100 \quad (1)$$

Where Ao and A_t are the absorbance of the dye solution before and after photocatalytic activity [77,82].

3.5.1 The Degradation Reaction Kinetics of (MB) by Prepared Photocatalysts

The kinetics degradation reaction of MB by prepared photocatalysts in the dark and under UV and solar irradiation was determined by using the Langmuir-Hinshelwood equation, can be described as a degradation reaction within pseudo-first order, and the rate equation for the degradation reaction can be expressed in absorbance data at λmax 665nm wavelength. The key concept here is that the concentration of methylene blue (MB) is directly proportional to its absorbance within degradation with photocatalysts under irradiation, according to the Beer-Lambert law:

$$A = \epsilon.\ C.\ l \quad (2)$$

Where:

A: Absorbance

C: Concentration

l: length

ϵ: molar Absorptivity coefficient

from rate low of pseudo-first order reaction equation:

$$ln\ (C_t/C_0) = k_1.t \quad (3)$$

Since absorbance is directly proportional to concentration, the equation (3) rate of reaction law can be rewritten as:

$$ln\ (A_t/A_0) = k_1.t \quad (4)$$

The rate constant could be expressed as a positive value by slightly modifying this equation:

$$ln\ (A_0/A_t) = k1.t \qquad (5)$$

$$ln\ (A_0/A_t)\backslash t = k \qquad (6)$$

Where:

A_0: Initial absorbance (measure absorbance before degradation reaction)

A_t: Absorbance at time t (measure absorbance at regular time of degradation reaction)

K: rate constant

t: irradiation time

The rate constant of photocatalysts can be determined from the slopes of the plot of ln (A_t/A_0) versus irradiation time (t) [1] and half time $t_{1/2}$:

$$t_{1\backslash 2} = (\frac{ln\ 2}{k}) \qquad (7)$$

3.5.2 Factors Affecting Photocatalytic Activity

The most effective conditions for the photocatalytic degradation of methylene blue (MB) using green-prepared photocatalysts were determined through parameter optimization experiments. These experiments focused on key factors such as pH, initial MB concentration, and irradiation time under UV and solar irradiation. The goal was to enhance the efficiency and effectiveness of the photocatalysts for environmental applications [90,91].

3.5.2.1 Effect of Doping Silver NPs on Degradation Efficiency (%)

The effect of silver doping on the degradation of methylene blue (MB) dye was investigated, as it is a critical factor in enhancing photocatalytic activity. Doping involves incorporating metal atoms into the lattice of metal oxides, which helps tailor the chemical and physical properties of the photocatalysts. This process enhances photocatalytic activity by reducing the bandgap energy of zinc oxide (ZnO) and nickel oxide (NiO) nanoparticles. The degradation of MB dye was studied at a concentration of 10 mg/L under both ultraviolet

(UV) and solar radiation. The experiments were conducted with a reaction time of 140 minutes, a pH of 7, and a photocatalyst dosage of 60 mg.

3.5.2.2 Effect of Irradiation Time on Degradation Efficiency (%)

The effect of time on the efficiency of the synthesised photocatalyst for degrading organic dye pollutants was investigated, along with the relationship between the two. The aqueous solution of the organic dye, with a concentration of 20 ppm and a pH of approximately 7, was irradiated for 140 minutes under both UV and solar irradiation. A photocatalyst dosage of 60 mg was used in the experiments.

3.5.2.3 Effect of Initial Concentration of Dye on Degradation Efficiency (%)

The effect of the initial concentration of dye on the efficiency of the degradation reaction was studied; it is an essential factor in photocatalysis. Different methylene blue (MB) dye concentrations were used: 10 mg/L, 12.5 mg/L, 15 mg/L, and 20 mg/L under ultraviolet and solar radiation at a reaction time of 140 min and pH of 12. The amount of catalyst used was 60 mg.

3.5.2.4 Effect of pH on Degradation Efficiency (%)

The degradation efficiency (%) of MB dye was affected by pH. It was studied at different pH values varying from 3 to 12 at constant parameters since the pollutant concentration (MB) is 10 mg\L, exposing the reaction mixture to UV light and sunlight irradiation for 140 min. The amount used from photocatalysts is 60 mg.

3.6 Reusability of the Photocatalysts

The photocatalysts prepared by green synthesis were recycled after being used in the first experiment of dye degradation by photocatalysts under sunlight. The photocatalyst was collected from the solution by centrifugation and washed three times with distilled water and ethanol (50:50). It was dried in an electric oven at 120°C for 12 hours and used for two repeated experiments of dye degradation. Then, the reusability of the prepared photocatalyst was calculated [108].

CHAPTER 4

RESUTLS AND DISCUSION

4.1 Green Synthesis of Pure ZnO Nanoparticles

The green synthesis method was employed to prepare pure zinc oxide (ZnO) and pure nickel oxide (NiO) nanoparticles from aqueous solutions of zinc acetate ($Zn(CH_3CO_2)_2 \cdot 2H_2O$) and nickel chloride ($NiCl_2 \cdot 6H_2O$) in the presence of *Thymelaea hirsuta* extract. The pH of the solution was adjusted to 8 by adding drops of 1 M NaOH solution.

Table 5 summarises the weights of $Zn(CH_3CO_2)_2 \cdot 2H_2O$ and $NiCl_2 \cdot 6H_2O$ salts used to synthesise 18.76 grams of zinc oxide nanoparticles and 15.96 grams of nickel oxide nanoparticles. Assuming a 1:1 molar ratio between the produced zinc oxide nanoparticles and the reacted zinc acetate, the production rates were calculated to be 92.4% for ZnO and 85% for NiO [62].

Table 4: The production rate of ZnO and NiO NPs.

Type Metal salt	Weight of salts used	The theoretical yield	The average yield	%
Zinc salt	54.875 grams	20.3 grams	18.76 grams	92.4%
Nickel salt	59.48 grams	18.75 grams	15.96	85%

Based on the calculations and experimental results, green synthesis proves to be an effective method for preparing zinc oxide (ZnO) and nickel oxide (NiO) nanoparticles. However, some sample losses were observed during the purification and separation processes.

This reaction method appears reliable, high-quality, and efficient from a yield amount, complexity, and safety standpoint. However, its overall quality will be determined from the direct characterisation of the produced nanoparticles.

After preparation, the resulting ZnO NPs were ground into light white powder and black powder of NiO NPs ,as shown in **Figure** 16. The resulting samples were ground down into fine powders with a mortar and stored for characterisation.

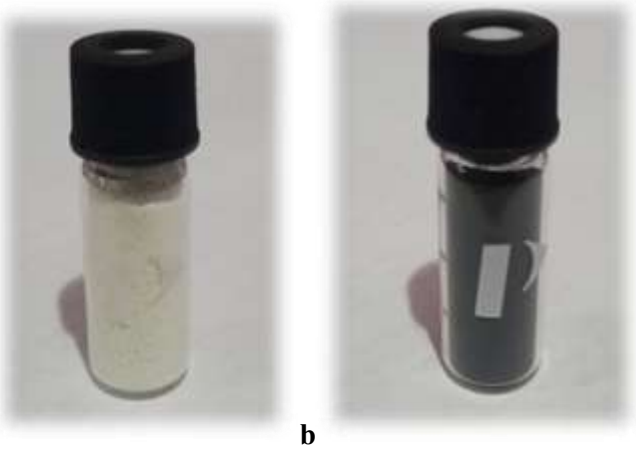

a **b**

Figure 16: The colour of pure (a) ZnO NPs and (b) NiO NPs.

4.2 Green Synthesis of Doped ZnO and NiO NPs with Ag NPs

The green synthesis method prepared ZnO NPs doped with Ag NPs (Ag-ZnO) nanoparticles and NiO NPs doped with Ag NPs (Ag-NiO) nanoparticles from an aqueous solution of zinc oxide nanoparticles and nickel oxide nanoparticles in the presence of *Thymeala hirsuta* extract and source Ag ions (Ag^{+}) from silver nitrate ($AgNO_3$). The solution's pH was adjusted to 8 by adding NaOH solution drops (1 M). Specific weights of zinc oxide and nickel oxide were used to prepare the Ag-ZnO and Ag-NiO nanoparticles, as detailed in Table 6.

Table 5: Weights of ZnO and NiO NPs used in the synthesis of Ag-doped photocatalysts

Type Metal Oxide	Weight of oxide used	Weight of result doped metal oxide
ZnO NPs	15 grams	12.53 grams
NiO NPs	15 grams	13.74 Grams

After preparation, the resulting Ag-ZnO NPs were ground into a light brown powder and a deep grey powder of Ag-NiO NPs, as shown in **Figure** 17. The resulting samples were ground down into fine powders with a mortar and stored for characterisation.

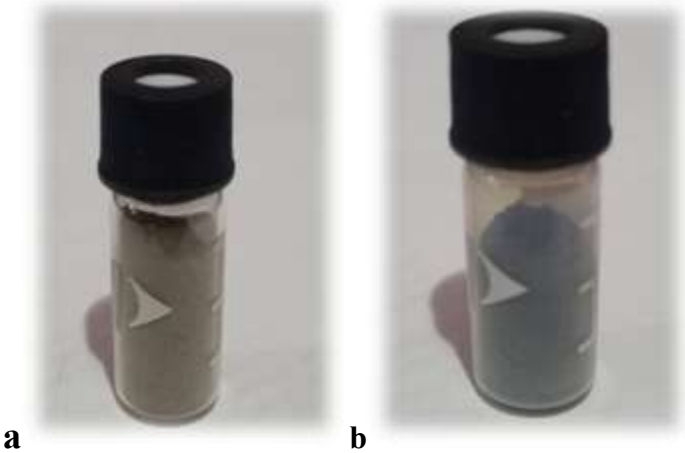

a **b**

Figure 17: The colour of (a) Ag-ZnO NPs and (b) Ag-NiO NPs

Confirmation of Silver Doping in Metal Oxide Nanoparticles: To confirm the doping of the metal oxide by nano silver ions through the characterisation of these prepared samples, energy-dispersive X-ray spectroscopy (EDX) coupled with scanning electron microscopy (SEM) can provide elemental mapping and compositional analysis, showing the uniform distribution of silver within the metal oxide matrix.

Transmission electron microscopy (TEM) provides high-resolution images showing the integration of silver ions at the atomic level. UV-visible diffuse reflectance spectrometers can further support doping by detecting changes in optical properties, such as changes in band gap energy.

4.3 Characterization of Photocatalysts Nanoparticles

The prepared pure and doped photocatalysts were characterised using DRS, FT-IR, TEM, FESEM, and EDX.

Field Emission Scanning Electron Microscopy (FESEM) with EDX was used to study the morphology and chemical composition of the pure metal oxides and doped metal oxide nanoparticles and indicate present Ag NPs in metal oxide lattice, A UV-visible Diffuse Reflectance Spectrophotometer (DRS) was used to study optical properties and measure the

band gap energy of prepared samples, Fourier-transform infrared spectroscopy (FTIR) was used to study functional groups.

Using ImageJ software from TEM images, a transmission electron microscope (TEM) was used to measure the size distribution of the prepared pure and doped metal oxide nanoparticles.

4.3.1 UV-Visible Diffuse Reflectance Analysis

UV-Visible Diffuse reflectance spectroscopy is preferred over UV-vis absorption spectroscopy, primarily to circumvent the challenges of enhanced scattering in certain materials. Scattering can complicate UV-vis absorption for powder, rough surfaces, or highly turbid substances.

In these scenarios, the light often does not penetrate the sample effectively; instead, it scatters in various directions. As a result, scattering interference with obtaining an accurate absorption value makes diffuse reflectance spectroscopy more suitable for these materials. To increase the accuracy of the sample's absorption data, diffusely reflected light comprised of both absorbed and dispersed light was captured using UV-Vis diffuse reflectance spectroscopy.

The diffused reflectance spectra for pure (ZnO-NiO) and doped (ZnO-NiO) with Ag nanoparticles are presented in **Figures** 18 and 19, the Kubelka–Munk equation which is analysed using:

$$F(R)\lambda \equiv \frac{(1-R)2}{2R} = \frac{K}{S}$$

Absolute reflectance is the 'R' of the sample, and 'F(R)' is the Kubelka-Munk function. **Figure** 18 shows the diffused reflectance spectra of pure ZnO, Ag-doped ZnO, pure NiO, and Ag-doped NiO NPs. Taking the case of an infinitely thick sample where the thickness of the sample holder was neglected, the Kubelka-Munk equation becomes:

$$F(R_\infty) = \frac{(1-R_\infty)^2}{2R}$$

Where

$$R_{\infty} = \frac{R_{sample}}{R_{standard}}$$

Eq. (hv) represents the relationship between the band gap (E_g) and absorption coefficient (α) for a direct band gap semiconductor:

$$\alpha h\nu = C_1(h\nu - Eg)^{\frac{1}{2}}$$

Where 'hν' is the photon energy and C_1 is a proportionality constant. Kubelka–Munk scattering coefficient S as constant concerning wavelength, the Eq. (hν) changes to:

$$[F(R_{\infty})h\nu]^2 = C_2(h\nu - E_g)$$

Plotting $[F(R_{\infty})\ h\nu]^2$ against hν determined the band gap Eg, as shown in Figure (inset plot) [109].

As shown in **Figure** 18, the UV-visible spectra of ZnO and Ag-ZnO nanoparticles were synthesised by green synthesis using Thymeala hirsuta extract. The optical band gap energy of prepared nanoparticles measurement by using the Kubelka–Munk relation, the calculated Eg value was found to be 3.3 eV for ZnO NPs and 3.15 eV for Ag-ZnO NPs, findings align with those of previous studies [7,110,111], which reported similar changes in the optical properties of ZnO after doping with Ag nanoparticles reported similar optical properties chemical methods and green synthesis techniques. The optical band gap energy narrows after doping ZnO NPs with Ag nanoparticles, causing the material to absorb light at longer wavelengths (redshift). This means that the broad absorption band in the diffuse reflectance spectra becomes sharper and more defined as the band gap decreases. The results show that a shift in the band gap is observed, indicating Ag's surface modification on pure ZnO, allowing the material to interact with light at these longer wavelengths more effectively.

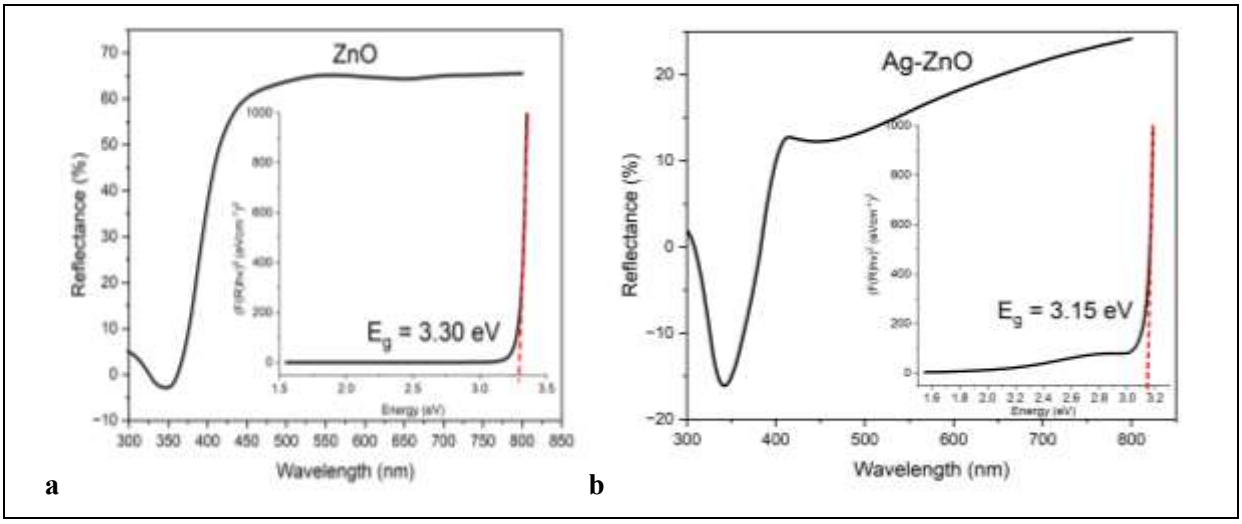

Figure 18: UV-Vis diffused reflectance spectra and band gap calculation graph of (a) pure ZnO& (b) Ag-ZnO NPs.

In Figure 19**,** the band gap energy of NiO NPs and Ag-NiO obtained from this study, equal Eg=3.16 eV and 3.14 eV, are comparable to that reported in the previous research [112], who studied nanocrystalline nickel oxide thin films prepared by hydrothermal and sol-gel methods. "The results show that a mild shift in band gap is observed, indicating surface modification of Ag on pure NiO NPs.

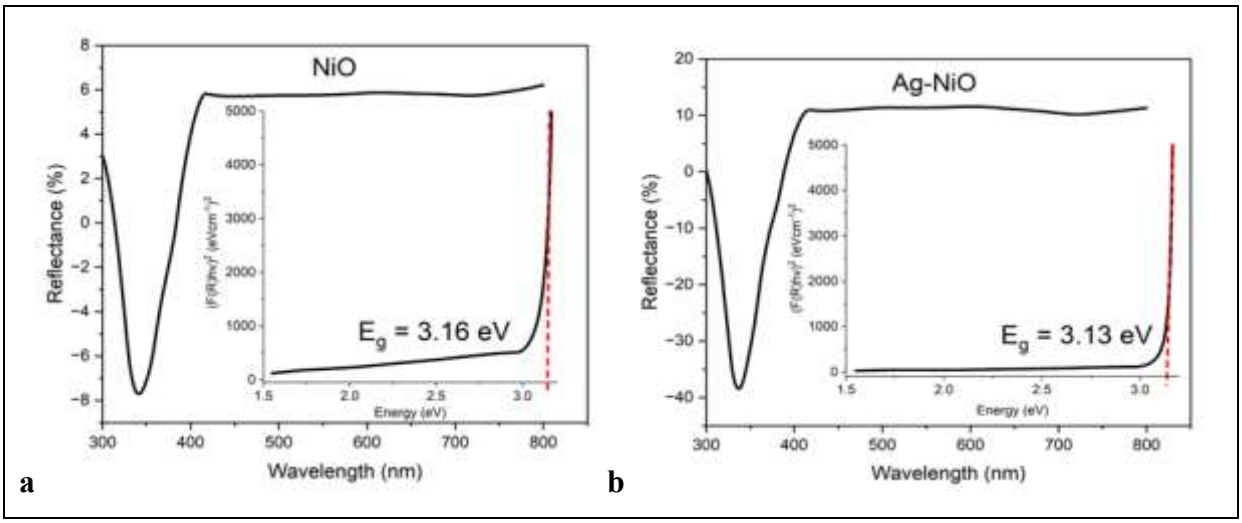

Figure 19: UV-Vis diffused reflectance spectra and band gap calculation graph of (a) pure NiO & (b) Ag-O Ni NPs.

4.3.2 Fourier-Transform Infrared Spectroscopy (FTIR) Analysis

FTIR analysis was performed using Shimadzu IR, the range of Spirit FTIR spectrometer, 400–4000 cm^{-1}, using the KBr technique with 8 cm^{-1} resolution.

The information from the chemical bonding of the samples was obtained by performing FTIR analysis in the range 4000-400 cm^{-1}. **Figures** 20 and 21 display the FTIR spectra for pure ZnO and Ag-doped ZnO, confirming that the pure ZnO NPs had 1441, 867, 373, and 350 cm^{-1} absorption bands. Absorption bands below 1000 cm^{-1} represent interatomic vibrations absorption [79,82,84]. The peak bands at 867, 373, and the wavenumber 350 cm^{-1} confirm the presence of the Zn-O bond in the sample due to Zn-O bond stretching vibrations [77,78]. Meanwhile, the peak at 1441 cm^{-1} represents C=C stretching in polyphenols and C–N stretching in primary amines, which may result from the use of a solvent in the synthesis of ZnO NPs; these findings are consistent with those reported by [7,110]. The above inference justifies that primary amines and polyphenols in the plant extract could be implicated in the capping and stabilisation of ZnO nanomaterials.

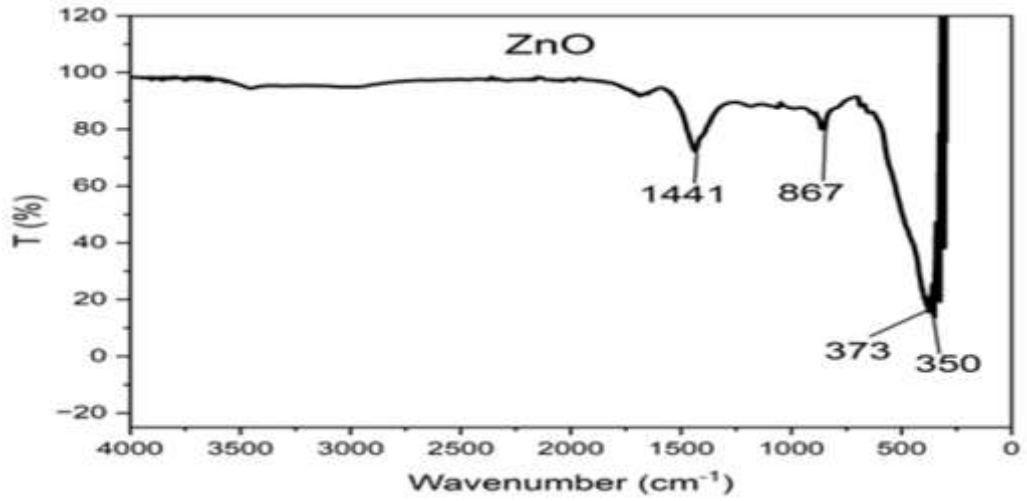

Figure 20: FT-IR analysis of pure ZnO NPs.

The FTIR spectrum of Ag-doped ZnO NPs shows similar absorption bands to those obtained from the FTIR spectrum of pure ZnO NPs but shifted to slightly lower wavenumbers from (1441 to 1410 cm^{-1}), (867 to 860 cm^{-1}), (373 to 366 cm^{-1}) and (350 to 339 cm^{-1}) as shown in **Figure** 21.

FTIR spectrum of Ag-doped ZnO NPs also shows absorption bands similar to those observed in studies [113,114] in which the bands shifting might be due to changes in the local environment around the Zn ions caused by Ag doping.

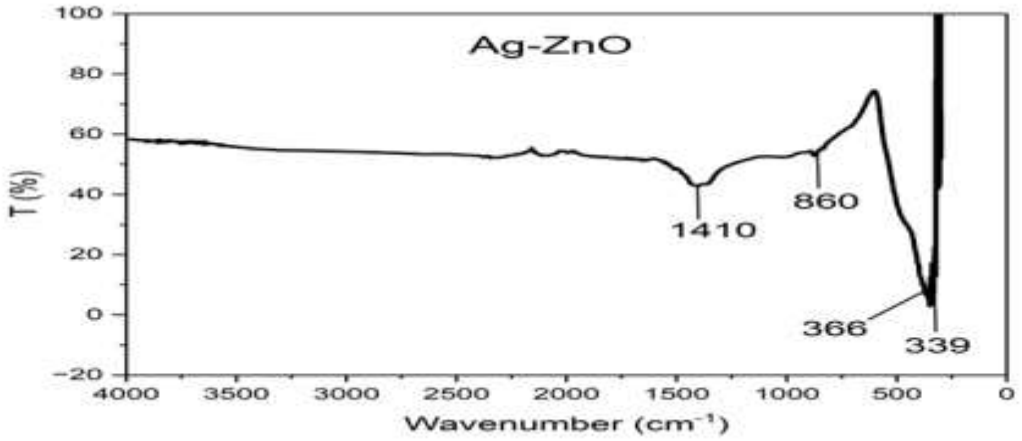

Figure 21: FT-IR analysis of Ag-ZnO NPs.

Figure 22 displays the FTIR spectra of pure NiO, which has peak bands at 850, 400, and 295 cm^{-1}. The FTIR spectrum of NiO falls within the stretching frequencies of metal-oxygen, which agrees with [84], which is in the range 1000-400, confirming the presence of NiO. The FTIR spectra NiO and Ag-doped NiO NPs exhibit are presented in **Figure** 22, with absorption features comparable to those obtained from the FTIR spectra of pure ZnO and Ag-doped ZnO NPs. Furthermore, the FTIR spectrum of Ag-doped NiO NPs shows absorption at lower wavenumbers than that of pure NiO NPs [86]. This test revealed that the biomolecules in the structure of Thymeala hirsuta extract play an active role in the synthesis of ZnO, Ag-ZnO, NiO, and Ag-NiO NCs.

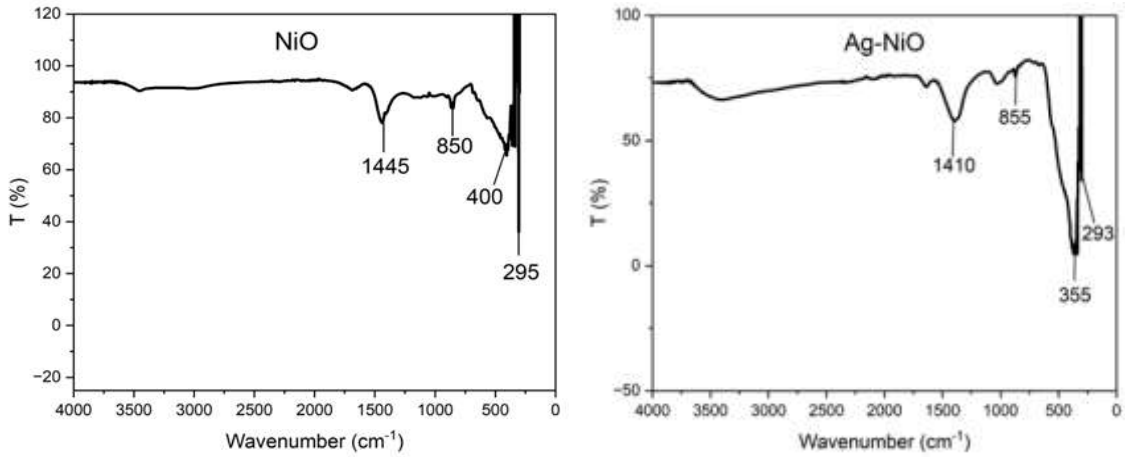

Figure 22 : FTIR spectra of pure NiO and Ag-NiO NPs.

4.3.3 Energy Dispersive X-ray Spectroscopy Analysis

EDX analysis confirmed the prepared samples' chemical formation and elemental composition by green synthesis. EDX spectra mean energy-dispersive X-ray spectroscopy. This spectrum is a plot of the intensity of X-rays scattered or emitted when a sample is irradiated with an electron beam versus the energy of the X-rays [104]. The EDX spectra confirm the presence of zinc, oxygen, Ni, and Ag NPs; **Figure** 23 shows the EDX spectra of pure ZnO and NiO and Ag-doped ZnO and NiO. The sharp EDX peaks indicated that the synthesised nanoparticles had crystalline structures, and the vigorous intensity and the narrow width of pure ZnO and NiO diffraction peaks indicate that the resultant products were highly crystalline in nature.

- **Analysis of Atomic Ratios:**

  Pure ZnO:

  Zn = 40.94% at%

  O = 35.52% at%

  The atomic ratio of Zn to O = $40.94/35.52 = 1.18$

  This ratio suggests that the Zn content is slightly higher than O, which indicates zinc vacancies (V_{Zn}). The structure is likely Zn-rich, which might lead to defects such as Zn vacancies or excess oxygen in the system.

  Ag-ZnO:

  Zn=46.07%

  O =34.99%

  The atomic ratio of Zn :O = 1.3

  After Ag doping, the Zn content increases, and the Zn O ratio increases to 1.3, indicating that the material is still Zn-rich. This suggests that Ag doping could fill Zn vacancies and compensate for some defect sites in the ZnO lattice. The increase in Zn and the slight decrease in O could indicate that oxygen vacancies (V_o) are created or modified during the doping process, while Ag helps stabilise the structure.

  Pure NiO:

  The atomic ratio of Ni :O =1.52

  Ag-NiO:

  The atomic ratio of Ni :O =1.2

With a Ni :O With a ratio of 1.51, the material could improve its various properties, depending on the application. The Ni excess, Ni, and oxygen vacancies can lead to better electrical conductivity, magnetic properties, and structural stability. These improvements make the material more suitable for advanced electronics, energy storage, and magnetism applications.

With the Ni :O The ratio decreases to 1.2, and the material becomes closer to stoichiometric or at least more balanced. This suggests improvements in several aspects:

- More balanced electrical conductivity.
- Improved catalytic efficiency due to more stable active sites.
- Better structural stability, fewer defects or vacancies [102-104,125].

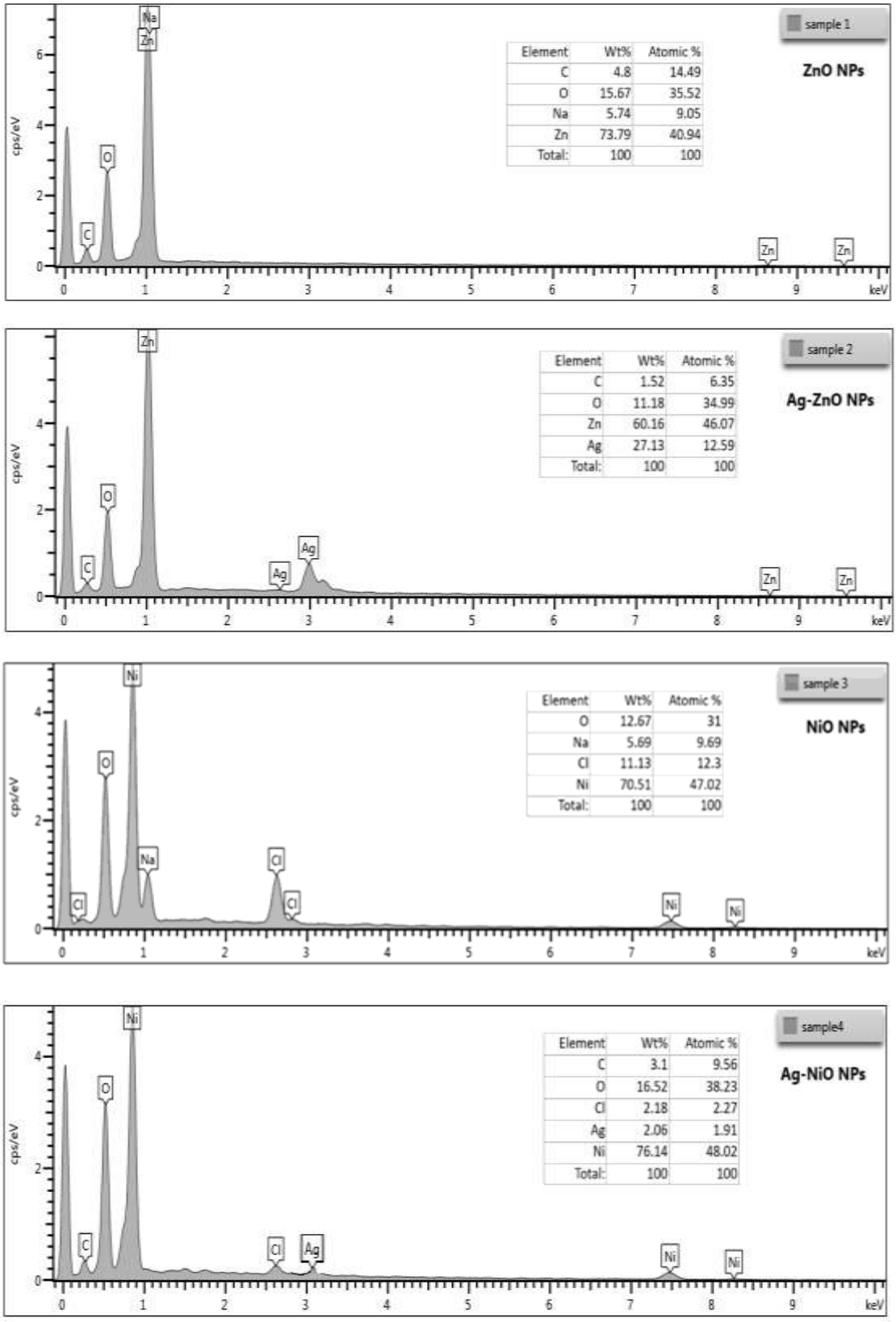

Figure 23: EDX spectra of green synthesised ZnO (a), Ag-ZnO (b), NiO (c), and Ag-NiO NPs (d).

Peaks and Identified Elements in ZnO NPs (a) Spectrum:

1- C (Carbon): The significant peak was around 0.2-0.3 Kev, which refers to the present—c in the sample, which is possible from an organic plant extract used to synthesise ZnO NPs with type transition Kα.
2- O (Oxygen): The peak at 0.5 Kev refers to the oxygen in the prepared sample as oxide (O^-), with the type transition being Kα.
3- Na (Sodium): An energy peak equal to ~1.0 corresponding to sodium indicates that a NaOH solution was used in the preparation process.
4- Zn (Zinc): Significant peaks were in the lower energy region of the spectrum, about one keV, and the second peak at 8-9 Kev; these peaks refer to the Zn atom present in the prepared sample, and this means Zn is an essential component in the prepared sample

   Possible Explanation:

   Present Zn and O refer to the prepared sample, ZnO NPs. C was impurities from organic compounds, and Na was from a hydrogen hydroxide solution.

Peaks and Identified Elements in Ag-ZnO NPs (b) Spectrum:

1- C (Carbon): The significant peak near zero was around 0.2-0.3 Kev, which refers to the present—c in the sample, which is possible from an organic plant extract used to synthesise ZnO NPs with type transition Kα.
2- O (Oxygen): The peak at 0.5 Kev refers to the oxygen in the prepared sample as oxide (O-), with the type transition being Kα.
3- Zn (Zinc): Significant peaks were in the lower energy region of the spectrum, about one keV, and the second peak at 8-9 Kev; these peaks refer to the Zn atom present in the prepared sample, and this means Zn is an essential component in the prepared sample
4- Ag (Silver): There are peaks at around three keV, which refer to the presence of silver within the nanoparticles.

Type of sample:

The spectrum confirms that Ag-ZnO nanoparticles have been prepared with zinc oxide (ZnO) as the core and silver (Ag) as the additive material.

Peaks and Identified Elements in NiO NPs (c) Spectrum:

1- Ni (Nickel): Significant peaks are around one keV and 7-8 keV.
2- Cl (Chlorine): two resolved peaks around 0.5 and 2.5 keV.
3- O (Oxygen): A smaller peak near 0.5 keV, this corresponds to oxygen
4- Na (Sodium): A peak near one keV.

The spectrum confirms the existence of nickel oxide (NiO).

Peaks and Identified Elements in Ag-NiO NPs Spectrum:

1- C (Carbon): The significant peak near zero was around 0.2-0.3 Kev, which refers to the present—c in the sample, which is possible from an organic plant extract used to synthesise ZnO NPs with type transition Kα.
2- O (Oxygen): The peak at 0.5 Kev refers to the oxygen in the prepared sample as oxide (O-), with the type transition being Kα.
3- Ni (Nickel): Peaks around one keV refer to a significant presence of nickel, and smaller peaks near 7 and 8 keV correspond to characteristic nickel X-ray emissions.
4- Cl (Chlorine): A peak near 2.5 keV, possibly from sample preparation or residuals.
5- Ag (Silver): There are peaks at around three keV, which refer to the presence of silver within the nanoparticles.

Sample Explanation:

The spectrum confirms the presence of nickel oxide (NiO) with strong Ni and O signals. The silver peak suggests Ag has been incorporated into or is present in the sample; trace chlorine and carbon might result from preparation methods.

The energy of such transitions, and consequently the position of the peaks in the spectrum, is determined by the energy level differences between the involved shells, which are unique to each element.

The EDX spectra help identify elements since the absence of Kβ transition can be used to refer to the presence of the elements in the sample. In addition, it can improve element identification in spectra with a complex composition, mainly when other elements produce peaks that overlap [104,115]. These results agree with literature reports [84,116], except for slight variations due to the differences in chemical composition.

4.3.4 Field Emission Scanning Electron Microscope Analysis

The study of the morphology and size of prepared photocatalyst nanoparticles using FESEM used high-resolution images from FESEM to determine the structure, particle distribution, and surface characterisation of NPs [71,97,98].

The essential morphological parameters, including the number of particles, total area, average particle size, perimeter, circularity, and solidity, were considered to analyse the morphological properties in the samples. These parameters are essential to understanding the performance of nanoparticles in photocatalysis, sensing, and energy storage applications [117,118,119,120]. **Figure** 24 shows FESEM images of pure ZnO NPs at one micro and 500 nm magnifications, with a work distance of 5.3 cm.

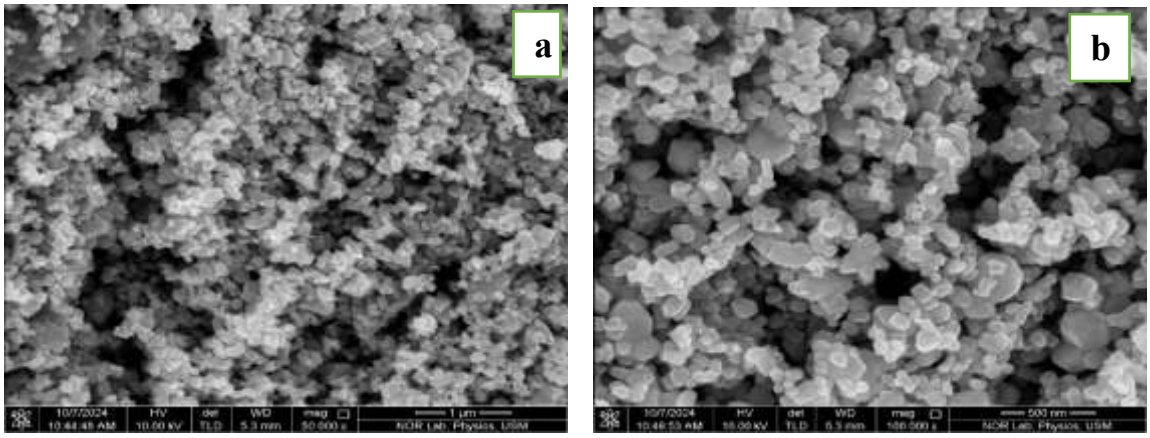

Figure 24: FESEM images at magnification (a) 50000x and (b) 100000x.

The following are the morphology and shape results for ZnO nanoparticles that were calculated by ImageJ software:

- **Particle Count:** 1526 particles
- **Area:** 23961.938 nm² (total area of all particles)
- **Average Size:** 15.702 nm² (area of each particle on average)
- **Perimeter:** 12.658 nm (average perimeter of the particles)
- **Circularity (Circ):** 0.939
- **Solidity:** 0.938

1. Average Particle Size Calculation:

The average size of each nanoparticle is expressed in **square nanometres (nm²),** with an area measurement of 15.702 nm². This helps to understand how big each particle is on a microscopic scale. To find the average diameter of the nanoparticles, assuming spherical particles (since the circularity is close to 1), can use the following formula:

Plugging in the area: $$D = 2 \times \sqrt{\frac{\text{Area}}{\pi}} \quad (8)$$

The **average diameter** of ZnO nanoparticles calculated by equation No. 8 is approximately **4.46 nm**, which refers to the nanoparticles as very small and not in micrometre scale, as expected for ZnO NP synthesis at this scale from a methodology used in preparing NPs [119,120].

2. Perimeter of NPs:

Its perimeter is 12.658 nm, relatively small for nanoparticles, given that its diameter is about 4.46 nm. The ratio of the perimeter to the area can tell us something about the shape.

If the particles were perfectly spherical, we would expect that the perimeter varies with diameter according to the following expression for the circumference of a circle:

$$D = 2 * \sqrt{\frac{15.702}{\pi}} \approx 4.46\ nm$$

$$P = \pi \times D = \pi \times 4.46 = 14.0\ nm$$

The exact perimeter of NPs is 12.658 nm, which is lower than the expected value for a perfect sphere. This shows that some nanoparticles may be slightly faceted or non-spherical but close to spherical [120].

3. circularity of NPs:

The circularity of NPs refers to how close the particle shape is to being a circle. Near 0 for very irregular particles, and near 1, the NPs are ideal circular particles. The measured value for circularity is 0.939, which is near 1. The value confirms that the synthesised nanoparticles are nearly spherical with minute irregularities. This value is for particles with smooth edges and compactness and slight deviations from the form of an ideal sphere [120].

4. Solidity of NPs:

The Solidity of NPs means how much particle fills in her convex hull. The closer the value is to 1, the more solid the particle is (indicating no significant voids or hollows). The solidity value is 0.938, close to 1, indicating that the nanoparticles are solid in structure with very little fragmentation [117,120].

5. Morphology and Structure Summary of NPs:

The nanoparticles exhibit near-spherical morphology with slight faceting, as suggested by the observed perimeter, which is marginally lower than the theoretical value for perfect spheres. The calculated circularity of 0.939 indicates that while the particles are predominantly spherical 1, they exhibit minor surface irregularities or faceted edges contributing to this deviation.

- **Size of NPs:** The average diameter of the nanoparticles is about 4.46 nm, which is typical for ZnO nanoparticles in many synthesis methods. This size indicates that the particles are within the nanoscale range.
- **Clustering/agglomeration:** The massive sample size of 1526 nanoparticles refers to a significant dispersive condition that could be met with relatively slight aggregation. The fact that the solidity is 0.938 with a near-round particle morphology further supports that assumption since agglomerated particles typically have lower solidity values and distort from circularity.
- **Surface Texture:** The smooth circularity and high solidity suggest that the surface of the nanoparticles is likely to be soft without significant defects, fragmentation, or hollow regions. This would be typical of well-formed compact nanoparticles []117,118,120].

Final Analysis:

ZnO nanoparticles in this sample are mostly nearly spherical, with a diameter size of 4.46 nm. The ZnO NPs are relatively uniform in shape, with tiny irregularities, as evidenced by their high circularity and solidity. The smoothness of the particles is supported by the high solidity and circularity, indicating that they are compact and solid with only minimal surface defects. Because these nanoparticles have a low aspect ratio, close to a perfect circularity factor, they may show excellent stability in suspension. **Figure** 25 shows FESEM

images of Ag doping ZnO NPs at one micro and 500 nm magnifications, with a work distance of 5.3 cm.

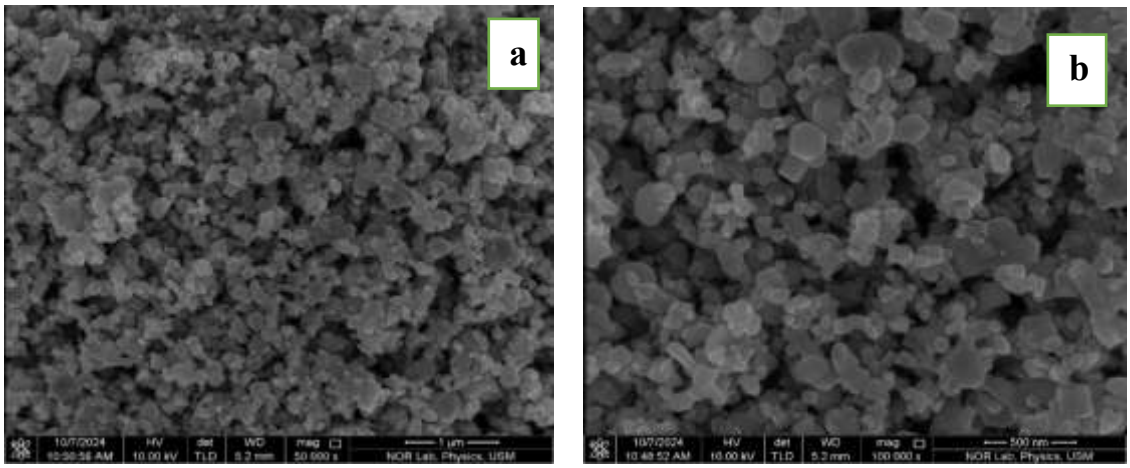

Figure 25: FESEM images of ZnO NPs doping with Ag NPs at magnification (a) 50000x and (b) 100000x.

The analysis of data obtained from the FESEM images of Ag-doped ZnO nanoparticles on the following specified parameter in **Table** 7:

Table 6: Some parameters are calculated from data obtained from images by ImageJ software.

Particle count	1552
Surface area	231159.727 nm^2
Average area	14.932 nm^2
Perimeter	12.414 nm
Circularity	0.937
Solidity	0.935

1. Calculation of Average Particle Size:

The total number of particles in the obtained micrograph was 1,552; therefore, one would expect a variation in their size. However, because the calculated average area is small, the distribution should be narrow, pointing to similar particle sizes. From Equation No. 1, the estimated average diameter in the case of spherical particles is approximately 4.35 nm.

2. Perimeter of NPs:

The average perimeter was 12.414 nm, smaller than the theoretically calculated perimeter for exactly spherical NPs with a diameter calculated to be 4.35 nm.

$$P\ theoretical = \pi \times D = \pi \times 4.35 \approx 13.67\ nm$$

This deviation (~9.2%) refers to the particles are not perfectly spherical and might be more compact or dense due to Ag doping [117,120].

3. Circularity and Solidity of NPs:

A high circularity of 0.937 and solidity of 0.935 signify that the particles' surfaces are smooth and well-rounded, with tiny surface irregularities.

4. Clustering or Aggregation:

The particle count (1552) and high solidity indicate that the nanoparticles are well dispersed in the observed region. There is no significant evidence of clustering or aggregation, which would otherwise manifest as irregular shapes, lower circularity, or lower solidity values.

5. Morphology and Shape:

Circularity (0.937): Indicates that the particles are nearly spherical, with slight irregularities or faceted surfaces. Adding **silver (Ag)** might influence the **ZnO particle** morphology, but the particles maintain a predominantly spherical structure.

Doping Effects: Doping **silver (Ag^+)** ions into the **zinc oxide (ZnO) lattice** reduces the overall particle size due to **lattice distortion** and the **inhibition of growth kinetics**. This process creates strain and defect states because of the size mismatch between **Ag^+** and **Zn^{+2}** ions, affecting ZnO **optical** and **electronic** properties. Ag doping creates **localised surface plasmon resonance (LSPR)** and modifies **bandgap energy** [69,71,113]. The doping effect alters **crystal growth**, leading to irregular shapes and a slight reduction in **circularity**. Values of **0.937** for Ag-doped ZnO are compared to **0.939** for pure ZnO. While Ag-doped ZnO shows **high solidity** at **0.935**, it slightly decreases from **0.938** pure ZnO, suggesting potential surface distortions. Doping by **Ag** allows the **nucleation rate**, and hence, a more significant particle number of **1552** from Ag-doped ZnO compared with **1526** from pure

ZnO. Small and more numerous particles with a reduced perimeter from **12.414 nm** against that of pure ZnO of **12.658 nm** agree with the earlier size reduction and increased smoothening. $\mathbf{Ag^{+}}$ ions can replace $\mathbf{Zn^{+2}}$ ions or occupy intermediate positions within the ZnO lattice, resulting in distortions that affect ZnO's **particle size**, **shape**, and **optical and electronic properties**.

Figure 26 shows FESEM images of NiO NPs and their Ag-doped form, comparing particle characteristics. The morphological parameters from the FESEM analysis are compared for all four samples- ZnO NPs, Ag-doped ZnO NPs, NiO NPs, and Ag-doped NiO NPs- in **Table** 8.

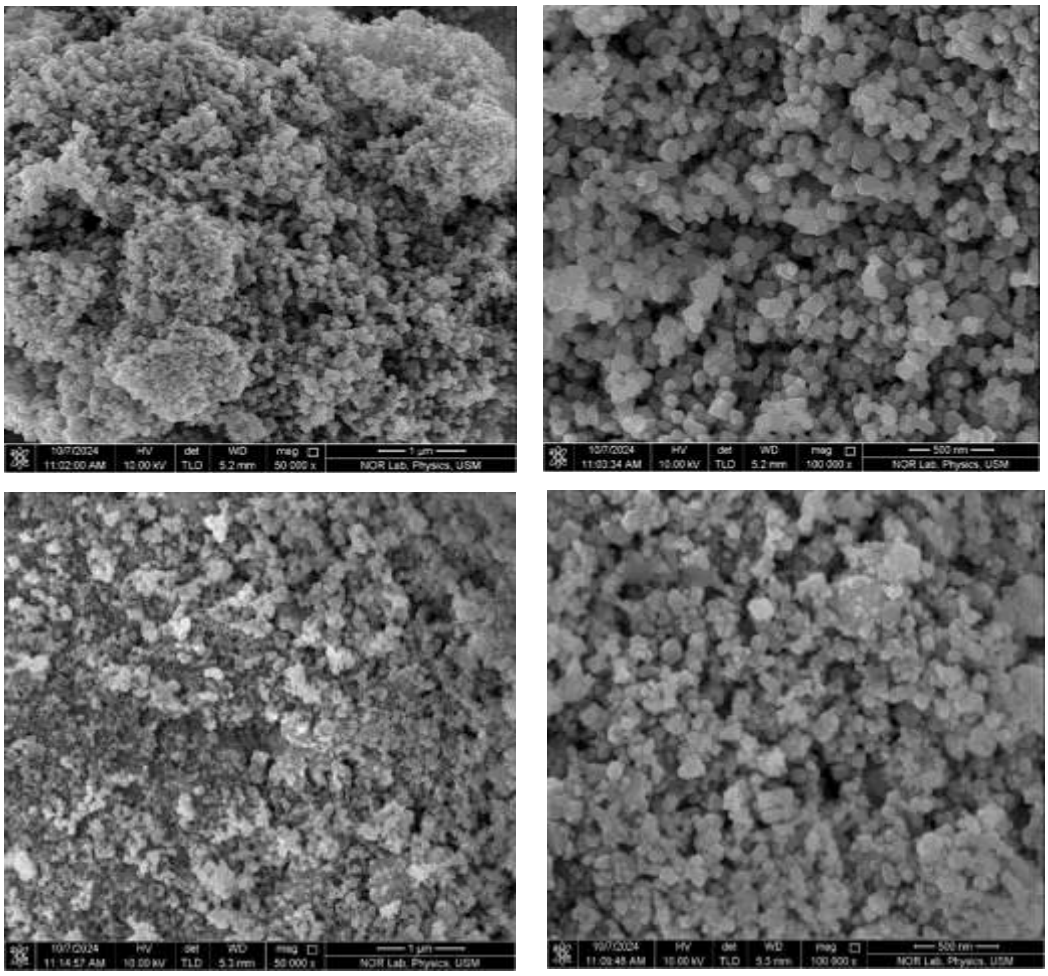

Figure 26: FESEM images of (a-b) NiO and (c-d) Ag-NiO NPs at magnification 50000x and 100000x.

Table 7: values the morphological parameters of the NiO and Ag-NiO nanoparticles.

Property	NiO NPs	Ag-NiO NPs
Particle Count	677	829
Total Area	9421.654 nm²	12380.003 nm²
Average size Area	13.917 nm^2	14.934 nm^2
Average particle Diameter	4.21 nm	4.36 nm
Circularity	0.952	0.947
Solidity	0.952	0.942

Significantly affects the morphology and surface characteristics of NiO nanoparticles, resulting in a higher particle count (829 vs. 677) and increasing the total occupied area from 9421.654 nm² to 12380.003 nm², suggesting better particle nucleation and lesser aggregation. The average particle size increases slightly, 14.934 nm versus 13.917 nm, with a marginally more significant perimeter, 12.118 nm versus 11.638 nm, reflecting less perfect spherical shapes due to Ag incorporation. Besides, a slight reduction of circularity, 0.947 versus 0.952, and solidity, 0.942 versus 0.952, reflects increased surface irregularities, most presumably induced by Ag atoms, which disturb the homogeneous growth of the particles. These morphological changes increase surface area and introduce structures that facilitate catalytic activity, sensing application, and energy storage as they enhance active sites, sensitivity, and efficient charge transfer.

4.3.5 Transmission Electron Microscope (TEM) Analysis

TEM analyses were conducted to determine the precise particle sizes of the synthesised ZnO and NiO and their silver nanoparticle-doped counterparts. **Figures** 27-28 show the prepared photocatalyst nanoparticles' TEM images at one micro, 200 nm, 100 nm, and 50 nm magnifications, highlighting their morphological characteristics. The nanoparticles appear to have a spherical shape in TEM images. **Table** 9 shows that the nanoparticles' diameter measurements were calculated from the surface average size (d_{surf}) [121]. The results of the study outperform many other studies.

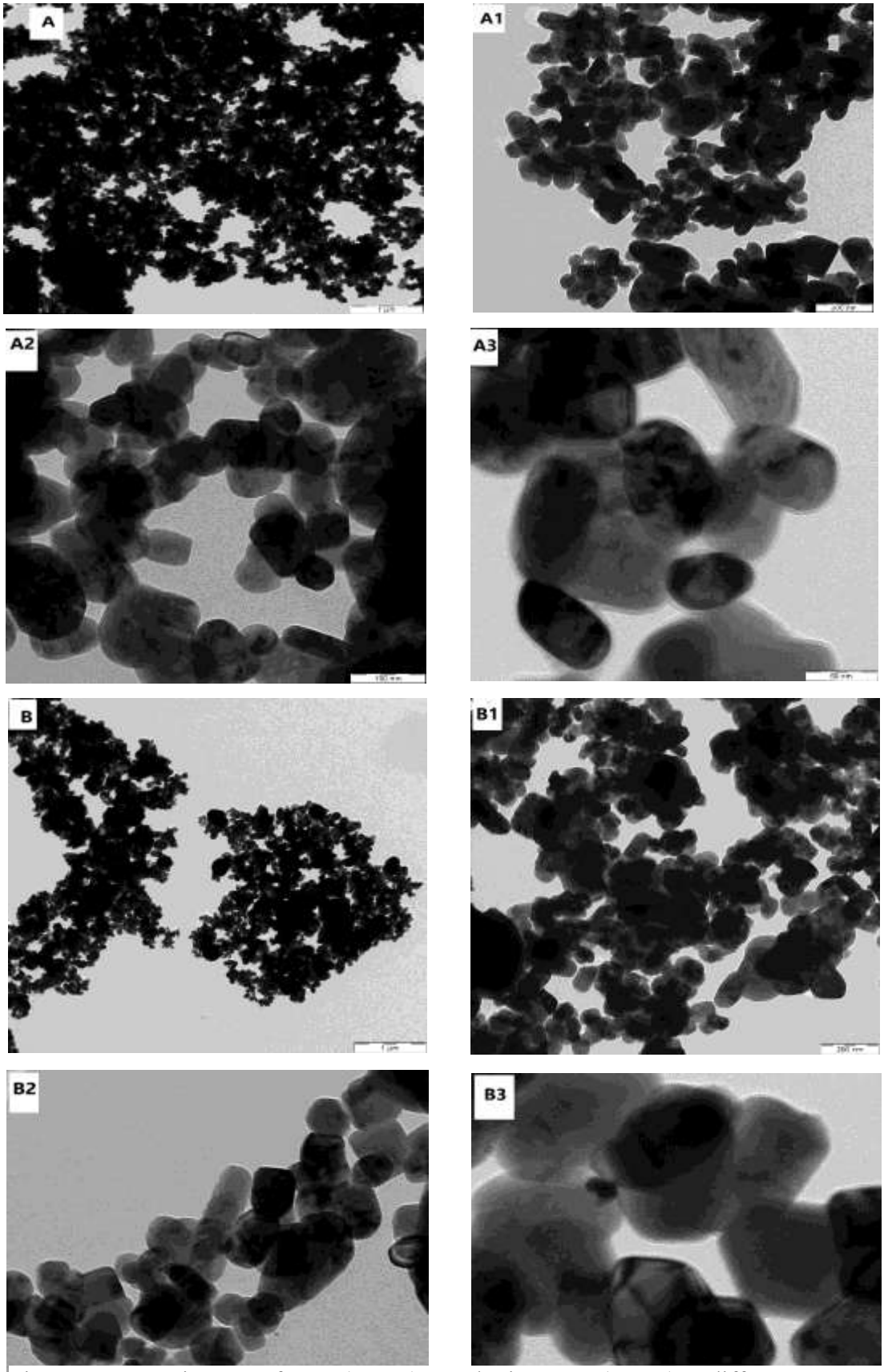

Figure 27: TEM images of ZnO (A, A3), Ag doping ZnO (B, B3) at different nanoscale.

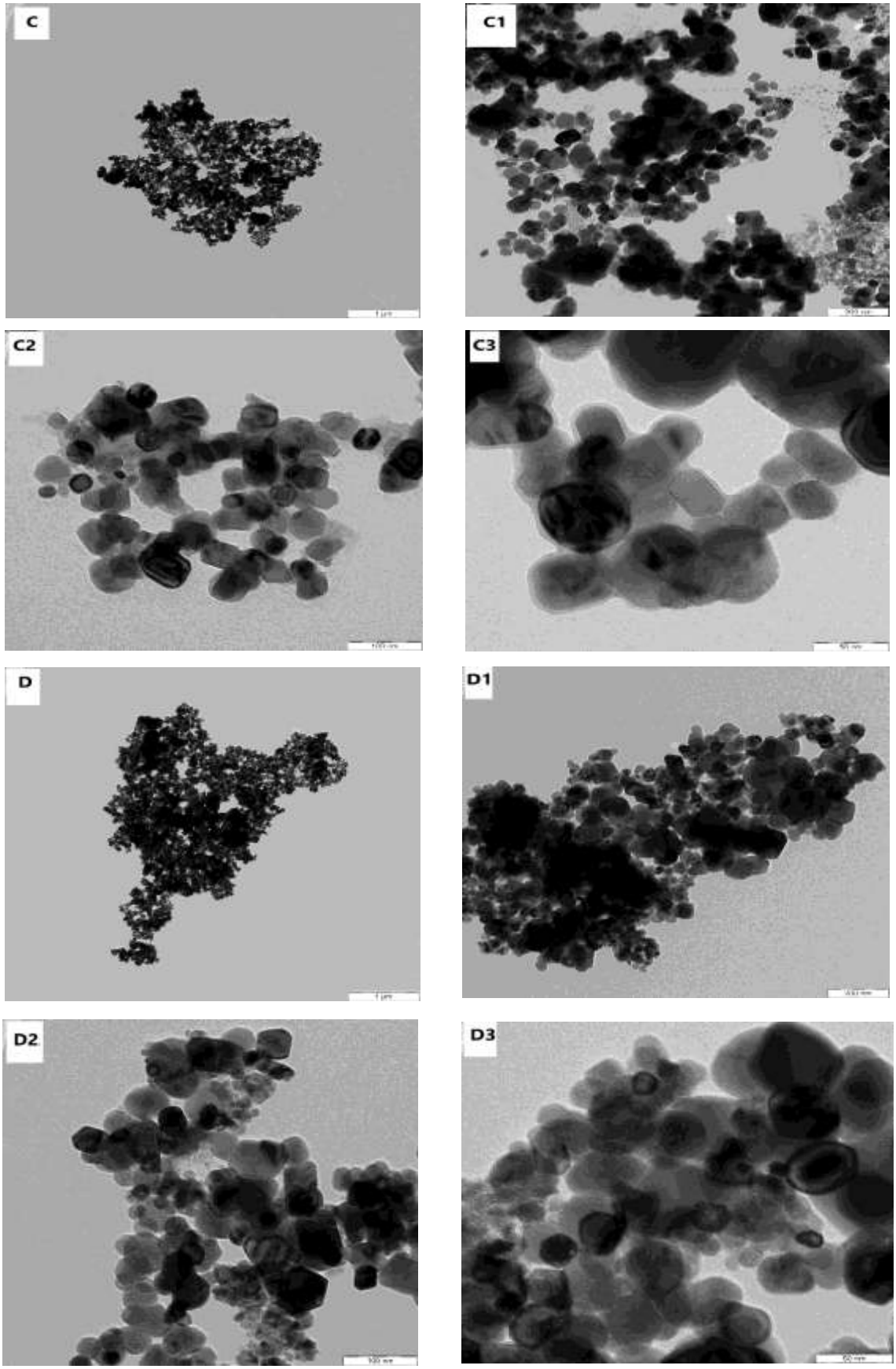

Figure 28: TEM images of NiO (C, C3), Ag doping NiO (D, D3) at different nanoscale.

Table 8: The nanoparticles' diameter of the prepared photocatalysts.

Photocatalyst	Morphology	Average Particle Diameter by TEM	Average Particle Diameter by FESEM
ZnO	Spherical	3.05 nm	4.46 nm
Ag-ZnO	Spherical	3.04 nm	4.35 nm
NiO	Spherical	3.34 nm	4.21 nm
Ag-NiO	Spherical	3.43 nm	4.36 nm

The photocatalysts synthesised in this study demonstrated spherical morphologies across all samples, as observed through TEM and FESEM analysis. The average particle diameter measured by TEM revealed that pure ZnO nanoparticles had the smallest size, averaging 3.05 nm, followed closely by Ag-ZnO (3.044 nm) and NiO (3.346 nm). The Ag doping NiO NPs exhibited a slightly larger particle size of 3.434 nm. These results, which highlight the impact of Ag doping on particle size, indicate that doping with Ag or combining NiO with Ag introduces minor changes to the particle size, likely due to the influence of dopant ions on the nucleation and growth dynamics during synthesis [120,121].

Similarly, FESEM measurements confirmed the nanoscale particle sizes, albeit with slightly larger diameters than TEM results. For instance, ZnO nanoparticles measured 4.46 nm on average via FESEM, while Ag-ZnO, NiO, and Ag-NiO recorded sizes of 4.35 nm, 4.21 nm, and 4.36 nm, respectively[6]. Compared to TEM, the minor size increase in FESEM is attributed to particle aggregation, a common occurrence in SEM analysis due to the high-resolution imaging of more significant sample regions [117].

The origin of the differences in the particle sizes obtained by SEM and TEM images can be understood from the sample supply step for these analyses. Some powders are usually utilised for an SEM analysis of powdered materials. The powder is stuck onto an SEM stub and coated by Au or other conductors for nonconductive materials. In the case of a TEM analysis, the desired material is usually suspended in a solvent by a high-power ultrasonic instrument to spread the sample well. Then, the suspension was put onto a TEM grid, and the solution was air-dried to obtain a thinly sliced sample. Therefore, the images obtained from TEM analysis have higher resolution, and the agglomerations could be distinguished with this instrument. In contrast, in an SEM image, the agglomerated particles are usually

observed with larger sizes. Hence, TEM analysis is the best technique to obtain the actual sizes of materials compared to SEM analysis, which is challenging to study real particle sizes[5]. It is noticed that to get the best size distribution using TEM analysis [117,118,119].

Comparing these findings with other studies, the particle sizes achieved here are notably smaller, particularly for green synthesis methods. This demonstrates the ability of natural capping agents to effectively limit particle growth, producing uniformly spherical and ultra-small nanoparticles. Furthermore, the small particle sizes observed here enhance the surface-to-volume ratio, a critical factor for photocatalytic efficiency. This aligns with findings from previous green synthesis studies, emphasising the advantages of eco-friendly methods in achieving high-quality nanomaterials.

4.4 Absorption Spectra Test of The Methylene Blue Dye

UV-vis spectroscopy analysis of various aqueous solutions of methylene blue dye demonstrated the peak absorption maximum at 665 nm. The relations among various concentrations of dyes versus their absorbances are in **Table** 10 and **Figure** 29. In this series, by increasing the dye concentration in water linearly, the absorbencies also increased according to the Beer-Lambert law. This linear relation refers to the fact that this spectrophotometric method is reliable for measurement. The plotted data and related graph serve as a sound basis for studying the degradation efficiency of methylene blue dye, employing the prepared photocatalysts for photocatalytic activity.

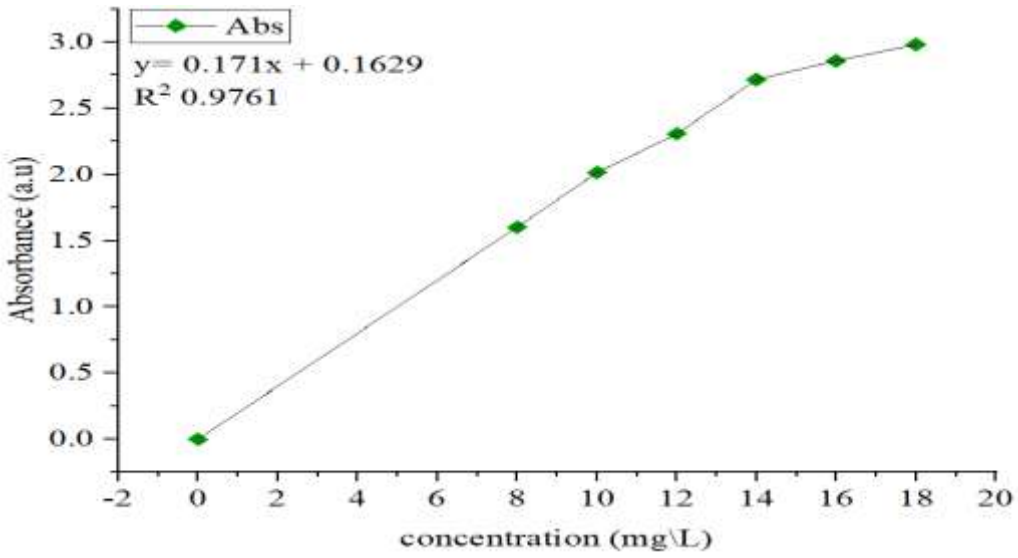

Figure 29: Calibration curve of methylene blue dye standard solution.

Table 9: The absorbance of standard aqueous methylene blue solutions.

No.	Sample	Concentration (ppm)	Absorbance
1	Blank	0	0
2	Standard 1	8	1.6
3	Standard 2	10	2.01
4	Standard 3	12	2.31
5	Standard 4	14	2.72
6	Standard 5	16	2.86
7	Standard 6	18	2.98

With increasing concentrations of **methylene blue**, there is a much greater chance for dimerisation because of the **π-π stacking** between the aromatic rings of individual methylene blue molecules. Thus, **dimers** are formed wherein two methylene blue molecules associate and interact, resulting in a much larger, extended conjugated system. As the concentration increases, so does the strength of the interactions between these molecules, leading to a more effective dimerisation process. This leads to dimerisation, causing a **red shift** of the absorption spectrum, shifting the absorption peak from around **660 nm** in its monomeric form to **665–750 nm** in its dimeric form. The change to the red region occurs because dimer formation extends the conjugated **π-system**, thus decreasing the energy of the electronic transition. Therefore, less energy will be required to excitation electrons [107].

By using high concentrations such as 8, 10, 12, 14, 16, and 18 ppm, one could realise how dimers gradually form in such a concentration range and observe how the absorption spectrum shifts. Such a concentration would, therefore, reveal the dependency of methylene blue in solution and hence will allow for determining beyond which the dye's threshold value will exhibit strong dimerisation and, importantly, alteration in its property upon increasing its concentration. The higher the concentration, the more the shifting in absorbance, hence giving more reliable information about the dependence on the concentration of molecular interactions of methylene blue, which includes aggregate or dimer formation [122]. This forms the basis for photocatalytic studies, where the photocatalytic degradation rate can depend on methylene blue's form and its interaction with the photocatalyst surface. For example, the interaction of dimers with photocatalysts can be different from monomers, thus generally influencing the photocatalytic process, and can infer the effects on concentration and acidity using concentrations ranging from 8 to 18 ppm.

At these concentrations, methylene blue can dimerise significantly, and variations in concentration help assess its interaction with the photocatalyst. The pH of the solution, protonation, and dimer formation can influence the charge state, affecting photocatalytic degradation rates. A study examining a concentration gradient from 8 ppm to 18 ppm can explore the combined effects of dimerisation, concentration, and acidity on photocatalytic efficiency. This approach may provide insights into optimising the photocatalytic degradation process based on methylene blue concentration and solution acidity.

4.5 Photocatalytic Activity Testing and Effect of Doping Silver NPs

4.5.1 Photocatalytic Activity of Photocatalysts Under Sunlight

The prepared photocatalytic activity was evaluated by photodegradation methylene blue (MB) aqueous solution under direct sunlight on clear sky days during June- July 2024 between 9.00 am and 12.00 pm, when the daily temperature was 30-35 C. Under ambient conditions, the solutions were exposed to sunlight for 140 min. Every 20 minutes, the reaction solutions were sampled, centrifuged, and filtered to remove the photocatalysts.

The degradation efficiency of MB is calculated for both samples by recording the absorption spectra of the test dye, finding the absorption intensity at the characteristic absorption peak at 665 nm, and adjusting Ph to 7 using a UV-Vis spectrophotometer, then quantifying the dye degradation rate. The UV-visible absorption spectra shown in **Figure** 30 of the four samples, where (a, b) represent the ZnO and Ag-ZnO NPs efficiency, respectively, and (c & d) represent the NiO and Ag-NiO NPs efficiency, respectively.

The results indicate that the Ag doping ZnO NPs had high photodegradation activity ZnO NPs, as shown in Figure 7, with a degradation rate of 74.62% and 98.32% for Ag doping ZnO NPs. The Ag doping NiO NPs also showed a high level of photodegradation activity, with degradation rates of 76.59% and 51.37% for NiO NPS, respectively.

Various factors reportedly enhanced the catalyst's photocatalytic action on the dye, including the catalyst's particle size, phase composition, shape, crystallinity, size distribution, surface area, and bandgap energy [43,54].

a

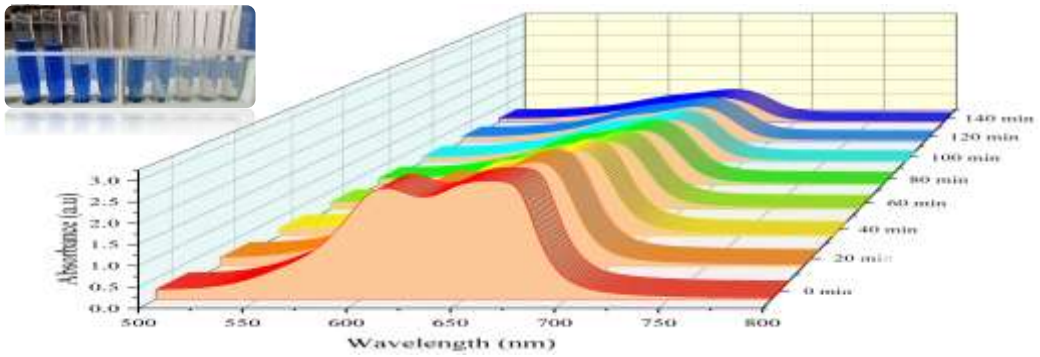

b

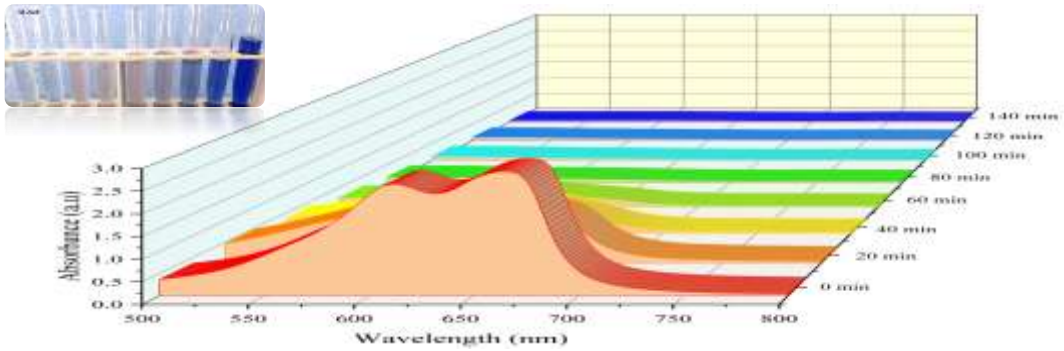

c

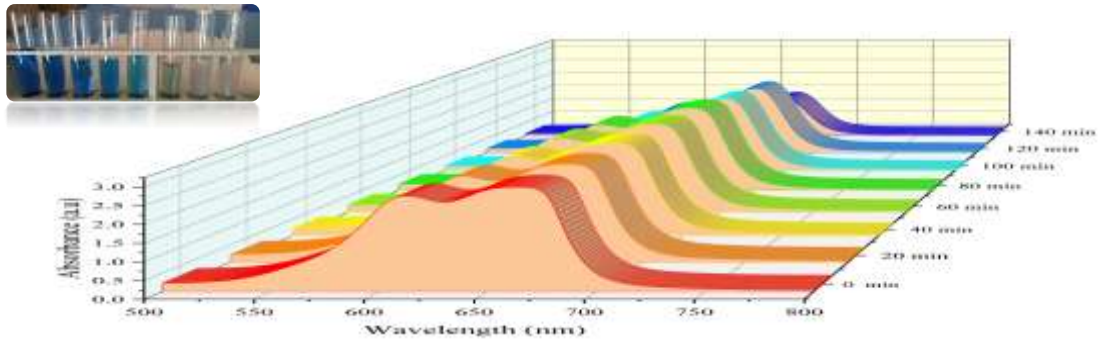

d

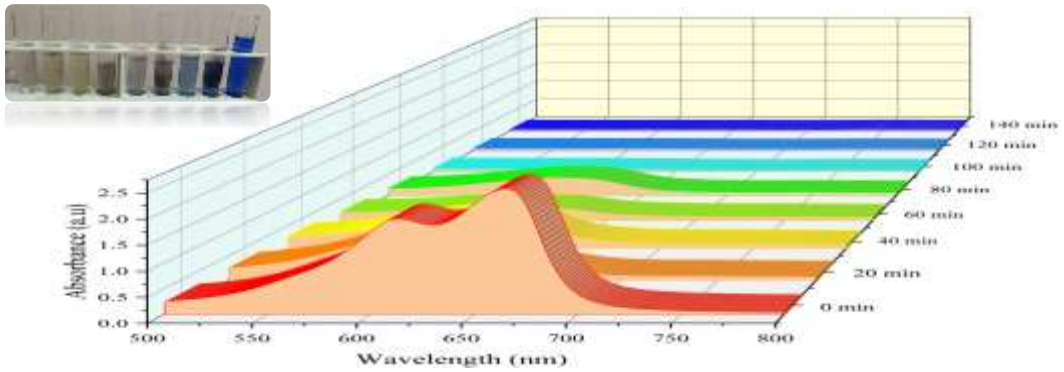

Figure 30: UV–visible spectra showing the reduction in the intensity of MB solution under sunlight irradiation by using ZnO NPs (a), Ag-ZnO NPs (b), (c) NiO NPs, and Ag-NiO NPs (d).

4.5.2 Photocatalytic Activity of Photocatalysts Under UV Light

Figure 31 displays the two samples (a, b) representing the efficiency of the ZnO and Ag-ZnO NPs. Figure 32 shows (c, d) representing the efficiency of the NiO and Ag-NiO NPs, respectively. Such improved photocatalytic activity of Ag-doped ZnO and NiO NPs upon UV light irradiation is believed to be due to the enhanced charge carrier dynamics, LSPR of Ag, and a slight bandgap reduction. Ag NPs doping of photocatalysts generates defect states that trap the charge carriers, reducing recombination and improving the formation of ROS, which is crucial for the degradation of pollutants [46].

Therefore, Ag-doped ZnO degraded with the efficiency of 55.87%. For reference, pure ZnO had deteriorated by 52.68%, and Ag-doped NiO was 45.34% effective compared to 42.71% of pure NiO, proving that Ag significantly improved the material's photocatalytic activity. Photodegradation efficiencies matched reported work by other authors [44,45,47], wherein Ag-doped ZnO nanoparticles exhibited high photocatalytic efficiency under sunlight and UV light.

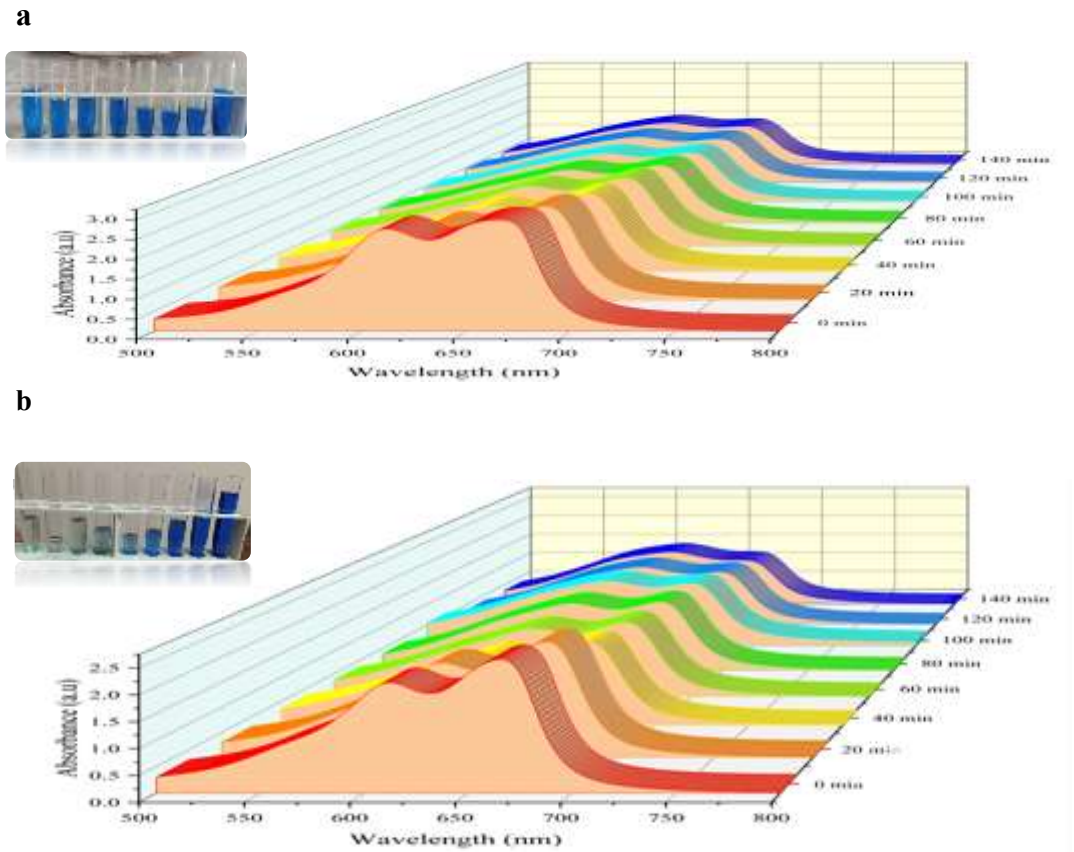

Figure 31: UV-visible spectra showing the reduction in the intensity of MB solution under UV light irradiation using ZnO NPs (a) and Ag-ZnO NPs (b).

a

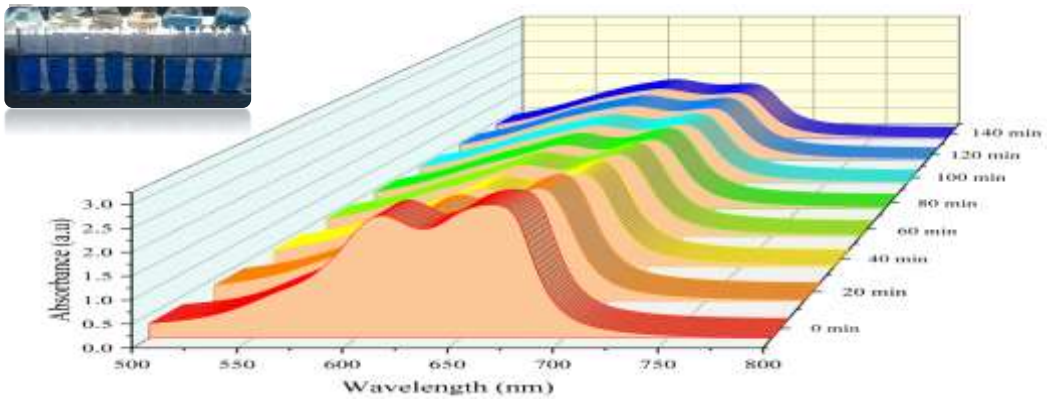

b

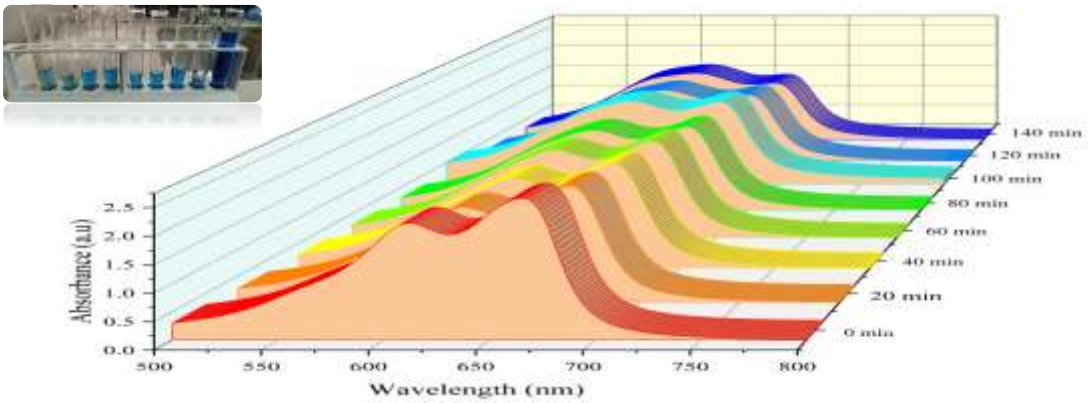

Figure 32: UV-visible spectra showing the reduction in the intensity of MB solution under UV light irradiation using NiO NPs (a) and Ag-NiO NPs (b).

4.5.3 Photocatalytic Activity of Photocatalysts in Dark Conditions

The photocatalytic efficiency of the synthesised catalysts under dark conditions was studied to examine their capacities of adsorption and their intrinsic catalytic activities in the absence of illumination. In **Figure** 33 below, it can be observed that without light, the degradation of the organic dye pollutant barely occurred. This finding is further supported by **Table** 10, which presents that without light activation being essential to excite the photocatalyst and form reactive species able to destroy the dye, the degradation process practically does not occur.

However, significant adsorption of pollutant molecules onto the photocatalyst surface was observed, which coincides with literature reports [1,2,21]. This implies that the catalyst

surface has a strong affinity for pollutant molecules, which is quite helpful in the photocatalytic action under illuminated conditions. This observed adsorption can be ascribed to the high surface area and active sites on the catalyst surface, which allow pollutant molecules to accumulate before photodegradation [3]. Such adsorption characteristics agree with reports showing the importance of pollutant-catalyst interactions in the dark phase as a precursor to enhanced photocatalytic efficiency [4]. These results illuminate the dual role of the photocatalyst surface in adsorption and photocatalysis, providing valuable insight into optimising material design for environmental remediation applications.

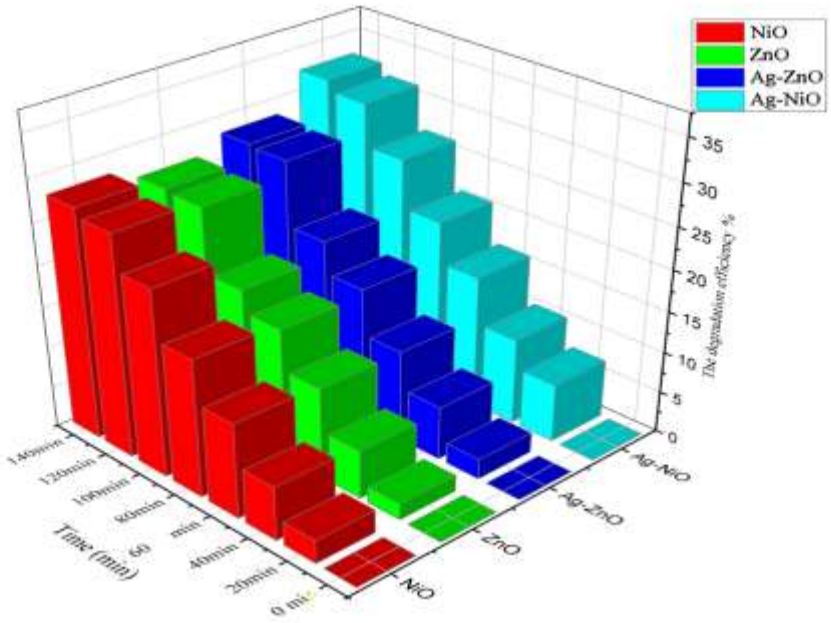

Figure 33: UV-visible spectra showing the reduction in the intensity of MB solution in dark conditions using ZnO, Ag-NiO, NiO NPs, and Ag-NiO NPs.

4.5.4 The Degradation Reaction Kinetics of (MB) Under Sunlight

The reaction rate was determined from the slope of the linear relation between plotting $\ln(A_0/A_t)$ against irradiation time, as shown in **Figure** 34. The kinetics observed tend to a pseudo-first-order reaction profile. The calculated rate constants, k, were 0.01, 0.0052, 0.0263, and 0.0104 min^{-1} for pure ZnO, NiO, and ZnO: NiO co-doped with Ag nanoparticles. Indeed, the results also showed that with the presence of silver nanoparticles, there is an enhanced reaction rate, proving its effect on efficient dye degradation in an aqueous environment [84].

The calculated values of the reaction rate constant, k, for the different samples—pure ZnO, NiO, and ZnO: NiO doped with Ag NPs are given in **Table** 11 below. The optimal concentration of silver dopant may have played a role in achieving these photocatalytic results. Energy characterisation indicates that oxygen vacancies were mainly generated with new energy levels that act as electron traps. This decreases the recombination of charge carriers and promotes higher photocatalytic activities.

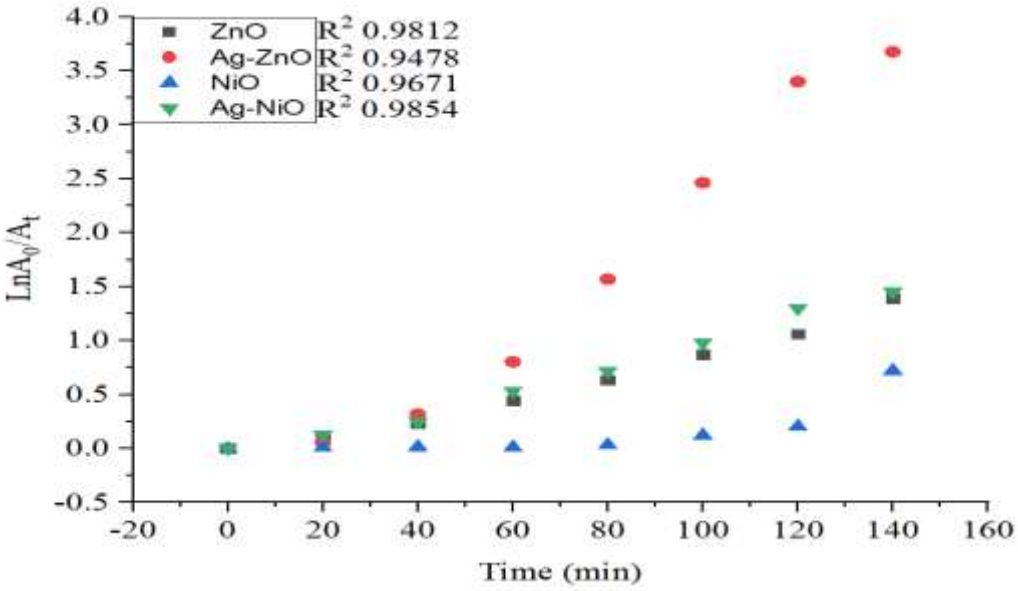

Figure 34: The Degradation Reaction Kinetics of (MB) Under Sunlight of prepared photocatalysts.

Silver nanoparticles dope photocatalysts, increasing the photocatalytic activity due to their surface plasmon resonance effect, which enhances light absorption and generates more reactive species. This increase in the degradation rate constant (k) will directly reduce the half-life ($t_{1/2}$) of dye degradation and, hence, increase the degradation rate.

Table 10: K pseudo-first-order rate constant values of prepared photocatalysts.

Photocatalysts	K (min^{-1})	t ½ (min)	R^2
ZnO	0.00995	69.69	0.9912
Ag-ZnO	0.02626	26.39	0.9478
NiO	0.00515	134.57	0.9671
Ag-NiO	0.01037	66.82	0.9458

4.5.5 The Degradation Reaction Kinetics of (MB) Under UV Light

The photocatalytic efficiencies of UV light-irradiated ZnO, Ag-ZnO, NiO, and Ag-NiO nanoparticles show significant differences in their degradation kinetics, as illustrated in **Figure** 35.

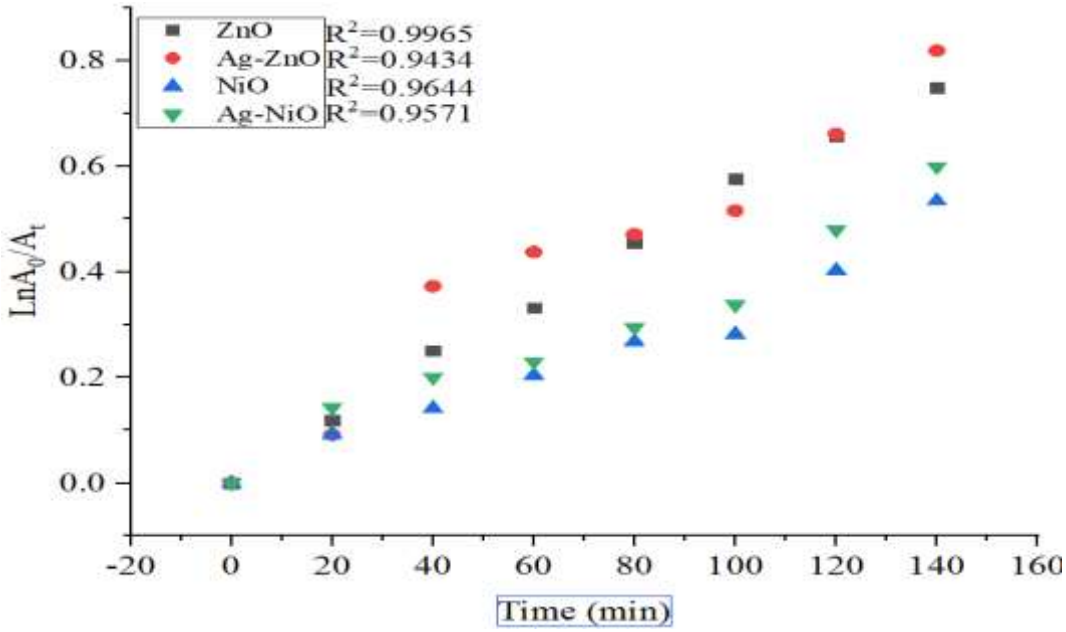

Figure 35: The Degradation Reaction Kinetics of (MB) Under UV light of prepared photocatalysts.

Table 12 shows the rate of the degradation reaction and half-time of the MB dye by using Ag-ZnO nanoparticles as a photocatalyst. Indeed, for this material, a maximum rate constant was obtained, with a value of k = 0.00584 min^{-1}, and correspondingly, the minimum half-life, t½ = 118.6 min, illustrating its superior photocatalytic activity. This can be explained by adding silver, which enhances the charge carrier separation and surface plasmon resonance and, finally, enhances the efficiency of the degradation reactions. While the photocatalytic activities of ZnO nanoparticles were low, having a rate constant of 0.00535 min^{-1} and half-time of 129.66 min, it could be attributed to the undoped condition with silver. The NiO nanoparticles showed the lowest photocatalytic efficiency with a rate constant of 0.00381 min^{-1} and a half-time of 181.80 min. This is probably due to the poor mobility of charge carriers and sluggish reaction kinetics under UV irradiation.

The Ag-NiO nanoparticles exhibited moderate photocatalytic performance, with a rate constant of 0.00428 min^{-1} and a half-life of 162.06 min. Although silver doping improved their performance, it remains inferior to the ZnO-based systems. These results emphasise the critical role of doping and material type in influencing photocatalytic activity under UV light exposure [1,38].

Table 11: K pseudo-first-order rate constant values of prepared photocatalysts.

Photocatalysts	K (min^{-1})	t ½ (min)	R^2
ZnO	0.00535	129.65	0.9965
Ag-ZnO	0.00584	118.60	0.9434
NiO	0.00381	181.80	0.9644
Ag-NiO	0.00428	162.05	0.9571

4.5.6 The Degradation Reaction Kinetics of (MB) Under Dark Conditions

Figure 36 presents the relationship between $\ln(A_0/A_t)$ and time for the degradation of methylene blue under dark conditions for all photocatalysts. The figure shows that all catalysts show a linear trend, confirming that the response follows pseudo-first-order kinetics since the slope of each line gives a value of the rate constant, K.

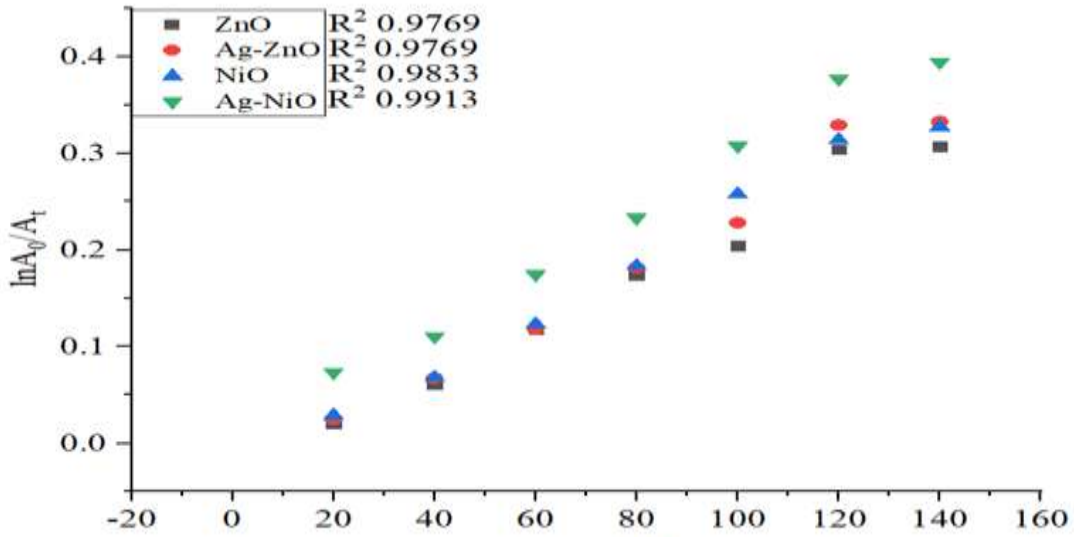

Figure 36: The Degradation Reaction Kinetics of (MB) in Dark Conditions of prepared photocatalysts.

ZnO has the least steep slope, corresponding to the lowest rate constant (k=0.002193 min^{-1}), representing the slowest degradation rate. Ag-ZnO shows a slightly steeper slope, k=0.002375 min^{-1}, reflecting an improved performance due to the electron-trapping properties of Ag. NiO also exhibits moderate activity, k=0.002337min^{-1}, with a slope similar to Ag-ZnO. Ag-NiO exhibited a steeper slope, with k=0.002816min^{-1} indicating the fastest degradation rate probably because of the synergistic effect of Ag doping and redox capability of NiO. These results also agree with the rate constant values calculated from **Table** 13, further confirming that Ag-NiO exhibits higher catalytic activity than other materials.

Table 12: K pseudo-first-order rate constant values of prepared photocatalysts.

Photocatalysts	K (min^{-1})	t ½ (min)	R^2
ZnO	0.00219	316.03	0.9769
Ag-ZnO	0.00237	291.8	0.9769
NiO	0.00233	296.63	0.9833
Ag-NiO	0.00281	246.1	0.9913

Figure 36 presents the plot of ln (A_0/A_t) as a function of time for the dark degradation of methylene blue, representing the pseudo-first-order kinetics of the reaction on each used photocatalyst. Linearity for all catalysts ensures that pseudo-first-order kinetics has been followed; the slope for each straight line is exactly k (rate constant) corresponding to the slope. Among the catalysts considered, ZnO exhibited the least steep slope, indicating the lowest rate constant, k = 0.002193 min^{-1}, representing a relatively slow degradation rate. In contrast, Ag-ZnO showed a somewhat steeper slope with a k value of 0.002375 min^{-1}, reflecting the improvement in its degradation performance brought about by the electron-trapping efficiency of silver. Among them, NiO has moderate catalytic activity with k = 0.002337 min^{-1}, whose slope is as steep as Ag-ZnO.

The highest slope was obtained for Ag-NiO, k = 0.002816 min^{-1}, corresponding to the fastest degradation rate. The synergistic effects of Ag doping and NiO natural redox properties can explain the improved performance. These observations are further confirmed

by the calculated values of the rate constant presented in **Table** 13, which shows that Ag-NiO exhibits higher catalytic activities than other photocatalytic materials tested.

4.5.7 Factors Affecting Photocatalytic Activity

4.5.7.1 Effect of Irradiation Time on Degradation Efficiency (%)

Figure 37 shows the degradation efficiency (%) versus irradiation time under sunlight, indicating performance differences between ZnO, Ag-ZnO, NiO, and Ag-NiO. Because of the limited visible light absorption, the lowest efficiency of ZnO is 75.15% after 140 minutes. Ag-ZnO shows a much higher efficiency of 97.47% within the same time due to the Ag LSPR effect, enhancing visible light absorption and charge separation. NiO exhibits mediocre activity with a maximum of 51.38% at 140 minutes, reflecting the intrinsic redox properties.

In contrast, Ag-NiO reaches 76.60% degradation, higher than that of ZnO and NiO, especially in the early stages of the reaction, due to the synergistic effect of Ag doping and the redox capability of NiO [114,123]. **Figure** 37 shows that Ag doping enhances the photocatalytic activity of materials, specifically Ag-ZnO and Ag-NiO, under sunlight irradiation compared to their undoped form.

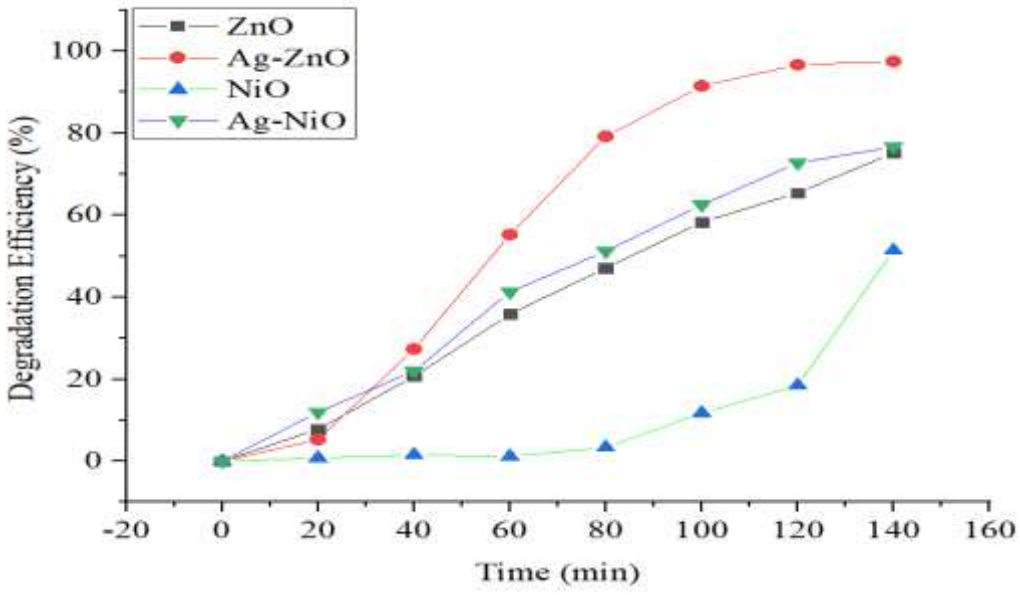

Figure 37: Effect of Irradiation time on the Degradation of MB dye by prepared photocatalysts.

4.5.7.2 Effect of pH on Degradation Efficiency (%)

Figure 38 depicts that the degradation efficiency of ZnO, Ag-ZnO, NiO, and Ag-NiO shows a significant variation with pH, generally showing an increasing efficiency as the pH rises from acidic to alkaline conditions. The efficiencies for ZnO increase gradually from 26.44% at pH 3 to 98.33% at pH 12. In the case of NiO, though it increased along a similar trend, it was worse in acidic conditions, with a gradually increased efficiency from 23.23% at pH 3 to 98.29% at pH 12. This can be explained by the fact that more hydroxyl radicals are generated, and the separation of electron-hole pairs is favoured in alkaline conditions, which applies to what he received from the hydroxyl ions (OH^-) improve the degradation reaction of MB in the alkaline medium, leading to higher photocatalytic activity [7,84]. Ag doping considerably enhances ZnO and NiO degradation efficiency [114,123], especially at low pH. For example, the efficiency at pH 3 is 96.53% for Ag-ZnO, whereas, in the case of pure ZnO, it was only 26.44%. The observed improvement in photocatalytic activity can be attributed to silver nanoparticles induced by the surface plasmon resonance (SPR) effect. Enhancing the light absorption by Ag nanoparticles, acting as an electron sink that reduces the recombination rate, and enhancing charge carrier separation [7,69]. Similarly, Ag-NiO outperforms pure NiO at all pH values, increasing from 62.85% at pH 3 to 98.59% at pH 12. Among all the materials, Ag-ZnO exhibits the highest efficiency in the whole pH range, with a more than 96% value. This demonstrates its superior photoactivity and stability across a broad pH spectrum. Thus, it is an ideal candidate for applications related to environmental concerns under broad pH conditions**.**

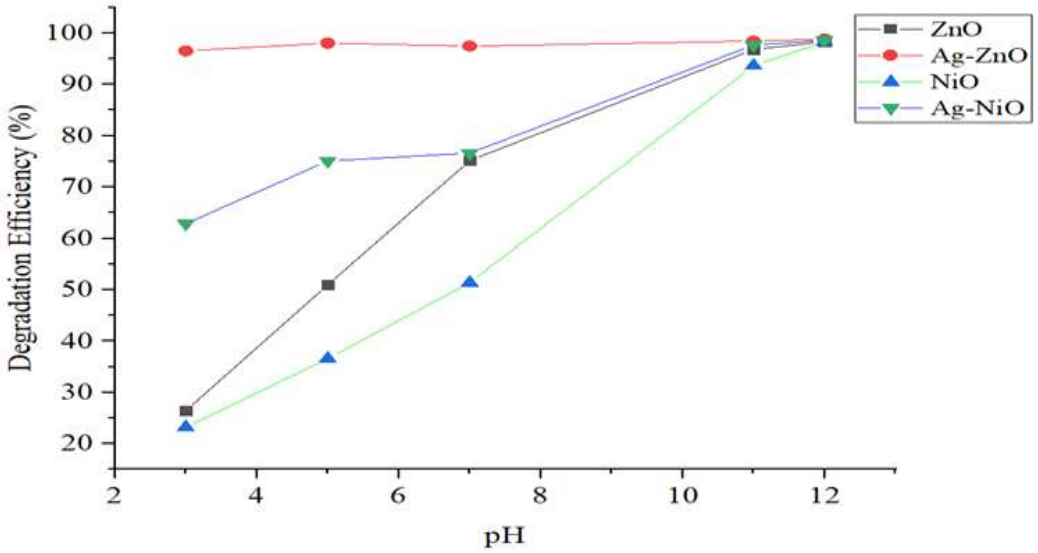

Figure 38: Effect of pH on methylene blue degradation Efficiency (%) using prepared photocatalysts.

4.5.7.3 Effect of MB Dye Dose on Degradation Efficiency (%)

Figure 39 illustrates that the **degradation efficiency (%)** of **ZnO, Ag-ZnO, NiO**, and **Ag-NiO** decreases with increasing catalyst dosage from **20 to 40 mg/L** [7,84,114]. In the case of ZnO, it decreases from **98.33%** at **20 mg/L** to **93.26%** at **40 mg/L**, while for Ag-ZnO, it decreases, though at a higher efficiency across all dosages, starting from **98.81%** and going down to **94.67%**. Of the three, the NiO exhibits the most significant decline. The efficiency was reduced from **98.29%** to **84.51%** from **20** to **40 mg/L** dosing, indicating that it has lower capacity and fails to maintain higher dosages. The **Ag-NiO** also followed a decreasing trend but exhibited better performances than **NiO**, while **Ag-NiO** showed **92.13%** at **40 mg/L**. This may be because increasing the photocatalyst dosage leads to an excessive concentration of catalyst particles, which causes light-scattering phenomena and reduces light penetration into the solution, limiting the generation of reactive species. Among all materials, **Ag-ZnO** performed better, again indicative of its superior **photocatalytic activity** and **stability** at different dosages**.**

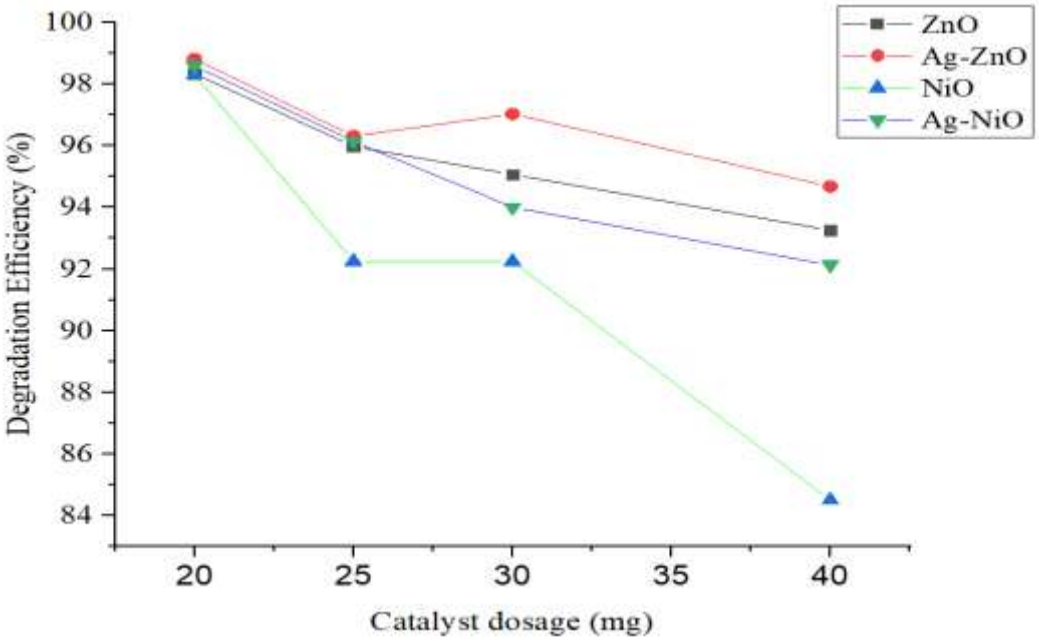

Figure 39: Effect of Dye dose on Degradation Efficiency (%).

4.6 Reusability of Prepared Photocatalysts

4.6.1 Reusability of Pure ZnO and Ag-ZnO Nanoparticles as Photocatalysts

Figures 40 and **41** show the photocatalytic performance of ZnO and Ag-ZnO, respectively, illustrating the relationship between time and **degradation efficiency (%)**, an explanation of which is given in the significant enhancement achieved through Ag doping [38,39,66,114]. For ZnO, the highest degradation efficiency was about **98.33%** at 140 minutes in the first cycle, while it showed a noticeable drop in subsequent cycles with lower starting efficiencies and reduced stability over time. In contrast, **Ag-ZnO** had the highest activity for all three cycles, with **98.81%** degradation at **140 minutes** in the first cycle and a high efficiency of **97.13%** in the third cycle. This can be ascribed to increased stability and efficiency due to Ag doping effects such as enhanced light absorption through the localised surface plasmon resonance effect, effective charge separation, and decreased electron-hole recombination. Also, the initial efficiency of **Ag-ZnO** was higher than that of **ZnO** for shorter times, showing faster degradation kinetics. These results conclude that **Ag-ZnO** has higher photocatalytic activity, reusability, efficiency and sustainability as a catalyst for pollutant degradation than **ZnO**.

Figures 40 and **41** illustrate the photocatalytic efficiency of ZnO and Ag-doped ZnO (Ag-ZnO) in terms of **degradation efficiency (%)** over time. Ag doping significantly boosts performance; pristine ZnO achieves a maximum degradation of **98.33%** after **140 minutes** in the first cycle but shows a notable decline in subsequent cycles. In contrast, Ag-ZnO maintains high activity across all cycles, reaching **98.81%** degradation after **140 minutes** in the first cycle and retaining **97.13%** by the third cycle. This enhanced stability and efficiency is attributed to improved light absorption from the LSPR effect, better charge separation, and reduced electron-hole recombination rates [24,56]. **Ag-ZnO** also shows higher initial degradation efficiencies, even at shorter reaction times.

Considering the mentioned facts, Ag-ZnO photocatalytic activity and recyclability exceed ZnO; thus, it is more effective and applicable in actual pollutant degradation.

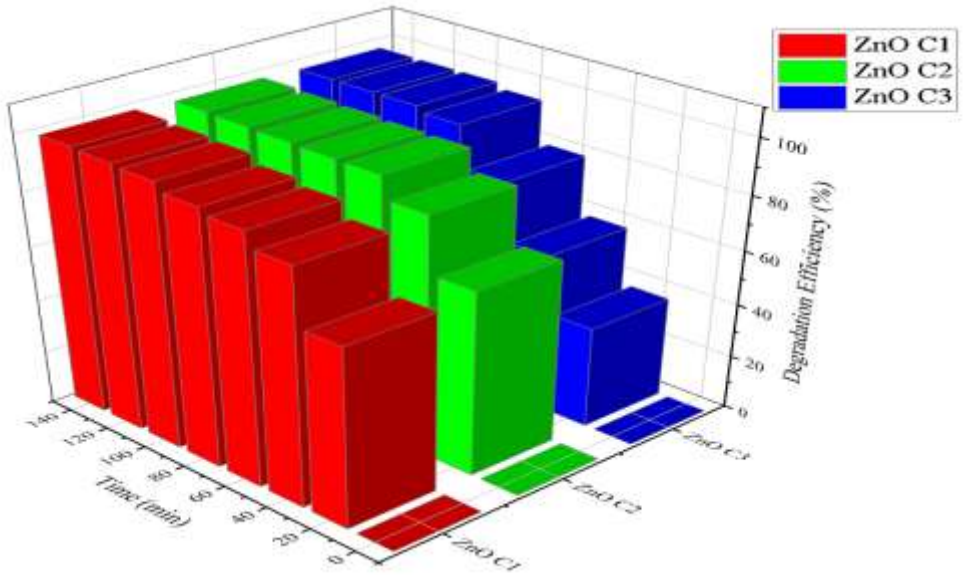

Figure 40: Recyclability of ZnO NPs for the degradation of MB in three cycles under solar irradiation.

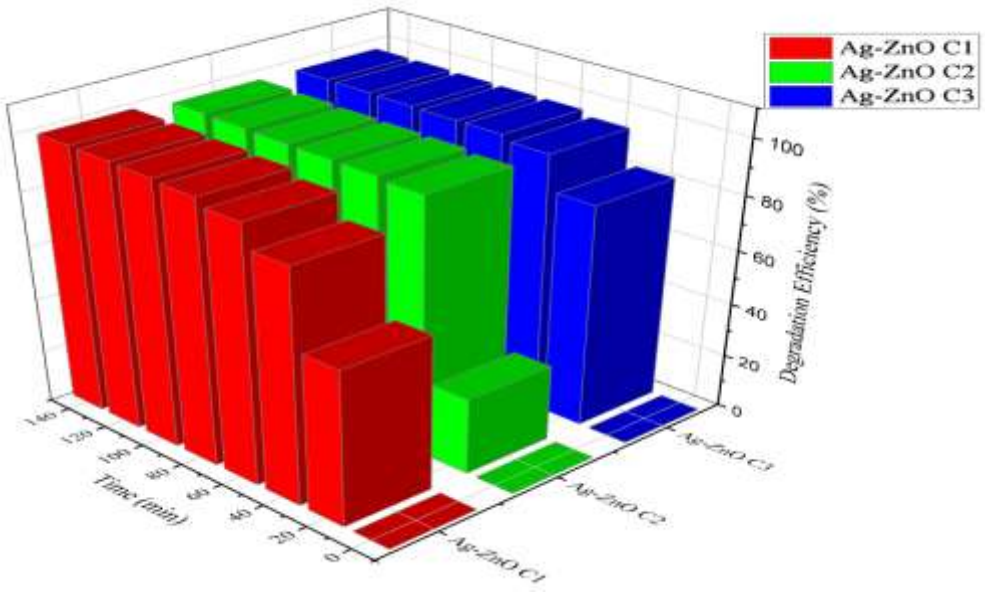

Figure 41: Recyclability of Ag-ZnO NPs for the degradation of MB in three cycles under solar irradiation.

4.6.2 Reusability of Pure NiO and Ag-NiO Nanoparticles as Photocatalysts

Figures 42 and **43** depict the reusability results comparing the catalytic performances of **NiO** and **Ag-NiO** over three cycles, respectively. Figure 41: In the case of **NiO**, there is an increase in the efficiency of degradation as time progresses, with slight variation between cycles in each cycle, thus showing stability in catalytic activity [84]. This peaks at about **98%** at **140 minutes** for all three cycles, showing excellent reusability.

Figure 43 highlights the activity of **Ag-NiO**, which manifests faster degradation kinetics compared to **NiO**. Indeed, higher efficiencies are recorded during the reaction's early stages. The efficiency in **Ag-NiO** reaches its maximum **(~98.6%)** earlier, around **100-120 min**. However, a slight decrease in performance during the second and third cycles, particularly in the earlier time intervals, is present, probably due to surface fouling or partial deactivation of the catalyst [69].

The comparison of the discussion between Figure **42** and Figure **43** highlights that **Ag-NiO** exhibits superior initial activity and faster kinetics owing to the enhancement of Ag doping. At the same time, **NiO** showed superior cycle performance, proving long-term strong reusability.

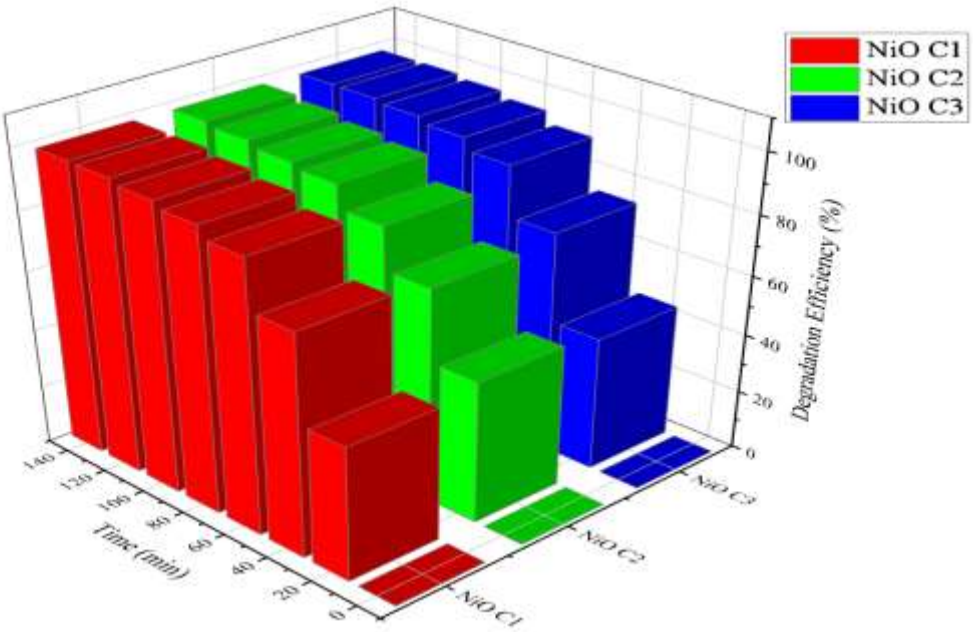

Figure 42: Recyclability of NiO NPs for the degradation of MB in three cycles under solar irradiation.

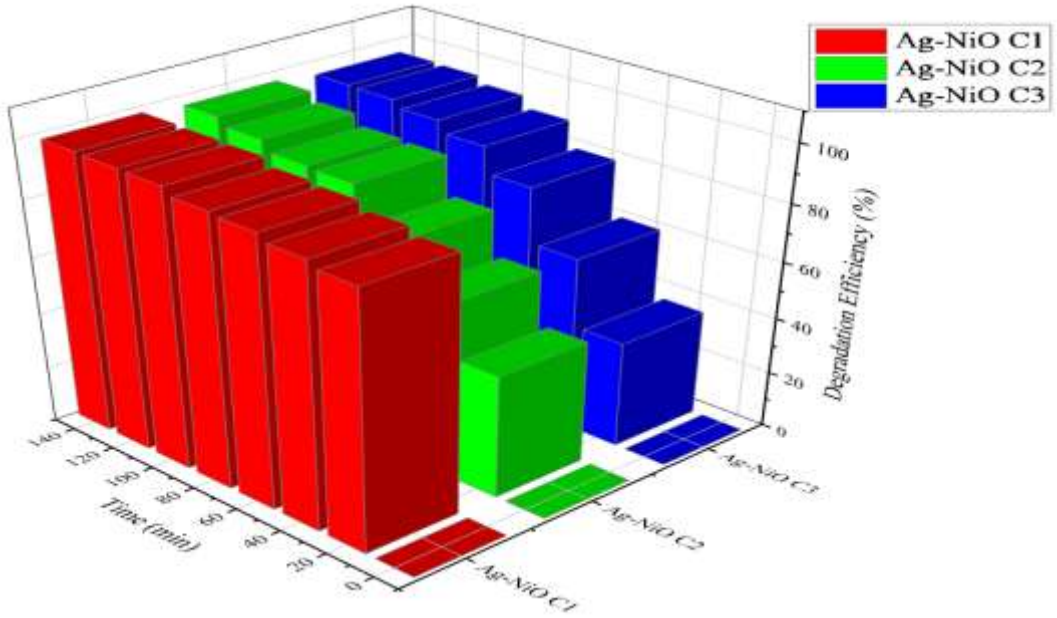

Figure 43: Recyclability of Ag-NiO NPs for the degradation of MB in three cycles under solar irradiation.

4.7 Photodegradation Mechanism of Methylene Blue as an Organic Pollutant

Pure ZnO and Pure NiO:

- **UV Light:** Pure photocatalysts are excited by UV light, promoting electrons from the VB to the CB, where electron-hole pairs are formed. However, in undoped systems, this kind of carrier recombines faster, eventually reducing the photocatalytic performance.
- **Visible Light:** Photocatalysts with wide bandgaps can absorb visible light, but recombination rates remain high without further modification [77,84].

Ag-Doped ZnO (Ag-ZnO) and Ag-Doped NiO (Ag-NiO):

- **UV Light:** Photogenerated electrons in the photocatalysts, CB, are transferred to the Ag nanoparticles because of the lower Fermi level in the Ag-doped semiconductors. This traps them and prohibits their recombination with the holes in VB, thus improving the charge separation and photocatalytic efficiency.
- **Visible Light:** Semiconductor Ag nanoparticles absorb visible light through the LSPR. These "hot electrons" are excited and may be transferred to the

semiconductors' CB, extending the photocatalytic activity into the visible spectrum [38,56,69,123].

Figure 44 shows the Photodegradation mechanism of **ZnO NPs** after doping with silver nanoparticles in UV light and Visible light (from sunlight). The degradation reaction of methylene blue (MB) by **ZnO** and **NiO** nanoparticles (NPs) involves reactive **oxygen species (ROS)** formation through a series of reactions influenced by **bandgap** and **Fermi level** positioning [38]. Pure ZnO, with a bandgap of **3.30 eV**, experiences fast electron-hole recombination [66], resulting in a degradation efficiency of **74.62%**. Doping ZnO with Ag lowers the bandgap to **3.15 eV**, creating a Schottky junction that enhances electron transfer and reduces recombination, increasing efficiency to **98.32%.** NiO, a p-type semiconductor with a bandgap of **3.16 eV**, generates holes that oxidise **MB**, while electrons form superoxide radicals. Ag doping reduces its bandgap to **3.13 eV**, improving light absorption and creating a similar Schottky junction that enhances charge separation [75]. **Ag's localised surface plasmon resonance (SPR)** effect also boosts **ROS** production and degradation efficiency [69,125].

Overall, the shifts in Fermi levels, Schottky junction formation, and improved charge separation through Ag doping enhance **ZnO** and **NiO** photocatalytic activity for **MB degradation**.

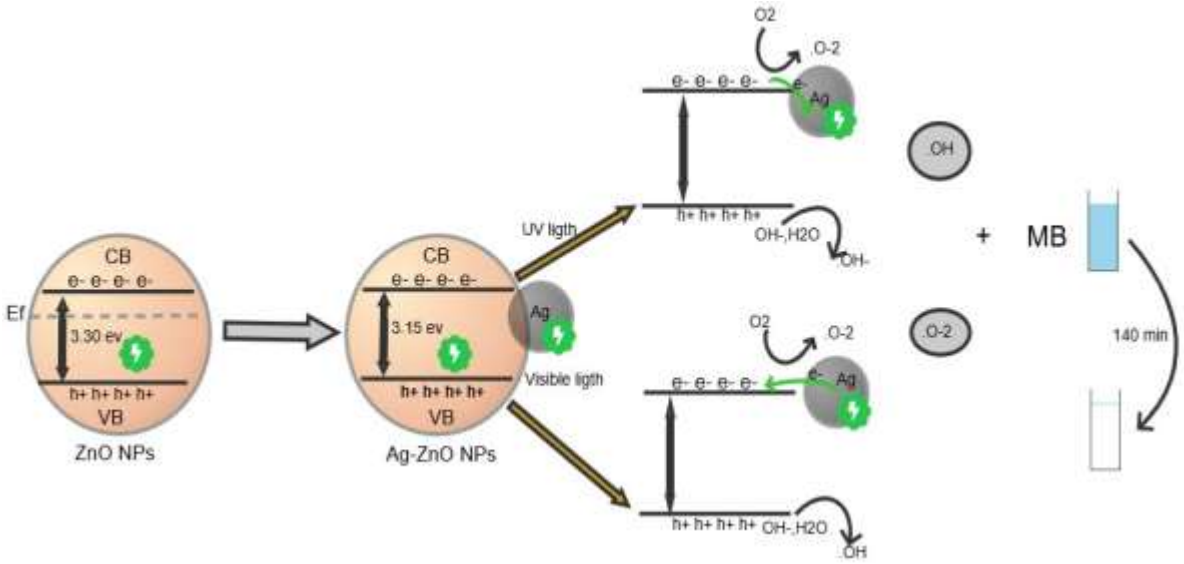

Figure 44: Photodegradation Mechanism of ZnO NPs after doping with silver NPs.

4.8 Comparison of Photocatalytic Activity of Pure ZnO and NiO NPs and when Doped by Silver NPs: Improved Size, Morphology, and Methylene Blue Degradation in Sunlight.

Table 14 Compared to the literature studies, in this study, synthesised pure **ZnO**, **NiO**, and Ag-doped nanoparticles are much smaller in size **(~3 nm)** compared to the literature **(10–87 nm)**, making them more photocatalytic activity for many reasons for their higher surface area and better charge separation. While previously, **ZnO NPs** exhibited degradation efficiencies of **48%–88%** under **UV** and **sunlight** [1–5], in this study, **ZnO NPs** exhibited **52.68% (UV)** and **74.62% (sunlight)**, which performed equally well despite their smaller size. Likewise, Ag-ZnO NPs exhibited the highest efficiency, possessing **55.87% (UV)** and **98.32% (sunlight)**, outperforming previous **Ag-ZnO** research **(87% under UV)** [8]. For the case of NiO and Ag-NiO NPs, our samples also showed good performances, with NiO up to **51.37% (sunlight)** and **Ag-NiO 76.59% (sunlight)**, which is better than the earlier **Ag-NiO NPs (50% under UV)** [6,7,9]. This shows that the smaller nanoparticle size, spherical shape and doping **ZnO** and **NiO NPs** with **Ag NPs** significantly contribute to improved photocatalytic activity in the degradation reaction of **MB dye**, especially under sunlight conditions and higher concentration of organic dye, making my synthesised materials more efficient and sustainable for environmental applications.

Table 13: comparison of synthesised photocatalysts in photocatalytic activity with other studies.

Photocatalyst	Size	Shape	pollutant	Light source	E%	R
ZnO NPs	19.45 nm	Nanoflower	MB	Sun/270 min	88%	[79]
ZnO NPs	20 nm	Hexagonal	MB	UV/48 min	48%	[80]
ZnO NPs	By 10g/60-80 nm	Flaky	MB	UV/120 min	55%	[81]
	By 20g/8-12 nm	Spherical			<55%	
	By 30g/8-10 nm	Spherical			81%	
NiO NPs	10.5 nm	Cubic	MB	Sun/130 min	72.6%	[84]
NiO NPs	28.6 nm	Spherical	MB	UV/270 min	80%	[86]
Ag-ZnO NPs	59.73 -87.05 nm	Spherical	MB	UV /90 min	87%	[71]
Ag-NiO NPs	42 -76 nm	Spherical	MB	UV/120 min	50%	[124]
ZnO NPs	3.05 nm	Spherical	MB	UV/140 min	52.68%	This study
				Sun/140 min	74.62%	
Ag-ZnO NPs	3.044 nm	Spherical	MB	UV/140 min	55.87%	This study
				Sun/140 min	98.32%	
NiO NPs	3.346 nm	Spherical	MB	UV/140 min	42.71%	This study
				Sun/140 min	51.37%	
Ag-NiO NPs	3.434 nm	Spherical	MB	UV/140 min	45.34%	This study
				Sun/140 min	76.59%	

CHAPTER 5

CONCLUSION AND RECOMMENDATIONS

Pure ZnO and NiO NPs and silver nanoparticles doping ZnO and NiO were synthesised by *Thymelaea hirsute* extract as photocatalysts to be applied in environmental remediation in methylene blue (MB) degradation under UV and sunlight. Characterisation showed that nanoparticles whose dimensions were reduced down to 3 nm exhibited increased efficiency in photocatalysis, with high efficiency under sunlight. From the synthesised compounds, 98.32% efficiency under sunlight showed high activity in Ag-ZnO NPs, which is an improved value compared to values reported in the literature.

Degradation experiments in sunlight and under UV for efficiency and kinetic reaction determination showed that the nanoparticles' spherical shape improved charge separation and high performance. Doping effects were also observable, with high activity in Ag-ZnO and Ag-NiO NPs compared to their undoped counterparts. Nanoparticles' dimension effects were also visible with high efficiency when nanoparticles had lower dimensions, following high radiation absorption and surface. The FTIR, UV-Vis with Diffuse Reflection, FESEM, and EDX methods characterise the synthesised ZnO, NiO, and ZnO/NiO silver-doped nanoparticles. The characterisation of shape and structure reflected its photocatalyst activity by affirming shape and size and the role of doping in enhancing performance.

Despite these promising results, further research is recommended to pave the way for the optimum utilisation of ZnO, NiO, and ZnO/NiO NPs in high-performance photocatalysis under environmental conditions. Further studies can involve application to the degradation of other pollutants and develop multi-component nanocomposites (e.g., ZnO/NiO/Ag with carbon-based materials like graphene) for synergistic photocatalytic enhancement and application under actual environmental conditions.

REFERENCES

[1] Wu Q, Miao WS, Zhang YD, et al. Mechanical properties of nanomaterials: a review. Nanotechnol Rev. 2020; 9:259–73. https://doi.org/10.1515/ntrev-2020-0021.

[2] Rahmawati T, Butburee T, Sangkhun W, Wutikhun T, Padchasri J, Kidkhunthod P, et al. Green synthesis of Ag-TiO2 nanoparticles using turmeric extract and its enhanced photocatalytic activity under visible light. Colloids Surf A Physicochem Eng Asp. 2023; 665:131206. https://doi.org/10.1016/j.colsurfa.2023.131206

[3] Lins A, Jerônimo AG, Barbosa R, Neves L, Trigueiro P, Almeida LC, et al. Facile synthesis of Ni-doped ZnO nanoparticles using cashew gum: investigation of the structural, optical, and photocatalytic properties. Molecules. 2023;28(23):7772. https://doi.org/10.3390/molecules28237772.

[4] Al-Ariki S, Yahya NA, Al-A'nsi SAA, Jumali MH, Jannah AN, Abd-Shukor R. Synthesis and comparative study on the structural and optical properties of ZnO doped with Ni and Ag's nanopowders fabricated by sol-gel technique. Sci Rep. 2021;11(1):11948. https://doi.org/10.1038/s41598-021-91398-6.

[5] Ahmad I, Zou Y, Yan J, Liu Y, Shukrullah S, Naz MY, et al. Semiconductor photocatalysts: A critical review highlighting the various strategies to boost the photocatalytic performances for diverse applications. Adv Colloid Interface Sci. 2023; 311:102830. https://doi.org/10.1016/j.cis.2023.102830.

[6] Cantarella M, Mangano M, Zimbone M, Sfuncia G, Nicotra G, Scalisi EM, et al. Green synthesis of photocatalytic TiO2/Ag nanoparticles for an efficient water remediation. J Photochem Photobiol A Chem. 2023; 443:114838. https://doi.org/10.1016/j.jphotochem.2023.114838.

[7] Alharthi FA, Alghamdi AA, Al-Zaqri N, Alanazi HS, Alsyahi AA, Marghany AE, et al. Facile one-pot green synthesis of Ag–ZnO nanocomposites using potato peel and their Ag concentration dependent photocatalytic properties. Sci Rep. 2020;10(1):20229. https://doi.org/10.1038/s41598-020-77426-y

[8] Güy N, Özacar M. The influence of noble metals on photocatalytic activity of ZnO for Congo red degradation. Int J Hydrogen Energy. 2016;41(36):16365–74. https://doi.org/10.1016/j.ijhydene.2016.07.063

[9] Joseph A, Vijayanandan A. Photocatalysts synthesized via plant-mediated extracts for degradation of organic compounds: A review of formation mechanisms and application in

wastewater treatment. Sustain Chem Pharm. 2021; 22:100453. https://doi.org/10.1016/j.scp.2021.100453.

[10] Logaranjan K, Raiza AJ, Gopinath SCB, et al. Shape- and size-controlled synthesis of silver nanoparticles using Aloe vera plant extract and their antimicrobial activity. Nanoscale Res Lett. 2016; 11:520. https://doi.org/10.1186/s11671-016-1725-x.

[11] Schneider J, Bahnemann D, Ye J, Li Puma G, Dionysiou DD, Schneider J, editors. Photocatalysis: Fundamentals and Perspectives. The Royal Society of Chemistry; 2016.

[12] Bonomo M. Synthesis and characterization of NiO nanostructures: a review. J Nanopart Res. 2018; 20:222. https://doi.org/10.1007/s11051-018-4327-y.

[13] Jeevanandam J, Kiew SF, Boakye-Ansah S, Lau SY, Barhoum A, Danquah MK, et al. Green approaches for the synthesis of metal and metal oxide nanoparticles using microbial and plant extracts. Nanoscale. 2022;14(7):2534-71.

[14] Barhoum A, Makhlouf ASH. Emerging applications of nanoparticles and architecture nanostructures. In: Barhoum A, Makhlouf ASH, editors. Emerging applications of nanoparticles and architecture nanostructures. Amsterdam, The Netherlands: Elsevier; 2018. p. 255-78.

[15] Gour A, Jain NK. Advances in green synthesis of nanoparticles. Artif Cells Nanomed Biotechnol. 2019;47(1):844–51. https://doi.org/10.1080/21691401.2019.1577878

[16] Kumar A, Pandey G. A review on the factors affecting the photocatalytic degradation of hazardous materials. Mater Sci Eng Int J. 2017;1(3):1–10.

[17] Bukhari A, Ijaz I, Gilani E, Nazir A, Zain H, Saeed R, et al. Green synthesis of metal and metal oxide nanoparticles using different plants' parts for antimicrobial activity and anticancer activity: a review article. Coatings. 2021;11(11):1374. https://doi.org/10.3390/coatings11111374

[18] Fujishima A, Honda K. Electrochemical photolysis of water at a semiconductor electrode. Nature. 1972;238(5358):37–8.

[19] Kumar S, Kumar A, Kumar A, Krishnan V. Nanoscale zinc oxide-based heterojunctions as visible light active photocatalysts for hydrogen energy and environmental remediation. Catal Rev. 2020;62(3):346–405. https://doi.org/10.1080/01614940.2019.1684649

[20] Díaz C, Segovia M, Valenzuela ML. Solid-state nanostructured metal oxides as photocatalysts and their application in pollutant degradation: a review. Photochem. 2022;2(3):609–27. https://doi.org/10.3390/photochem2030041

[21] Gueymard CA. The sun's total and spectral irradiance for solar energy applications and solar radiation models. Sol Energy. 2004;76(4):423–53. https://doi.org/10.1016/j.solener.2003.08.039

[22] Qin Z, Su T, Ji H, Guo Z, Chen Y, Lu NL. Photocatalytic nanomaterials for the energy and environmental application. In: Multifunctional nanocomposites for energy and environmental applications. 2018; 1:353–401

[23] Sarkar B, Daware AV, Gupta P, et al. Nanoscale wide-band semiconductors for photocatalytic remediation of aquatic pollution. Environ Sci Pollut Res. 2017;24(26):25775–25797. https://doi:10.1007/s11356-017-0252-3.

[24] Chen X, Rong H, Ndagijimana P, Nkinahamira F, Kumar A, Guo D, et al. Towards removal of PPCPs by advanced oxidation processes: a review. Results Eng. 2023;101496. https://doi.org/10.1016/j.rineng.2023.101496

[25] Rahman MA. A review on semiconductors including applications and temperature effects in semiconductors. Am Sci Res J Eng Technol Sci. 2014;7(1):50–70.

[26] Kisch H. Semiconductor photocatalysis—mechanistic and synthetic aspects. Angew Chem Int Ed. 2013;52(3):812–47. https://doi:10.1002/anie.201201200.

[27] Rusdi R, Abd Rahman A, Mohamed NS, Kamarudin N, Kamarulzaman N. Preparation and band gap energies of ZnO nanotubes, nanorods and spherical nanostructures. Powder Technol. 2011;210(1):18–22. https://doi:10.1016/j.powtec.2011.02.005.

[28] Arif A, Belahssen O, Gareh S, Benramache S. The calculation of band gap energy in zinc oxide films. J Semicond. 2015;36(1):013001. https://doi:10.1088/1674-4926/36/1/013001.

[29] Li S, Li JL, Jiang Q, Yang GW. Electrical field induced direct-to-indirect bandgap transition in ZnO nanowires. J Appl Phys. 2010;108(2). https://doi:10.1063/1.3462407.

[30] Schneider K. Optical properties and electronic structure of V2O5, V2O3 and VO2. J Mater Sci: Mater Electron. 2020; 31:10478–10488. https://doi:10.1007/s10854-020-03596-0.

[31] Hong SJ, Mun HJ, Kim BJ, Kim YS. Characterization of nickel oxide nanoparticles synthesized under low temperature. Micromachines. 2021;12(10):1168. https://doi.org/10.3390/mi12101168

[32] Beach ER, Shqau K, Brown SE, Rozeveld SJ, Morris PA. Solvothermal synthesis of crystalline nickel oxide nanoparticles. Mater Chem Phys. 2009;115(1):371-7. https://doi.org/10.1016/j.matchemphys.2008.12.018

[33] Narender SS, Varma VV, Srikar CS, Ruchitha J, Varma PA, Praveen BVS. Nickel oxide nanoparticles: a brief review of their synthesis, characterization, and applications. Chem Eng Technol. 2022;45(3):397-409. https://doi.org/10.1002/ceat.202100442

[34] Medhi R, Marquez MD, Lee TR. Visible-light-active doped metal oxide nanoparticles: review of their synthesis, properties, and applications. ACS Appl Nano Mater. 2020;3(7):6156-85. https://doi.org/10.1021/acsanm.0c01035

[35] Sun N, Qi D, Jin Y, Wang H, Wang C, Qu C, et al. Porous pyrene organic cage with unusual absorption bathochromic-shift enables visible light photocatalysis. CCS Chem. 2022;4(8):2588-96. https://doi.org/10.31635/ccschem.021.202101202

[36] Sohrabnezhad S, Seifi A. The green synthesis of Ag/ZnO in montmorillonite with enhanced photocatalytic activity. Appl Surf Sci. 2016; 386:33-40. https://doi.org/10.1016/j.apsusc.2016.05.102

[37] Nagasundari SM, Muthu K, Kaviyarasu K, Al Farraj DA, Alkufeidy RM. Current trends of silver doped zinc oxide nanowires photocatalytic degradation for energy and environmental application. *Surfaces Interfaces.* 2021; 23:100931. https://doi.org/10.1016/j.surfin.2021.100931

[38] Liu H, Hu Y, Zhang Z, Liu X, Jia H, Xu B. Synthesis of spherical Ag/ZnO heterostructural composites with excellent photocatalytic activity under visible light and UV irradiation. Appl Surf Sci. 2015;355:644-52. https://doi.org/10.1016/j.apsusc.2015.07.012

[39] Dhiman P, Rana G, Kumar A, Dawi EA, Sharma G. Rare earth doped ZnO nanoparticles as spintronics and photocatalyst for degradation of pollutants. Molecules. 2023;28(6):2838. https://doi.org/10.3390/molecules28062838

[40] Naseer H, Iqbal T. Green synthesis of silver-doped zinc oxide nanoparticles for investigation of their photocatalytic activity and shelf-life applications. Biomass Convers Biorefinery. 2023:1-17. https://doi:10.1007/s13399-023-04380-w.

[41] Khalid NR, Hammad A, Tahir MB, Rafique M, Iqbal T, Nabi G, Hussain MK. Enhanced photocatalytic activity of Al and Fe co-doped ZnO nanorods for methylene blue degradation. Ceram Int. 2019;45(17):21430-5. https://doi.org/10.1016/j.ceramint.2019.07.132

[42] Kudo A, Niishiro R, Iwase A, Kato H. Effects of doping of metal cations on morphology, activity, and visible light response of photocatalysts. Chem Phys. 2007;339(1-3):104-10. https://doi.org/10.1016/j.chemphys.2007.07.024

[43] Sun S, Chang X, Li X, Li Z. Synthesis of N-doped ZnO nanoparticles with improved photocatalytical activity. Ceram Int. 2013;39(5):5197-203. https://doi.org/10.1016/j.ceramint.2012.12.018

[44] Asahi RYOJ, Morikawa TAKESHI, Ohwaki T, Aoki K, Taga Y. Visible-light photocatalysis in nitrogen-doped titanium oxides. Science. 2001;293(5528):269-71. https://doi.org/10.1126/science.1061051

[45] Choi W, Termin A, Hoffmann MR. The role of metal ion dopants in quantum-sized TiO_2: correlation between photoreactivity and charge carrier recombination dynamics. J Phys Chem. 2002;98(51):13669-79. https://doi.org/10.1021/j100102a038

[46] Ramesh MN. Fe-doped NiO nanoparticles for enhanced photocatalytic degradation of azo dye methylene blue in the presence of visible light. SN Appl Sci. 2021;3:817. https://doi.org/10.1007/s42452-021-04803-1.

[47] Liu C, Liu Y, Ma R, Sasaki T, Wang X, Xiong P, et al. Atomic cation-vacancy engineering of two-dimensional nanosheets for energy-related applications. Mater Chem Front. 2023;7(6):1004-24. https://doi.org/10.1039/d2qm01166b

[48] Pan L, Wang S, Mi W, Song J, Zou JJ, Wang L, et al. Undoped ZnO abundant with metal vacancies. Nano Energy. 2014;9:71-9. https://doi.org/10.1016/j.nanoen.2014.06.029

[49] Wang J, Wang Z, Huang B, Ma Y, Liu Y, Qin X, et al. Oxygen vacancy induced band-gap narrowing and enhanced visible light photocatalytic activity of ZnO. ACS Appl Mater Interfaces. 2012;4(8):4024-30. https://doi.org/10.1021/am300835p

[50] Thangadurai P, Beura R, Kumar JS. Nanomaterials with different morphologies for photocatalysis. In: Naushad M, Rajendran S, Lichtfouse E, editors. Green Photocatalysts. Environmental Chemistry for a Sustainable World, vol 34. Cham: Springer; 2020. p. [47-87]. https://doi:10.1007/978-3-030-15608-4_3.

[51] Hussain A, Nguyen DA, Ali S, Hussain I, Junejo A, et al. Advancement in nanomaterials for environmental pollutants remediation: a systematic review on bibliometrics analysis, material types, synthesis pathways, and related mechanisms. J Nanobiotechnol. 2024;22(1):26. https://doi:10.1186/s12951-023-02151-3.

[52] Ba-Abbad MM, Kadhum AAH, Mohamad AB, Takriff MS, Sopian K. Optimization of process parameters using D-optimal design for synthesis of ZnO nanoparticles via sol–gel technique. J Ind Eng Chem. 2013;19(1):99-105. https://doi.org/10.1016/j.jiec.2012.07.010

[53] Kajbafvala A, Hamed G, Asieh P, Joshua PS, Ehsan K, Sadrnezhaad SK (2012) Effects of morphology on photocatalytic performance of Zinc oxide nanostructures synthesized by

rapid microwave irradiation methods. Superlattice Microst 51:512–522. https://doi.org/10.1016/j.spmi.2012.01.015

[54] Ezhilarasi AA, Vijaya JJ, Kennedy LJ, Kaviyarasu K. Green mediated NiO nano-rods using Phoenix dactylifera (Dates) extract for biomedical and environmental applications. Mater Chem Phys. 2020; 241:122419. https://doi.org/10.1016/j.matchemphys.2019.122419

[55] Moghaddas SMTH, Elahi B, Darroudi M, Javanbakht V. Green synthesis of hexagonal-shaped zinc oxide nanosheets using mucilage from flaxseed for removal of methylene blue from aqueous solution. J Mol Liq. 2019; 296:111834. https://doi.org/10.1016/j.molliq.2019.111834

[56] Wang J, Liu D, Yu N, Cheng P, Cheng L, Liu Y, et al. Low-cost Ag/ZnO nanosheets arrays as sensitive and recyclable surface-enhanced Raman scattering substrates. Opt Mater. 2024; 157:116187. https://doi.org/10.1016/j.optmat.2024.116187

[57] Khedkar CV, Vedpathak AS, Dhotre AV, Daware KD, Kolekar YD, Sartale SD, Gosavi SW, Patil SI. Synthesis, characterization, electrochemical and catalytic performance of NiO nanostructures and Ag-NiO nanocomposite. Chem Phys Impact. 2023; 6:100153. https://doi.org/10.1016/j.chphi.2022.100153

[58] Ferreira, R. M., Morawski, F. M., Pessanha, E. C., de Lima, S. L., da Costa, D. S., Ribeiro, G. A., ... & Garcia, M. A. (2023). Facile gram-scale synthesis of NiO nanoflowers for highly selective and sensitive electrocatalytic detection of hydrazine. ACS omega, 8(13), 11978-11986. https://doi.org/10.1021/acsomega.2c07638

[59] Almuhammady AK, Salem KFM, Alloosh MT, Saleh MM, Alnaddaf LM, Al-Khayri JM. Nanomaterials Fundamentals: Classification, Synthesis and Characterization. In: Al-Khayri JM, Ansari MI, Singh AK, editors. Nanobiotechnology. Cham: Springer; 2021. p. [77-99]. https://doi:10.1007/978-3-030-73606-4_4.

[60] Shivaji K, et al. Synthesizing green photocatalyst using plant leaf extract for water pollutant treatment. In: Naushad M, Rajendran S, Lichtfouse E, editors. Green Photocatalysts. Environmental Chemistry for a Sustainable World, vol 34. Cham: Springer; 2020. p. [25-46]. https://doi:10.1007/978-3-030-15608-4_2.

[61] Hano C, Abbasi BH. Plant-based green synthesis of nanoparticles: production, characterization and applications. Biomolecules. 2021;12(1):31. https://doi.org/10.3390/biom12010031

[62] Khan F, Shariq M, Asif M, Siddiqui MA, Malan P, Ahmad F. Green nanotechnology: plant-mediated nanoparticle synthesis and application. Nanomaterials. 2022;12(4):673. https://doi.org/10.3390/nano12040673

[63] Munir H, Bilal M, Mulla SI, Abbas Khan H, Iqbal HMN. Plant-Mediated Green Synthesis of Nanoparticles. In: Inamuddin, Boddula R, Ahamed MI, Khan A, editors. Advances in Green Synthesis. Advances in Science, Technology & Innovation. Cham: Springer; 2021. p. [75-89]. https://doi:10.1007/978-3-030-67884-5_4.

[64] Anand V, Srivastava VC. Zinc oxide nanoparticles synthesis by electrochemical method: optimization of parameters for maximization of productivity and characterization. J Alloys Compd. 2015; 636:288-92. https://doi.org/10.1016/j.jallcom.2015.02.189

[65] Hasanpoor M, Aliofkhazraei M, Delavari HJ. Microwave-assisted synthesis of zinc oxide nanoparticles. Procedia Mater Sci. 2015; 11:320-5. https://doi.org/10.1016/j.mspro.2015.11.101

[66] Rakkesh RA, Durgalakshmi D, Karthe P, Balakumar S. Anisotropic growth and strain-induced tunable optical properties of Ag–ZnO hierarchical nanostructures by a microwave synthesis method. Mater Chem Phys. 2020; 244:122720. https://doi.org/10.1016/j.matchemphys.2020.122720

[67] Abbas AM, Abid MA, Abbas KN, Aziz WJ, Salim AA. Photocatalytic activity of Ag-ZnO nanocomposites integrated essential ginger oil fabricated by green synthesis method. In: Journal of Physics: Conference Series. Vol. 1892, No. 1, p. 012005. IOP Publishing; 2021. https://doi.org/10.1088/1742-6596/1892/1/012005

[68] Al-Zaqri N, Umamakeshvari K, Mohana V, Muthuvel A, Boshaala A. Green synthesis of nickel oxide nanoparticles and its photocatalytic degradation and antibacterial activity. J Mater Sci Mater Electron. 2022;33(15):11864-80. https://doi.org/10.1007/s10854-022-08149-1

[69] Pandey SK, Tripathi MK, Ramanathan V, Mishra PK, Tiwary D. Highly facile Ag/NiO nanocomposite synthesized by sol-gel method for mineralization of rhodamine B. J Phys Chem Solids. 2021; 159:110287. https://doi.org/10.1016/j.jpcs.2021.110287

[70] He P, Jiao Z, Wang J, Lin T. Research and application of joining technology at nanometer scale. Trans China Weld Inst. 2013;(2):109-12.

[71] Nemma NM, Sadeq ZS. Eco-friendly green synthesis and photocatalyst activity of Ag-ZnO nanocomposite. East Eur J Phys. 2023;(3):271-8. https://doi.org/10.26565/2312-4334-2023-3-24

[72] Hassaan MA, El-Nemr MA, Elkatory MR, Ragab S, Niculescu VC, El Nemr A. Principles of photocatalysts and their different applications: a review. Top Curr Chem (Z). 2023; 381:31. https://doi:10.1007/s41061-023-00444-7.

[73] Rani N, Yadav S, Mushtaq A, et al. Azadirachta indica peel extract-mediated synthesis of ZnO nanoparticles for antimicrobial, supercapacitor and photocatalytic applications. Chem Pap. 2024; 78:3687-704. https://doi:10.1007/s11696-024-03340-6.

[74] Yadav LR, Pratibha S, Manjunath K, Shivanna M, Ramakrishnappa T, Dhananjaya N, Nagaraju G. Green synthesis of Ag-ZnO nanoparticles: structural analysis, hydrogen generation, formylation and biodiesel applications. J Sci Adv Mater Devices. 2019;4(3):425-31. https://doi.org/10.1016/j.jsamd.2019.03.001

[75] Singh Y, Sodhi RS, Singh PP, Kaushal S. Biosynthesis of NiO nanoparticles using Spirogyra sp. cell-free extract and their potential biological applications. Mater Adv. 2022;3(12):4991-5000. https://doi.org/10.1039/D2MA00114D

[76] Rajalakshmi D, Gunasekaran S, Paneerselvam PJ, Kostova I. Synthesis, characterization, and biomedical potential of nickel oxide and silver-doped nickel oxide nanoparticles via green synthesis method. Physica B: Condens Matter. 2024; 693:416237. https://doi.org/10.1016/j.physb.2024.416237

[77] Lakshmanaprubhu S, Ganesan D, Priyadharsini K, Hemavathi S. Green synthesis of ZnO nanoparticles using Moringa oleifera leaf extract for efficient photocatalytic degradation of organic dyes. Water Wastewater Treat. 2024;26(1):1-7. https://doi:10.30955/gnj.005411.

[78] Tripathi RM, Bhadwal AS, Gupta RK, Singh P, Shrivastav A, Shrivastav BR. ZnO nanoflowers: novel biogenic synthesis and enhanced photocatalytic activity. J Photochem Photobiol B: Biol. 2014; 141:288-95. https://doi.org/10.1016/j.jphotobiol.2014.10.001

[79] Abdullah FH, Bakar NA, Bakar MA. Low temperature biosynthesis of crystalline zinc oxide nanoparticles from Musa acuminata peel extract for visible-light degradation of methylene blue. Optik. 2020; 206:164279. https://doi.org/10.1016/j.ijleo.2020.164279

[80] Davar F, Majedi A, Mirzaei A. Green synthesis of ZnO nanoparticles and its application in the degradation of some dyes. J Am Ceram Soc. 2015;98(6):1739-46. https://doi.org/10.1111/jace.13467

[81] Bopape DA, Motaung DE, Hintsho-Mbita NC. Green synthesis of ZnO: Effect of plant concentration on the morphology, optical properties and photodegradation of dyes and antibiotics in wastewater. Optik. 2022; 251:168459. https://doi.org/10.1016/j.ijleo.2021.168459

[82] Ahmad KS, Jaffri SB. Phytosynthetic Ag doped ZnO nanoparticles: semiconducting green remediators: photocatalytic and antimicrobial potential of green nanoparticles. Open Chem. 2018;16(1):556-70. https://doi.org/10.1515/chem-2018-0060

[83] Fouladi-Fard R, Aali R, Mohammadi-Aghdam S, Mortazavi-derazkola S. The surface modification of spherical ZnO with Ag nanoparticles: A novel agent, biogenic synthesis, catalytic and antibacterial activities. Arab J Chem. 2022;15(3):103658. https://doi.org/10.1016/j.arabjc.2021.103658

[84] Gemachu LY, Birhanu AL. Green synthesis of ZnO, CuO and NiO nanoparticles using Neem leaf extract and comparing their photocatalytic activity under solar irradiation. Green Chem Lett Rev. 2024;17(1):2293841. https://doi.org/10.1080/17518253.2023.2293841

[85] Roopan SM, Elango G, Priya DD, Asharani IV, Kishore B, Vinayprabhakar S, et al. Sunlight mediated photocatalytic degradation of organic pollutants by statistical optimization of green synthesized NiO NPs as catalyst. J Mol Liq. 2019; 293:111509. https://doi.org/10.1016/j.molliq.2019.111509

[86] Sabouri Z, Akbari A, Hosseini HA, Darroudi M. Facile green synthesis of NiO nanoparticles and investigation of dye degradation and cytotoxicity effects. J Mol Struct. 2018; 1173:931-6. https://doi.org/10.1016/j.molstruc.2018.07.063

[87] Alfadhli S, Khasim S, Darwish AAA, Al-Nahdi K, Abdelkader M, Gamal R, Hamdalla TA. Facile green synthesis of silver-doped NiO nanoparticles using aloe vera latex for efficient energy storage and photocatalytic applications. Heliyon. 2025;11(1). https://doi.org/10.1016/j.heliyon.2024.e41322

[88] Chen X, Mao SS. Titanium dioxide nanomaterials: synthesis, properties, modifications, and applications. Chem Rev. 2007;107(7):2891-2959. https://doi.org/10.1021/cr0500535

[89] Hoffmann MR, Martin ST, Choi W, Bahnemann DW. Environmental applications of semiconductor photocatalysis. Chem Rev. 1995;95(1):69-96. https://doi.org/10.1021/cr00033a004

[90] Reza KM, Kurny ASW, Gulshan F (2017) Parameters affecting the photocatalytic degradation of dyes using TiO2: a review. Appl Water Sci 7(4):1569–1578. https://doi.org/10.1007/s13201-015-0367-y

[91] Akpan UG, Hameed BH (2009) Parameters affecting the photocatalytic degradation of dyes using TiO2-based photocatalysts: a review. J Hazard Mater 170(2):520–529. https://doi.org/10.1016/j.jhazmat.2009.05.039

[92] Kumar A, Pandey G. A review on the factors affecting the photocatalytic degradation ofhazardous materials. Mater Sci Eng Int J. 2017;1(3):1-10. https://doi.org/10.15406/mseij.2017.01.00018

[93] Malato S, Fernández-Ibáñez P, Maldonado MI, Blanco J, Gernjak W. Decontamination and disinfection of water by solar photocatalysis: recent overview and trends. Catal Today. 2009;147(1):1-59. https://doi.org/10.1016/j.cattod.2009.06.018

[94] Chatterjee and Dasgupta (2005) discussed visible light induced photocatalytic degradation of organic pollutants. https://doi.org/10.1016/j.jphotochemrev.2005.09.001

[95] Rajeshwar K, Osugi ME, Chanmanee W, Chenthamarakshan CR, Zanoni MVB, Kajitvichyanukul P, Krishnan-Ayer R. Heterogeneous photocatalytic treatment of organic dyes in air and aqueous media. J Photochem Photobiol C: Photochem Rev. 2008;9(4):171-192. https://doi.org/10.1016/j.jphotochemrev.2008.09.001.

[96] Cao D, Gong S, Shu X, et al. Preparation of ZnO nanoparticles with high dispersibility based on oriented attachment (OA) process. Nanoscale Res Lett. 2019;14:210. https://doi.org/10.1186/s11671-019-3038-3.

[97] Mourdikoudis S, Pallares RM, Thanh NT. Characterization techniques for nanoparticles: comparison and complementarity upon studying nanoparticle properties. Nanoscale. 2018;10(27):12871-12934. https://doi.org/10.1039/C8NR02278J

[98] Kumar A, Dixit CK. Methods for characterization of nanoparticles. In: Advances in nanomedicine for the delivery of therapeutic nucleic acids. Woodhead Publishing; 2017. p. 43-58. https://doi.org/10.1016/B978-0-08-100557-6.00003-1

[99] Hussain A, Fiaz S, Almohammedi A, Waqar A. Optimizing photocatalytic performance with Ag-doped ZnO nanoparticles: Synthesis and characterization. Heliyon. 2024;10(15). https://doi.org/10.1016/j.heliyon.2024.e35725

[100] Quevedo AC, Guggenheim E, Briffa SM, Adams J, Lofts S, Kwak M, et al. UV-Vis spectroscopic characterization of nanomaterials in aqueous media. 2021. https://doi:10.3791/61764.

[101] Lakshmi B, Thomas BJ, Gopinath P. Accurate band gap determination of chemically synthesized cobalt ferrite nanoparticles using diffuse reflectance spectroscopy. Adv Powder Technol. 2021;32(10):3706-3716. https://doi.org/10.1016/j.apt.2021.08.028

[102] Mishra RK, Zachariah AK, Thomas S. Energy-dispersive X-ray spectroscopy techniques for nanomaterial. In: Microscopy methods in nanomaterials characterization. Elsevier; 2017. p. 383-405. https://doi.org/10.1016/B978-0-323-46141-2.00012-2

[103] Bernardi J. Energy-dispersive X-ray spectroscopy. In: Imaging Modalities for Biological and Preclinical Research: A Compendium, Volume 1: Part I: Ex vivo biological imaging. Bristol, UK: IOP Publishing; 2021. p. I-9.

[104] Shindo D, Oikawa T. Energy Dispersive X-ray Spectroscopy. In: Analytical Electron Microscopy for Materials Science. Springer, Tokyo; 2002. p. 79-105. https://doi.org/10.1007/978-4-431-66988-3_4.

[105] Bitwell C, Indra SS, Luke C, Kakoma MK. A review of modern and conventional extraction techniques and their applications for extracting phytochemicals from plants. Sci Afr. 2023;19:e01585. Available from: http://dx.doi.org/10.1016/j.sciaf.2023.e01585

[106] Amari NO, Bouzouina M, Berkani A, Lotmani B. Phytochemical screening and antioxidant capacity of the aerial parts of Thymelaea hirsuta L. Asian Pac J Trop Dis. 2014;4(2):104-109. https://doi.org/10.1016/S2222-1808(14)60324-8

[107] Abd El Khalk AA, Betiha MA, Mansour AS, Abd El Wahed MG, Al-Sabagh AM. High degradation of methylene blue using a new nanocomposite based on zeolitic imidazolate framework-8. ACS Omega. 2021;6(40):26210-26220. https://doi.org/10.1021/acsomega.1c03195

[108] Teixeira S, Martins PM, Lanceros-Méndez S, Kühn K, Cuniberti G. Reusability of photocatalytic TiO2 and ZnO nanoparticles immobilized in poly (vinylidene difluoride)-co-trifluoroethylene. Appl Surf Sci. 2016;384:497-504. https://doi.org/10.1016/j.apsusc.2016.05.073

[109] Kubelka P. New contributions to the optics of intensity light scattering materials. J Opt Soc Am. 1948;38(5):448-457.

[110] Szczesny R, Scigala A, Derkowska-Zielinska B, Skowronski L, Cassagne C, Boudebs G, et al. Synthesis, optical, and morphological studies of ZnO powders and thin films fabricated by wet chemical methods. Materials (Basel). 2020;13(11):2559. https://doi.org/10.3390/ma13112559

[111] Rajith Kumar CR, Betageri VS, Nagaraju G, Pujar GH, Onkarappa HS, Latha MS. Synthesis of core/shell (ZnO/Ag) nanoparticles using Calotropis gigantea and their applications in photocatalytic and antibacterial studies. J Inorg Organomet Polym Mater. 2020;30(9):3410-3417. https://doi.org/10.1007/s10904-020-01507-8

[112] Kamarulzaman N, Kasim MF, Rusdi R. Band gap narrowing and widening of ZnO nanostructures and doped materials. Nanoscale Res Lett. 2015; 10:1-12. https://doi.org/10.1186/s11671-015-1034-9

[113] Koca FD, Halici MG, Işik Y, Ünal G. Green synthesis of Ag-ZnO nanocomposites by using Usnea florida and Pseudevernia furfuracea lichen extracts and evaluation of their neurotoxic effects. Inorg Nano-Met Chem. 2024;54(9):818-825. https://doi.org/10.1080/24701556.2022.2078351

[114] Naseer H, Iqbal T. Green synthesis of silver-doped zinc oxide nanoparticles for investigation of their photocatalytic activity and shelf life applications. Biomass Convers Biorefin. 2024;14(18):21895-21911. https://doi.org/10.1007/s13399-023-04380-w

[115] Prencipe I, Dellasega D, Zani A, Rizzo D, Passoni M. Energy dispersive x-ray spectroscopy for nanostructured thin film density evaluation. Sci Technol Adv Mater. 2015;16(1):015005. https://doi.org/10.1088/1468-6996/16/2/025007

[116] Shkir M, Baskaran P, Khan A, Khan MT. Remarkable improvement in photocatalytic activity of NiO nanoparticles through Ag doping: A kinetics-mechanism & recyclability. Int J Hydrogen Energy. 2024; 73:54-62. https://doi.org/10.1016/j.ijhydene.2024.05.466

[117] Bunker KL, McAllister D, Allison KA, Wagner K, Rickabaugh K, Levine AM, et al. TEM and FESEM: The right combination for enhanced particle characterization. Microsc Microanal. 2008;14(S2):580-581. https://doi.org/10.1017/S1431927608083682

[118] Akbari B, Tavandashti MP, Zandrahimi M. Particle size characterization of nanoparticles–a practical approach. Iranian J Mater Sci Eng. 2011;8(2):48-56.

[119] Tuoriniemi J, Johnsson ACJ, Holmberg JP, Gustafsson S, Gallego-Urrea JA, Olsson E, et al. Intermethod comparison of the particle size distributions of colloidal silica nanoparticles. Sci Technol Adv Mater. 2014;15(3):035009. https://doi:10.1088/1468-6996/15/3/035009

[120] Merkus, H. G. (2009). Particle size measurements: fundamentals, practice, quality (Vol. 17, pp. 13–73). Springer Science & Business Media.

[121] Zhang S, Wang C. Precise analysis of nanoparticle size distribution in TEM image. Methods Protoc. 2023;6(4):63. https://doi.org/10.3390/mps6040063

[122] Wani HA, Shaikh VR, More DH, Patil KJ. Applications of spectroscopic techniques to the study of monomer–dimer equilibria for methylene blue in aqueous solutions containing ionic liquid: Probing the structural interactions involving water and ionic liquids. Spectrochim Acta A Mol Biomol Spectrosc. 2023; 287:122058. https://doi.org/10.1016/j.saa.2022.122058

[123] Amrute V, Supin KK, Vasundhara M, Chanda A. Observation of excellent photocatalytic and antibacterial activity of Ag doped ZnO nanoparticles. RSC Adv. 2024;14(45):32786-32801. https://doi.org/10.1039/d4ra05197a

[124] Basavalingaiah, K. R., Harishkumar, S., & Nagaraju, G. (2019). NiO and Ag@ NiO Nanomaterials for Enhanced Photocatalytic and Photoluminescence Studies: Green Synthesis Using Lycopodium Linn. Asian Journal of Engineering and Applied Technology, 8(2), 79-85. https://doi.org/10.51983/ajeat-2019.8.2.1133

[125] Gowthaman K, Gowthaman P, Venkatachalam M, Saroja M, Kutraleeswaran M, Dhinesh S. Design and synthesis of TiO2/ZnO nanocomposite with enhanced oxygen vacancy: Better photocatalytic removal of MB dye under visible light-driven condition. Inorg Chem Commun. 2022; 146:110197. https://doi.org/10.1016/j.inoche.2022.110197

الطاقة الشمسية. كما يغير التنشيط البنية الإلكترونية ويسهل إنشاء فجوة النطاق الموضعية، مما يعزز كفاءة احتواء حاملات الشحنة ويعيق إعادة التركيب. هذا التأثير مهم بشكل خاص في التطبيقات التي تتطلب نشاطًا تحفيزيًا ضوئيًا ثابتًا تحت الإضاءة بأشعة الشمس حيث يمكن استخدام نسبة أكبر من طيف الضوء. في العمل الحالي، تم الإبلاغ عن محفزات ضوئية تعتمد على جسيمات نانوية من أكسيد الزنك وأكسيد النيكل، تم تعديلها وتصنيعها باستخدام مستخلصات نباتية مختلفة من خلال عملية بسيطة وغير سامة وغير مكلفة وصديقة للبيئة لإنشاء محفز ضوئي عالي الكفاءة يتميز بسمية منخفضة [6،7].

لأغراض التحفيز الضوئي، يعد أكسيد الزنك (ZnO) وأكسيد النيكل (NiO) المرشحين الأكثر وعدًا لمجموعة متنوعة من التطبيقات، بما في ذلك الأنودات المركبة لخلايا الوقود، وتقنيات استشعار الغاز، والنوافذ الساطعة، والمكثفات الفائقة، ومعالجة المياه. يتمتع أكسيد الزنك وأكسيد النيكل بفجوة طاقة واسعة النطاق، لذا فهما يظهران نشاطًا ضوئيًا عاليًا تحت الأشعة فوق البنفسجية ولكن نشاطًا منخفضًا في النطاق المرئي؛ وبالتالي، لتحسين النشاط الضوئي لأكسيد الزنك وأكسيد النيكل في المنطقة المرئية، يستخدم الباحثون محفزات ضوئية مشبعة بالمعادن وغير المعادن أو مركبات محفزات ضوئية. ركزت بعض الدراسات على التخليق الأخضر باستخدام مستخلصات نباتية وكتل حيوية وطحالب [4]. كانت هذه الدراسة هي الأولى التي تجمع بين التخليق الأخضر والتحكم في مورفولوجيا وحجم الجسيمات النانوية؛ استند اختيار نبات (*Thymelaea hirsuta*) إلى محتواها العالي من الفلافونويد والسابونين والقلويدات التي تعمل كعوامل اختزال وتغطية وتثبيت نظرًا لقدرتها على تثبيط ذرات المواد النانوية النامية إلى القطر الصغير لأشباه الموصلات، والتي من المتوقع أن تسهل تكوين الجسيمات النانوية وتعزز خصائصها الفيزيائية. تساهم هذه المنهجية الجديدة في مجال التكنولوجيا النانوية الخضراء المتنامي وتفتح طرقًا لاستخدام الأنواع النباتية غير المستغلة في تصنيع المواد النانوية. إنها تربط بين تكنولوجيا النانو والتكنولوجيا الحيوية النباتية في تقليل أيونات المعادن باستخدام المستخلصات النباتية دون تطبيق ضغط مرتفع أو طاقة أو درجة حرارة أو مواد كيميائية سامة. يمكن تحسين مساحة السطح ومورفولوجيا المحفزات الضوئية في أشباه الموصلات عن طريق التنشيط بمعادن مختلفة وغير معدنية. تمنع هذه الظاهرة إعادة تركيب أزواج الإلكترونات والفجوات وتزيد من امتصاص الضوء المرئي عن طريق إدخال حالات عيب في فجوة النطاق[5].

وعلاوة على ذلك، عند تدعيم المواد شبه الموصلة بالعناصر المعدنية وغير المعدنية تسبب في تعزيز نشاطها التحفيزي الضوئي، مما يوسع التطبيقات الواعدة في معالجة المياه وتنقية البيئة وتحويل

المقدمة

تتميز المواد النانوية بخصائص بنيوية على مقياس النانو، وتتكون عادةً من جزيئات صغيرة تتراوح من 1 إلى 100 نانومتر. وعادةً ما تسمى البلورات المفردة للجسيمات النانوية بالبلورات النانوية، وتسمى التجمعات بالمساحيق النانوية [1]. يمكن أن تحتوي هذه الجسيمات النانوية على معادن أو مواد عازلة أو أشباه موصلات. ويمكن تصميمها في أشكال هندسية ذات قلب وقشرة، والتي تظهر خصائص كهربائية وبصرية جديدة بسبب تأثيرات الحجم الكمومي التي تزيد من فجوة الطاقة الطبيعية مقارنة بالمواد السائبة. وتشمل الأمثلة الآبار الكمومية، والمساحيق النانوية، والأغلفة النانوية، والأسلاك النانوية، والقضبان النانوية، وأنابيب الكربون النانوية، والأغشية النانوية، والطلاءات النانوية، والتي غالبًا ما يتم دمجها في مركبات نانوية[2] .

تتمتع المواد النانوية في تطبيقات الطاقة بخصائص كيميائية وإلكترونية وميكانيكية وبصرية محسنة بسبب زيادة نسبة السطح إلى الحجم وتأثيرات الحجم الكمومي. وهذا يجعلها فريدة مقارنة بالمواد السائبة. تم إنشاء العديد من طرق تخليق المحفزات الضوئية: الفيزيائية، والحرارية المائية، والحرارية الذائبة، والسول–جل، والترسيب المشترك. ومع ذلك، فقد تصبح مكلفة وتتضمن مواد كيميائية خطيرة يمكن أن تهدد بشكل كبير سلامة البيئة والأنظمة البيولوجية [3]. يتم تطوير طرق تخليق مختلفة، بما في ذلك الأساليب الصديقة للبيئة باستخدام المستخلصات النباتية، لإنشاء مواد نانوية مثل ZnO و TiO_2و NiOوالمركبات النانوية ذات ملفات تعريف بيئية وسلامة أفضل.

تجعل الميزات المذكورة أعلاه المستخلصات النباتية خيارًا أكثر ملاءمة مقارنة بطرق التخليق الأخرى. وهذا يفتح آفاق أشباه الموصلات بحجم النانو. من بين أشباه الموصلات التي يمكن استخدامها

الملخص

يعتبر النهج الأخضر لتخليق جسيمات النانو ضوئية المحفزة بديلاً مجديًا للطرق التقليدية. اعتمدت هذه الدراسة التخليق الأخضر باستخدام مستخلص نبات الزعتر البري (المثنان) كعامل تغطية وتثبيت واختزال للحصول على جسيمات نانوية نقية من أكسيد الزنك وأكسيد النيكل، والتي تم تعديل سطحها بعد ذلك بواسطة جسيمات نانوية فضية. أكد تحليل بنية جسيمات النانو ضوئية المحفزة تكوين شكل كروي بقطر يساوي 3.05 نانومتر و3.044 نانومتر و3.346 نانومتر و3.434 نانومتر لجسيمات النانو من أكسيد الزنك وأكسيد النيكل وأكسيد الفضة وأكسيد النيكل على التوالي. بسبب انخفاض حجم الجسيمات النانوية وتكوينه D-O والتشويب بواسطة الجسيمات النانوية الفضية مما تسبب في انخفاض قيمة طاقة فجوة النطاق (E_g) لجسيمات النانو ZnO و NiO النقية، كانت 3.3 إلكترون فولت لجسيمات النانو (ZnO) و 3.15 إلكترون فولت لجسيمات النانو (Ag-ZnO) وكانت طاقة فجوة النطاق لجسيمات النانو (NiO) تساوي 3.16 إلكترون فولت و Ag-NiO كانت 3.14 إلكترون فولت، مما أدى إلى تحسين النشاط التحفيزي الضوئي للمحفزات الضوئية النقية عند درجة الحموضة 7 بمعدل تحلل 74.62٪ و 98.32٪ لجسيمات النانو ZnO المشوبة بالفضة. أظهرت جسيمات النانو NiO المشوبة بالفضة أيضًا مستوى عالٍ من نشاط التحلل الضوئي، بمعدلات تحلل 76.59٪ و 51.37٪ لجسيمات النانو NiO على التوالي. تؤكد هذه الدراسة زيادة النشاط الضوئي التحفيزي في وسط قلوي استقرار المحفزات الضوئية وإمكانية إعادة استخدام المحفزات الضوئية المحضرة في عمليات معالجة المياة .

قال الله تعالي:

بسم الله الرحمن الرحيم

"يَرْفَعِ اللَّهُ الَّذِينَ آمَنُوا مِنكُمْ وَالَّذِينَ أُوتُوا الْعِلْمَ دَرَجَاتٍ"

صدق الله العظيم

سورة الجادلة (11)

جامعـــة ســـــــرت

كليـــــة العـــلوم

قســم الكيميـاء

تحسين النشاط الضوئي لأكسيد النيكل وأكسيد الزنك عن طريق تدعيمه بجسيمات نانوية من الفضة باستخدام التوليف الاخضر لمستخلص (المثنان الاهلب)

إعداد الطالبة:

حميدة مصباح زيد حامد

تحت إشراف:

ا. د. احميد محمد يونس

د. سليمة مفتاح حسين

قدمت هذه الرسالة كأحد متطلبات الحصول على درجة الإجازة العالية (الماجستير)

في العلوم تخصص كيمياء

العام الجامعي 2024-2025